Ordre N° :

الجمهورية الجزائرية الديمقراطية الشعبية
République Algérienne Démocratique et Populaire
وزارة التعليم العالي والبحث العلمي
Ministère de L'enseignement Supérieur et de La Recherche Scientifique
جامعة عين تموشنت بلحاج بوشعيب
Université Ain Temouchent – Belhadj Bouchaib

Faculté des Sciences et de la Technologie
Département des Sciences de la Matière
Laboratoire des Sciences des Matériaux et Applications (LSMA)

THESE

Présentée en vue de l'obtention du diplôme de **DOCTORAT**
Domaine: Sciences de la Matière
Filière: Physique
Spécialité: Physique Photonique

Par: OUARDI Mohamed Esseddik

Intitulé

Etude Plasmonique et Photonique pour la Conception et l'Optimisation des capteurs en CPs a base de Matériaux photoniques multifonctionnels

Soutenue publiquement le 11/12/2025, devant le jury compose de:

Noms	Grade	Qualité	Etablissement de rattachement
TOUIA Amina	Professeur	Président	Université d'Ain Temouchent – Belhadj Bouchaib
TAYEBOUN Fatima	Professeur	Rapporteur	Université de Sidi bel Abbes – Djillali liabès
MERADI Kada Abdelhafid	MCA	Co-rapporteur	Université d'Ain Temouchent – Belhadj Bouchaib
BOUKABRINE Fouzia	Professeur	Examinatrice	Université de Sidi bel Abbes – Djillali liabès
SLIMANE Zohra	Professeur	Examinatrice	Université de Tlemcen-Abou bakr Belkaid
BENCHERIF Kaddour	Professeur	Examinateur	Université d'Ain Temouchent – Belhadj Bouchaib

Année académique: 2025/2026

Order No :

الجمهورية الجزائرية الديمقراطية الشعبية
République Algérienne Démocratique et Populaire
وزارة التعليم العالي والبحث العلمي
Ministère de L'enseignement Supérieur et de La Recherche Scientifique
جامعة عين تموشنت بلحاج بوشعيب
Université Ain Temouchent – Belhadj Bouchaib

Faculté des Sciences et de la Technologie
Département des Sciences de la Matière
Laboratoire des Sciences des Matériaux et Applications (LSMA)

THESIS

Presented for obtaining the **Doctor of Philosophy (PhD)** degree
Field: Material Sciences
Sector: Physics
Specialty: Photonic Physics

By: OUARDI Mohamed Esseddik

Title

Plasmonic and Photonic Study for The Design and Optimization of Photonic Crystal Sensors Based on Multifunctional Photonic Materials

Publicly defended, on 11/12/2025, in front of the jury composed of:

Names	Grade	Quality	Establishment of attachment
TOUIA Amina	Professor	President	University of Ain Temouchent – Belhadj Bouchaib
TAYEBOUN Fatima	Professor	Reporter	University of Sidi bel Abbes – Djillali liabès
MERADI Kada Abdelhafid	MCA	Co-reporter	University of Ain Temouchent – Belhadj Bouchaib
BOUKABRINE Fouzia	Professor	Examiner	University of Sidi bel Abbes – Djillali liabès
SLIMANE Zohra	Professor	Examiner	University of Tlemcen-Abou bakr Belkaid
BENCHERIF Kaddour	Professor	Examiner	University of Ain Temouchent – Belhadj Bouchaib

Academic year: 2025/2026

Dedications

I dedicate this work

To my father Okkacha (may God have mercy on his soul) without whom, none of this would have been possible.

To my wife, my engine, the one who always supported me.

To my daughter Tamara, who illuminated my life.

To the few friends who surrounded me through this journey.

To my father-in-law Mr. Omar Boudaoud (may God have mercy on his soul), in whom I found courage and comfort.

And above all, to myself.

Acknowledgements

I thank, first and foremost, Allah the Almighty for giving me the strength and courage to move forward every day.

I would like to thank the director of this thesis Pr. TAYEBOUN Fatima, as well as Dr. MERADI Abdelhafid, who showed great patience and a sense of sharing, who guided and helped me until this project saw the light of day. A big thank you to them for their valuable advice and the great trust they placed in me.

I also thank Mr. GUERINIK Amine for his support, his availability and the time he devoted to helping me.

Not forgetting to warmly thank Mr. Arafa H Aly, for his observations, his advice and his guidance during the preparation of the work carried out during my studies.

I would like to express my gratitude to Pr. TOUIA Amina from the university of Ain Temouchent for the honor she gave me to be president of the jury as well as the members of the jury, Pr. BOUKABRINE Fouzia from the university of Sidi Bel Abbès, Pr. SLIMANE Zohra from the university of Tlemcen, and Pr. BENCHERIF Kaddour from the university of Ain Temouchent for the honor they gave me by agreeing to examine my work and appoint the jury of the defense of my thesis.

The work presented in this thesis was carried out within the Laboratory of Materials Sciences and Applications, of the Faculty of Science and Technology at the University of Ain Temouchent - Belhadj Bouchaib.

My most sincere thanks go to the members of the administration for the efforts made to promote the university at higher levels. In particular Mr. BENCHERIF Kaddour, who welcomed us, guided us and helped us throughout our journey within the University of Ain Temouchent.

I must not not forget to thank everyone who supported me closely or from afar, or even with a simple word, from the first day until the day of my thesis defense presentation.

Table of Contents

List of Figures

List of Tables

List of Abbreviations

PC	*Photonic crystal.*
SP	*Surface plasmon.*
SPR	*Surface plasmon resonance.*
ATR	*Attenuated total reflection.*
TM	*Transverse magnetic.*
TE	*Transverse electric.*
PSP	*Propagating surface plasmons.*
LSP	*Localized surface plasmons.*
SERS	*Surface enhanced raman spectroscopy.*
PVD	*Physical vapor deposit.*
CVD	C*hemical vapor deposit.*
SAM	*Self-assembly monolayers.*
AFM	*Atomic force microscopy.*
UV	*Ultra-violet.*
IR	*Infra-red.*
1D	*Unidimensional.*
2D	*Bidimensional.*
3D	*Tridimensional.*
FEM	*Finite elements method.*
FDTD	*Finite difference time domain.*
TMM	*Transfer matrix method.*

FOM	*Figure of Merit.*
DA	*Detection accuracy.*
QF	*Quality factor.*
FWHM	*Full width at half maximum.*
TMDC	*Transition metal dichalcogenides.*
BP	*Black phosphorus.*
LRSP	*Long-range surface plasmons*.
SRSP	*Short-range Surface Plasmons*.
Deg	*Degrees.*
RIU	*Refractive index unit.*

General Introduction

General Introduction

In the modern era of advanced technologies, precision and accuracy in measurements constitute the foundation of scientific progress and applications across all domains [1, 2]. Optical sensors, in particular, have revolutionized detection systems due to their high precision, miniaturization, and cost-effectiveness, enabling their widespread integration into daily life. From temperature sensors and environmental monitoring systems to disease detection, optical sensors have proven indispensable across diverse fields [3-5]. Among these, surface plasmon resonance (SPR) sensors stand out as a cutting-edge technology due to their unique capability to perform real-time, label-free molecular measurements with ultrahigh sensitivity.

SPR arises from the collective oscillation of free electrons at the metal-dielectric interface, termed surface plasmons, excited via specific optical configurations such as the Kretschmann or Otto geometries. In the Kretschmann configuration, a thin metal film is deposited on a prism surface, where an evanescent wave excites surface plasmons at the metal-dielectric interface. In the Otto configuration, a dielectric layer separates the prism and metal, with surface plasmon excitation occurring through a mechanism analogous to the former configuration. Both configurations achieve momentum matching between incident light and surface plasmons, thereby enabling plasmon resonance. This phenomenon exhibits exceptional sensitivity to refractive index changes near the sensor surface, rendering SPR sensors ideal for applications in biodetection, environmental and food safety monitoring, among others. The SPR mechanism is governed by the precise alignment of the incident light momentum and the plasmon wave momentum, resulting in a sharp reflectance dip at the resonance angle. This sensitivity allows SPR sensors to detect subtle refractive index variations in the analyte medium, corresponding to changes in its composition. Consequently, these sensors find utility in applications spanning cancer cell and pathogen detection, water quality monitoring, and gas sensing.

Theoretical and experimental advancements have significantly enhanced the performance of SPR-based sensors. Innovations include the integration of advanced materials such as graphene, zinc oxide (ZnO), and MoS_2, which amplify detection sensitivity and precision. Hybrid nanostructures have demonstrated remarkable potential for detecting diverse biomolecules, bacteria, and environmental pollutants with unparalleled accuracy. Fiber-optic SPR configurations and Tamm plasmonic structures have further expanded the scope of SPR technology, offering compact, non-invasive, and reusable solutions for real-world applications.

This thesis explores the theoretical foundations, numerical modeling, and experimental implementations of SPR-based sensors. The objective is to optimize sensor design by leveraging advanced materials and innovative configurations to address challenges in sensitivity, precision, and versatility. The research spans a rigorous investigation of Maxwell's equations and electromagnetic theory underlying SPR to the development and simulation of biodetection systems. By advancing the field of SPR-based sensing, this work contributes to addressing critical needs in healthcare, environmental monitoring, and industrial process control.

Thesis Organization

This thesis is structured into four chapters:

Chapter 1: This chapter introduces the foundational concepts of surface plasmons, Maxwell's equations, and constitutive relations. Coupling modes are established, and the behavior of plasmons on metallic surfaces is analyzed. A distinction is drawn between localized and delocalized plasmons, followed by a brief historical overview. The chapter concludes with a detailed exposition of the electromagnetic theory governing surface plasmons.

Chapter 2: This chapter focuses on surface plasmon spectroscopy, elucidating the development of surface plasmon resonance (SPR)-based sensors and the criteria for evaluating sensor performance: sensitivity, figure of merit (FOM), detection accuracy, limit of detection (LOD), and signal-to-noise ratio (SNR). Emphasis is placed on the diverse applications of surface plasmons across interdisciplinary domains, ranging from medical diagnostics to environmental monitoring, highlighting their relevance to both researchers and end-users.

Chapter 3: This chapter delves into numerical methods, with a primary focus on the **Transfer Matrix Method (TMM)** employed in this work. The TMM framework is comprehensively detailed, followed by a description of the MATLAB programming environment utilized for simulations. The materials used in the study are systematically presented: glass substrates serving as prisms, noble metals for adhesion layers, and semiconductors and dielectric materials selected for their optoelectronic properties.

Chapter 4: This chapter presents the experimental work conducted during this research. It showcases **nine custom-designed SPR sensors** and their applications:

1. **Water Quality Monitoring Sensor (n=1.33):** Optimized by investigating the effect of $PtSe_2$ layer thickness on sensor response.
2. **Ethanol Concentration Sensor:** Analyzes the influence of silicon dioxide (SiO_2) layer thickness and black phosphorus (BP) layer count.
3. **Cancer Cell Detection Biosensor:** Addresses a prominent application of SPR in oncology.
4. **Blood Glucose Level Sensor:** Features a simplified architecture for real-time monitoring.
5. **High-Sensitivity Pregnancy Test Sensor:** Leverages SPR for ultrasensitive hormone detection.
6. **Dual-Analyte Sensor:** Demonstrates multifunctionality by detecting hemoglobin levels in blood and glucose in urine through analyte substitution.
7. **Pesticide Detection Sensor (Deltamethrin):** Targets agro-industrial applications for contaminant monitoring.
8. **HIV Infection Diagnostic Sensor:** Highlights SPR's potential in rapid pathogen detection.
9. **Blood Cancer Sensor:** Especially leukemia detection.

And a **general conclusion**.

Chapter I

Surface Plasmons

Introduction

This chapter introduces the fundamental theoretical concepts underlying plasmonics and surface plasmon resonance (SPR). It begins with Maxwell's equations and the behavior of electromagnetic waves at material interfaces, then explains the formation, propagation, and characteristics of surface plasmons. The mechanisms of SPR excitation, including grating and prism coupling (Otto and Kretschmann configurations), are examined. Historical developments and the distinction between surface plasmons, polaritons, and Tamm plasmons are also presented to establish a strong theoretical foundation for the remainder of this work.

I. Surface Plasmons

The term **"plasmon"** is a contraction of *plasma* and *electron* [6], introduced by David Pines in 1956 :

"We describe the term 'plasmon' to designate the quantum of elementary excitation associated with high-frequency collective motion" [7].

Plasmons are defined as quantized plasma oscillations on metallic surfaces, representing electromagnetic waves of electron density that perturb free electrons at the interface between a metal and a dielectric or vacuum. Plasmons can interact with light to form **polaritons**, which exhibit strong light-matter coupling and enable promising applications in optics and nanotechnology [8]. Plasmonic phenomena have been extensively studied since the mid-20th century, employing techniques such as electron energy loss spectroscopy (EELS) and optical methods like attenuated total reflection (ATR) [9].

These waves, being highly sensitive to the refractive index adjacent to the metal surface or surface roughness, have found diverse applications in medicine [10], chemistry, and biology [11].

The study of light-nanostructure interactions is termed **plasmonics**. This field focuses on generating, detecting, and manipulating optical-frequency signals along metal-dielectric interfaces. **Surface plasmons (SPs)** [12]; quantized plasma oscillations localized at the interface between two media (a metal and a dielectric), represent unique solutions to Maxwell's equations. These waves propagate parallel to the interface [13], with their electromagnetic field amplitude decaying exponentially perpendicular to the interface. Surface plasmons are widely exploited in biophysics through **surface plasmon resonance (SPR)** [14], a charge density

oscillation phenomenon occurring at the interface of materials with contrasting dielectric constants.

Surface plasmon resonance (SPR) has emerged as a critical tool in biophysics and related disciplines. It enables the analysis and manipulation of biological entities by leveraging the sensitivity of SPs to changes in the optical parameters of the surrounding medium. This principle has driven the development of **SPR-based sensors** (Figure I.1), which exploit the resonance condition to detect minute variations in refractive index, binding events, or molecular interactions in real time.

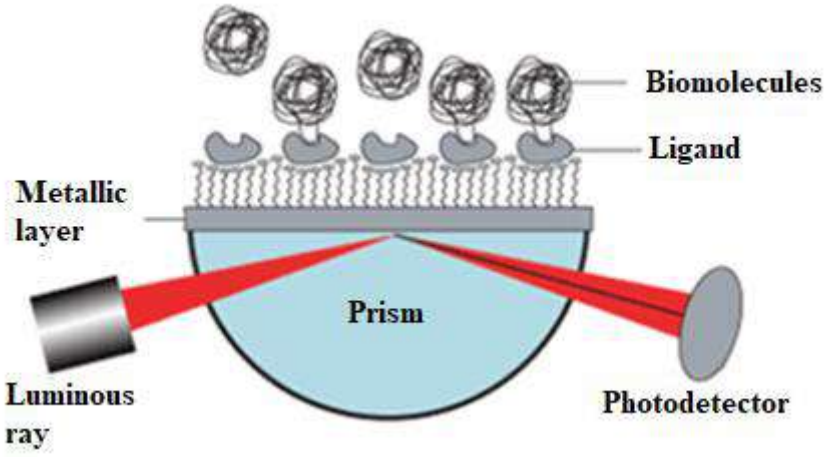

Figure I.1 Representation of a surface plasmon detector [12].

I.1. Principle of Surface Plasmon Resonance

The fundamental principle of SPR relies on the interaction between light and free electrons within a metallic film—typically gold or silver—generating surface plasmons, i.e., coherent electron oscillations at the metal-dielectric interface.

I.1.1 Basic Mechanism

1. Total Internal Reflection: Surface plasmon resonance occurs when in-plane polarized light is directed toward a thin metallic film under total internal reflection conditions. This configuration generates an evanescent field that penetrates a short distance into the dielectric medium adjacent to the metallic surface [15].
2. Evanescent Field Formation: When light interacts with the boundary between two materials (e.g., glass and air) at a critical angle, it undergoes total reflection, producing an evanescent field that decays exponentially with distance from the interface.

3. Surface Plasmon Generation: If the incident light is p-polarized and matches specific resonance conditions (wavelength and angle of incidence), it couples with the free electrons in the metal, exciting surface plasmon polaritons (SPPs)—electromagnetic waves that propagate along the metal-dielectric interface [16].
4. Detection of Refractive Index Changes: The resonance condition is highly sensitive to refractive index variations near the metallic surface, such as those induced by biomolecular binding events. When target molecules bind to the sensor surface, they alter the local refractive index, resulting in a measurable shift in the minimum reflectance angle, termed the SPR angle [17].

I.2. Components and Operation of the SPR Sensor

Surface plasmon resonance (SPR) sensors comprise several key components that collectively detect molecular interactions via refractive index changes at a metal-dielectric interface. These components include:

1. **Light Source:** Typically a laser emitting visible-range light (600–800 nm) to excite surface plasmons.
2. **Prism:** A coupling prism, often made of BK7 glass, directs light toward the metallic film at a specific angle to achieve total internal reflection.
3. **Metallic Film:** A thin layer of noble metal (commonly gold or silver) deposited on the prism surface to support surface plasmons.
4. **Dielectric Layer:** A functionalized dielectric layer immobilized on the metallic surface to facilitate analyte binding.
5. **Detector:** A photodetector monitors reflected light intensity or angular shifts, correlating to refractive index changes at the sensor surface.

SPR sensors operate using an optical configuration combining these components to enable real-time molecular interaction monitoring. Refractive index variations caused by binding events are detected as resonance angle or intensity shifts, enabling detailed analysis of biomolecular interactions. The operation of SPR sensors involves four key steps:

1. **Total Internal Reflection:** Light is directed onto the prism at an angle exceeding the critical angle, inducing total internal reflection. An evanescent field is generated, penetrating the dielectric layer adjacent to the metallic film [18].
2. **Surface Plasmon Excitation:** When specific resonance conditions (angle and wavelength) are met, light couples with free electrons in the metallic film, exciting surface plasmons that propagate along the interface [19].

3. **Refractive Index Changes:** Binding events between immobilized ligands and analytes alter the local refractive index at the sensor surface. This shifts the minimum reflectance angle, observable as a resonance angle deviation [20].
4. **Data Acquisition:** Reflected light intensity or angle is continuously measured as analytes flow over the sensor surface, generating a sensorgram that quantifies binding kinetics and affinities over time.

I.3. Factors Influencing the SPR Response

The response of surface plasmon resonance (SPR) is influenced by several key factors that impact measurement accuracy and sensitivity. Analyte concentration plays a critical role; higher concentrations typically induce stronger binding responses, measured as shifts in the SPR signal. Binding kinetics also significantly affect the SPR response, determining the rate of equilibrium attainment and the binding strength between analytes and immobilized ligands, thereby shaping the sensorgram's profile and amplitude. Surface ligand density is another crucial factor: optimal coverage ensures sufficient binding sites while minimizing steric hindrance that could limit analyte accessibility.

Additional factors include refractive index variations from both the analyte solution and surrounding medium, which directly influence sensitivity and precision [21]. Temperature fluctuations can alter refractive indices and molecular interactions, necessitating strict environmental control during experiments. Finally, the choice of metallic substrate (typically gold or silver) in SPR sensors impacts sensitivity and resonance conditions. By meticulously controlling these parameters, researchers can enhance SPR sensor performance, enabling more precise biomolecular interaction studies [22].

I.4. The Maxwell Equations

Named after the physicist James Clerk Maxwell who first formulated them in 1861. Maxwell's equations, also known as the Maxwell-Lorentz equations, are a set of partial differential equations, they form the basis of classical electromagnetism and optics and the electric and magnetic fields.

The interaction between electromagnetic waves and matter can be described by Maxwell's simplified equations [23]:

$$\begin{cases} \vec{\nabla} \wedge \vec{E}(\vec{r},t) = -\dfrac{\partial \vec{B}(\vec{r},t)}{\partial t} \\ \vec{\nabla} \wedge \vec{H}(\vec{r},t) = \vec{J} - \dfrac{\partial \vec{D}}{\partial t} \\ \vec{\nabla}.\vec{D}(\vec{r},t) = \rho \\ \vec{\nabla}.\vec{B}(\vec{r},t) = 0 \end{cases} \quad (I.1)$$

Where :

$\vec{E}$: the electric field.

$\vec{H}$: the magnetic field.

$\vec{J}$: the density of electric current.

$\vec{D}$: the electric displacement.

In a vacuum, we note the presence of the electric field $\vec{E}$ and the magnetic induction $\vec{B}$. On the other hand, in matter, we have three other vectors:

$$\begin{cases} \vec{D} = \varepsilon_0 \varepsilon \vec{E} = \varepsilon_0 \vec{E} + \vec{P} \\ \vec{B} = \mu_0 \mu \vec{H} \\ \vec{J} = \sigma \vec{E} \end{cases} \quad (I.2)$$

These relationships are called constitutive.

I.5. The Evanescent Wave

The evanescent wave is an electromagnetic wave that presents components of the electromagnetic field with the same real part at the same time at any point, at least in one direction. It is generated in the process of total reflection at the interface between two different media, the amplitude of the evanescent wave decreases rapidly until it becomes negligible at a few wavelengths, this decrease is not due to absorption [24].

Evanescent waves are part of a very general type of solutions of Maxwell's equations called near field [25].

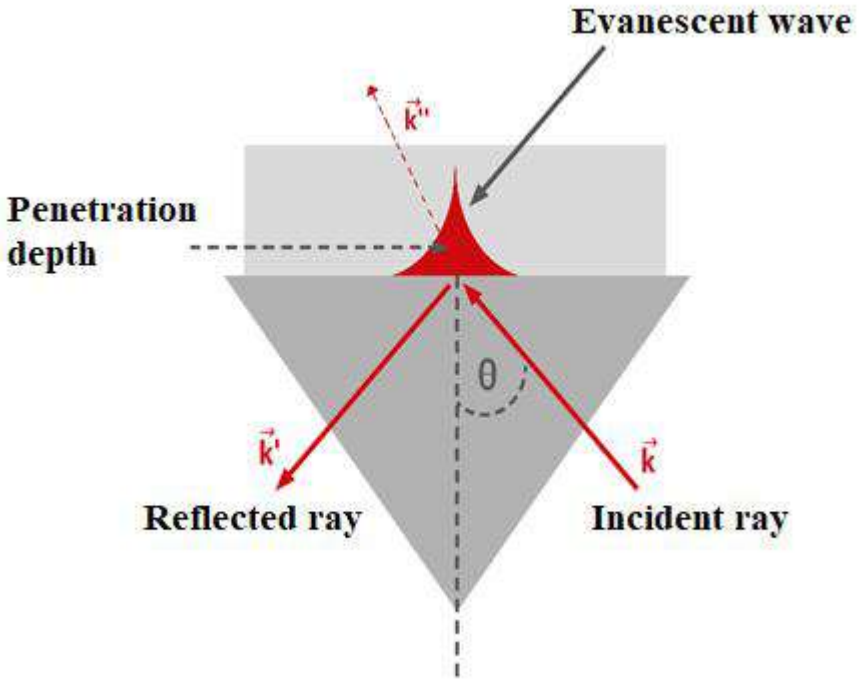

Figure I.2 Representation of an evanescent wave [25].

$$\begin{cases} k_x = k\cos\theta = n\frac{\omega}{c}\cos\theta \\ k'_x = -k\cos\theta' = -n_1\frac{\omega}{c}\cos\theta' \\ k''_x = n_2\frac{\omega}{c}\cos\beta = n_2\frac{\omega}{c}\sqrt{1-\sin^2\beta} = n_1\frac{\omega}{c}\sqrt{\left(\frac{n_2}{n_1}\right)^2 - \sin^2\theta} \end{cases} \quad (I.3)$$

Because : $n_1 \sin\theta = n_2 \sin\beta$ (Snell-Descartes law).

With :

θ : incident angle.

θ': reflected angle.

β : refracted angle.

n_1 and n_2 : refractive indices of the two mediums.

For angles greater than the limiting angle of incidence called the “critical angle” there is total reflection; $\theta > \arcsin(\frac{n_2}{n_1})$ that is, when $\sin\theta > \frac{n_2}{n_1}$ no waves are transmitted.

Evanescent waves do not propagate in a medium, but are stationary and attenuated. Despite this, they can very well influence the interaction between interfaces and waves [26].

I.6. History

In 1704, Isaac Newton demonstrated the existence of evanescent waves by observing the phenomenon of attenuated total reflection at the face of a prism when directing a light beam through a converging lens. Through this experiment, he also discovered the evanescent electromagnetic field.

In 1957, R. H. Ritchie introduced the term “surface plasmon” for the first time, theoretically proving the existence of transverse plasmons on metal surfaces [27]. In 1958, E. A. Stern and R. A. Ferrell provided a theoretical framework for the coupling of electromagnetic radiation with surface plasmons at a metal-dielectric interface, showing that such waves generate an electromagnetic field coupled to surface plasmons [28].

T. Turbadar first experimentally observed surface plasmons in 1959, while their excitation at a metallic interface was practically demonstrated by Powell and Swan in 1960 [29]. Turbadar’s findings were later explained by A. Otto in 1968, who attributed the observed reflectivity dip to surface plasmon excitation. Otto proposed the frustrated total reflection (FTR) configuration, which couples electromagnetic waves with surface plasmons to highlight their properties [30].

In 1971, E. Kretschmann refined Otto’s geometry by introducing the attenuated total reflection (ATR) configuration [30], which remains the most widely used setup to date.

Homer Neff developed the first SPR-based biosensor in 1972, utilizing the Kretschmann configuration with a prism-coupled evanescent field to excite surface plasmons [31].

Subsequent years saw a surge in SPR-related research, though interest waned in the 1990s as focus shifted toward more practical applications, such as surface-enhanced Raman spectroscopy (SERS) [32].

Today, advances in coupling techniques have expanded the current understanding of surface plasmons, reigniting research interest due to their interdisciplinary applications in medicine, biology, biophysics, optics, and environmental science.

I.7. Polariton and Surface Plasmon

A coupling between an electromagnetic field and the local polarization induced in a material subjected to it may occur. This excitation is referred to as a polariton [33]. When the polarizable system (i.e., the material) is a metal or exhibits metallic characteristics, the coupling

occurs with collective, quantized oscillations of electrons. This phenomenon is termed a plasmon-polariton, or more simply, a **plasmon**. Plasma oscillations occur at the metal–dielectric interface, where they are known as surface plasmons.

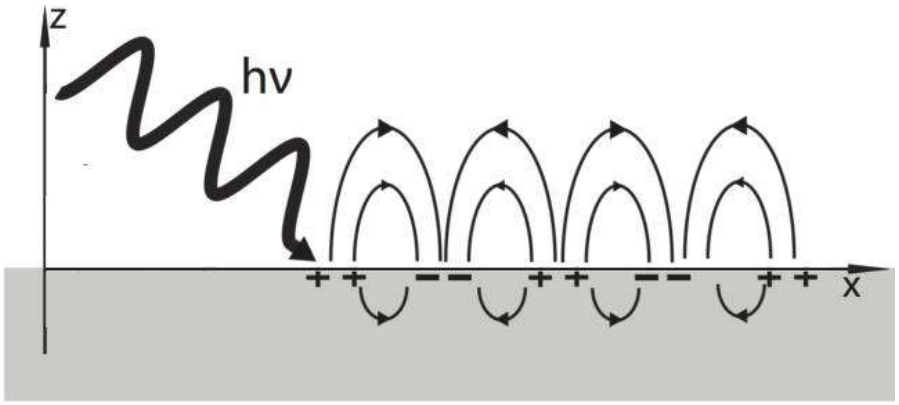

Figure I.3 Representation of the propagation of free electron plasma oscillations on the metal surface [28].

Two types of surface plasmons can be distinguished:

- **Localized Surface Plasmons (LSP).**
- **Propagative (Delocalized) Surface Plasmons (PSP).**

These surface plasmons are excitations whose electromagnetic field decays exponentially in the media on either side of the interface, yet they can propagate along the entire surface. Discovered by Ritchie in 1957, they are mainly differentiated by their propagation lengths.

I.7.1 Localized Surface Plasmons (LSP):

Localized surface plasmons are confined to a nanometric scale, as their name suggests. They are generated in the vicinity of nanometric particles that make up the rough metallic surface. These localized plasmons are considered “radiative” since they can spontaneously couple with an electromagnetic wave. The confinement of these plasmons is a key property that leads to the enhancement of the electromagnetic field near the metal particles, forming so-called “hot spots.” This phenomenon underpins the electromagnetic theory of Surface-Enhanced Raman Spectroscopy (SERS) [34].

I.7.2 Propagative (Delocalized) Surface Plasmons (PSP):

In contrast, propagative surface plasmons appear on the surface of thin metallic films and can propagate over micrometer-scale distances. Generated at the interface of smooth metallic layers, these plasmons are non-radiative and, therefore, cannot directly couple with light. As a result, the use of a “coupler” becomes necessary, as will be discussed subsequently.

I.8. Electromagnetic Theory of Surface Plasmons

We consider the case of a linear, isotropic, inhomogenic and non -magnetic environment.

In the absence of external currents and charges, Maxwell's equations are written as follows:

$$\begin{cases} \vec{\nabla} \wedge \vec{\mathrm{E}}(\vec{\mathrm{r}},t) = -\dfrac{\partial \vec{\mathrm{B}}(\vec{\mathrm{r}},t)}{\partial t} \\ \vec{\nabla} \,.\, \vec{\mathrm{B}}(\vec{\mathrm{r}},t) = 0 \\ \vec{\nabla} \wedge \vec{\mathrm{H}}(\vec{\mathrm{r}},t) = \dfrac{\partial \vec{\mathrm{D}}(\vec{\mathrm{r}},t)}{\partial t} \\ \vec{\nabla} \,.\, \vec{\mathrm{D}}(\vec{\mathrm{r}},t) = 0 \end{cases} \qquad (I.4)$$

The environment is non -magnetic, therefore $\mu = \mu_0$ is the permeability of the vacuum.

Relative permittitivity of the environment ε depends on the direction $\vec{\mathrm{r}}$ Because the latter is inhomogenic, as:

$\vec{\mathrm{D}}(\vec{\mathrm{r}},t) = \varepsilon_0 \varepsilon(\vec{\mathrm{r}})\vec{E}(\vec{\mathrm{r}},t)$, ε_0 represents the permittitude of the void.

Maxwell's equations then become:

$$\begin{cases} \vec{\nabla} \wedge \vec{\mathrm{E}}(\vec{\mathrm{r}},t) = -\mu_0 \dfrac{\partial \vec{\mathrm{H}}(\vec{\mathrm{r}},t)}{\partial t} \\ \vec{\nabla} \,.\, \vec{\mathrm{B}}(\vec{\mathrm{r}},t) = 0 \\ \vec{\nabla} \wedge \vec{\mathrm{H}}(\vec{\mathrm{r}},t) = \varepsilon_0 \varepsilon(\vec{\mathrm{r}}) \dfrac{\partial \vec{\mathrm{E}}(\vec{\mathrm{r}},t)}{\partial t} \\ \vec{\nabla} \,.\, \vec{\mathrm{D}}(\vec{\mathrm{r}},t) = 0 \end{cases} \qquad (I.5)$$

From these equations, it is demonstrated that the electric and magnetic fields obey the following equations:

$$\begin{cases} \left(\Delta_t - \beta^2 + \omega^2 \varepsilon_0 \mu_0 \varepsilon(r)\right)\vec{e}(x,y) = -(\nabla_t + i\beta\vec{z}_0)\vec{e}_t(x,y).\nabla_t \ln\left(\varepsilon_0 \varepsilon(r)\right) \\ \left(\Delta_t - \beta^2 + \omega^2 \varepsilon_0 \mu_0 \varepsilon(r)\right)\vec{h}(x,y) = -(\nabla_t \ln\left(\varepsilon_0 \varepsilon(r)\right) \wedge \left[\left(i\beta\vec{z}_0 + \vec{\nabla}_t\right) \wedge h\right] \end{cases} \qquad (I.6)$$

With β : the constant of propagation ($\beta = k_z$).

I.8.1 Particular Case of Three Environments

We consider the case of three homogeneous environments with flat interfaces.

The vectors of the electromagnetic field depend only on X (axis perpendicular to the flat interfaces) and Z (axis parallel to the interfaces).

$$\begin{cases} \vec{E}(\vec{e},t) = \vec{e}(x)\exp\big(i(\beta z - t)\big) \\ \vec{H}(\vec{r},t) = \vec{h}(x)\exp\big(i(\beta z - \omega t)\big) \end{cases} \quad (I.7)$$

We are more interested in the TM polarization ('transverse magnetic'). The propagation constant of this multilayer system can be determined using the equation:

$$\tan 2\kappa_2 d = \frac{\gamma_1\varepsilon_2/\kappa_2\varepsilon_1 + \gamma_3\varepsilon_2/\kappa_2\varepsilon_3}{1 - (\gamma_1\varepsilon_2/\kappa_2\varepsilon_1)(\gamma_3\varepsilon_2/\kappa_2\varepsilon_3)} \quad (I.8)$$

With $\kappa_i^2 = \omega^2\varepsilon_i\varepsilon_0\mu_0 - \beta^2$

and $\gamma_i = i\kappa_i$, $i = 1,3$

It is an equation that can only be resolved digitally. We define n_{eff} the effective index, another parameter that can be deduced from the propagation constant:

$$n_{eff} = \frac{c}{\omega} Re\,(\beta) \quad (I.9)$$

I.8.2 Particular Case of One Environment

If the intermediate layer did not exist, there remains only the first layer (the metal) and the third (the dielectric), therefore:

$$\gamma_1/\varepsilon_1 + \gamma_3/\varepsilon_3 = 0 \quad (I.10)$$

Therefore:

$$\kappa_1/\varepsilon_1 = -\kappa_3/\varepsilon_3 \quad (I.11)$$

$$\frac{\sqrt{\omega^2\varepsilon_1\varepsilon_0\mu_0 - \beta^2}}{\varepsilon_1} = -\frac{\sqrt{\omega^2\varepsilon_3\varepsilon_0\mu_0 - \beta^2}}{\varepsilon_3} \quad (I.12)$$

$$\frac{\omega^2/c^2 - \beta^2}{\varepsilon_1} = \frac{\omega^2/c^2 - \beta^2}{\varepsilon_3} \quad (I.13)$$

So :

$$\beta = \frac{\omega}{c}\sqrt{\frac{\varepsilon_1\varepsilon_3}{\varepsilon_1 + \varepsilon_3}} \quad (I.14)$$

In the case of a metal whose real part is much higher than its imaginary part, in other words ; $|\varepsilon_1'| \gg \varepsilon_1''$, with $\varepsilon_1 = \varepsilon_1' + i\varepsilon_1''$:

$$\beta = k_0 \sqrt{\frac{(\varepsilon_1' + i\varepsilon_1'')\varepsilon_3}{(\varepsilon_1' + \varepsilon_3)i\varepsilon_1''}}\ , k_0 = \frac{\omega}{c} \qquad (I.15)$$

$$\beta = k_0 \sqrt{\frac{\varepsilon_3\left(\varepsilon_3\varepsilon_1' + \varepsilon_1'^{\,2} + \varepsilon_1''^{\,2}\right) + i\varepsilon_1''\varepsilon_3^2}{(\varepsilon_1' + \varepsilon_3)^2 + \varepsilon_1''^{\,2}}} \qquad (I.16)$$

$$\beta = k_0 \sqrt{\frac{\varepsilon_3\varepsilon_1'(\varepsilon_1' + \varepsilon_3) + i\varepsilon_1''\varepsilon_3^2}{(\varepsilon_1' + \varepsilon_3)^2}} \qquad (I.17)$$

The resolution of this equation is very simple:

$$\begin{cases} \beta' = k_0 \sqrt{\dfrac{\varepsilon_1{}'\varepsilon_3}{\varepsilon_1' + \varepsilon_3}} \\ \beta'' = \dfrac{k_0}{2}\dfrac{\varepsilon_1''}{\varepsilon_1'^2}\left(\dfrac{\varepsilon_1{}'\varepsilon_3}{\varepsilon_1' + \varepsilon_3}\right)^{\frac{3}{2}} \end{cases} \qquad (I.18)$$

The propagation constant is then written:

$$\beta\ = k_0 \sqrt{\frac{\varepsilon_1{}'\varepsilon_3}{\varepsilon_1' + \varepsilon_3}} + i\frac{k_0}{2}\frac{\varepsilon_1''}{\varepsilon_1'^2}\left(\frac{\varepsilon_1{}'\varepsilon_3}{\varepsilon_1' + \varepsilon_3}\right)^{\frac{3}{2}} \qquad (I.19)$$

I.9. Surface Plasmons Dispersion Relationship

The dispersion relation of surface plasmons is an expression that describes the dependence between the wavevector and the frequency of surface plasmons. This relation illustrates how these waves involve both the propagation of an electromagnetic wave (polariton) and the movement of charge in the metal (surface plasmon).

Consider a planar interface composed of two semi-infinite media—a metal and a dielectric. Both media are assumed to be isotropic, non-magnetic, and homogeneous, each characterized by a dielectric constant (ε_1 for the metal and ε_2 for the dielectric). An electromagnetic wave propagating along this interface can be described by Maxwell's equations, with the external charge and current density assumed to be zero:

$$\nabla^2 E - \frac{\epsilon}{c^2}\frac{\partial^2 E}{\partial t^2} = 0 \qquad (I.20)$$

By posing$E(r,t) = E(r)e^{-i\omega t}$, equation (I.30) becomes:

$$\nabla^2 E - k_0^2 \epsilon E = 0 \qquad (I.21)$$

Where $k_0 = \omega/c$.

The waves are considered to propagate towards the positive Xs with the plane z = 0 and deteriorate in the direction parallel to the axis (Oz) in the two environments, the equation of propagation of electromagnetic waves becomes.

$$E(x,y,z) = E(z)e^{i\beta x} \qquad H(x,y,z) = H(y)e^{i\beta x} \qquad (I.22)$$

Where β represents the constant of propagation of the wave that is parallel to the axis *(ox)*. By replacing in equation *(I. 22)* we obtain:

$$\frac{\partial^2 E(z)}{\partial z^2} + (k_0^2\epsilon - \beta^2)E = 0 \qquad \frac{\partial^2 H(y)}{\partial y^2} + (k_0^2\epsilon - \beta^2)H = 0 \qquad (I.23)$$

The resolution of the Maxwell equations (Maxwell-Faraday and Ampère law) gives:

$$\frac{\partial E_z}{\partial y} - \frac{\partial E_y}{\partial z} = i\omega\mu_0 H_x \qquad (I.24a)$$

$$\frac{\partial E_x}{\partial z} - \frac{\partial E_z}{\partial x} = i\omega\mu_0 H_y \qquad (I.24b)$$

$$\frac{\partial E_y}{\partial x} - \frac{\partial E_x}{\partial y} = i\omega\mu_0 H_z \qquad (I.24c)$$

$$\frac{\partial H_z}{\partial y} - \frac{\partial H_y}{\partial z} = -i\omega\mu_0 E_x \qquad (I.24d)$$

$$\frac{\partial H_x}{\partial z} - \frac{\partial H_z}{\partial x} = -i\omega\mu_0 E_y \qquad (I.24e)$$

$$\frac{\partial H_y}{\partial x} - \frac{\partial H_x}{\partial y} = -i\omega\mu_0 E_z \qquad (I.24f)$$

But the propagation is in the direction of the axis (OX) so the equations (I.24a-f) can be simplified [35] in:

$$\frac{\partial E_y}{\partial z} = -i\omega\mu_0 H_x \qquad (I.25a)$$

$$\frac{\partial E_x}{\partial z} - i\beta E_z = i\omega\mu_0 H_y \qquad (I.25b)$$

$$i\beta E_y = i\omega\mu_0 H_z \qquad (I.25c)$$

$$\frac{\partial H_y}{\partial z} = i\omega\mu_0 E_x \qquad (I.25d)$$

$$\frac{\partial H_x}{\partial z} - i\beta H_z = -i\omega\mu_0 E_y \qquad (I.25e)$$

$$i\beta H_y = -i\omega\mu_0 E_z \qquad (I.25f)$$

This equation set takes two solutions, which corresponds to two types of polarizations of the electro -stroke: polarization P (transverse magnetic "TM") and polarization s (transverse electric "TE") for $E_x, E_z, H_y \neq 0$ and $E_y, H_x, H_z \neq 0$ respectively.

The solutions of the equations (I.25a-f) for the polarization P (TM) give two cases:

1st case: for positive *z*:

$$H_y(z) = A_2 e^{i\beta x} e^{-k_{2,z}z} \qquad (I.26a)$$

$$E_x(z) = i\frac{A_2 k_2}{\omega\epsilon_0\epsilon_2} e^{i\beta x} e^{-k_{2,z}z} \qquad (I.26b)$$

$$E_z(z) = -\frac{A_2\beta}{\omega\epsilon_0\epsilon_2} e^{i\beta x} e^{-k_{2,z}z} \qquad (I.26c)$$

2nd case: for negative *z*:

$$H_y(z) = A_1 e^{i\beta x} e^{k_{1,z}z} \qquad (I.27a)$$

$$E_x(z) = -i\frac{A_1 k_1}{\omega\epsilon_0\epsilon_1} e^{i\beta x} e^{k_{1,z}z} \qquad (I.27b)$$

$$E_z(z) = -\frac{A_1\beta}{\omega\epsilon_0\epsilon_1} e^{i\beta x} e^{k_{1,z}z} \qquad (I.27c)$$

Where A_i, k_i are the amplitude coefficient and the normal component of the wave vector of each medium respectively. Since the components of the electric and magnetic fields must be continuous throughout the interface, we obtain:

$$A_1 = A_2 \quad \text{and} \quad \frac{k_{2,z}}{k_{1,z}} = -\frac{\epsilon_2}{\epsilon_1} \qquad (I.28)$$

Likewise concerning the polarization TE, and for positive z:

$$E_y(z) = A_2 e^{i\beta x} e^{-k_{2,z}z} \qquad (I.29a)$$

$$H_x(z) = -i\frac{A_2 k_2}{\omega\mu_0} e^{i\beta x} e^{-k_{2,z}z} \qquad (I.29b)$$

$$H_z(z) = \frac{A_2\beta}{\omega\mu_0} e^{i\beta x} e^{-k_{2,z}z} \qquad (I.29c)$$

For negative z:

$$E_y(z) = A_1 e^{i\beta x} e^{k_{1,z} z} \qquad (I.30a)$$

$$H_x(z) = i\frac{A_1 k_1}{\omega \mu_0} e^{i\beta x} e^{k_{1,z} z} \qquad (I.30b)$$

$$H_z(z) = \frac{A_1 \beta}{\omega \mu_0} e^{i\beta x} e^{k_{1,z} z} \qquad (I.30c)$$

Still, taking into account the continuity of the two tangential components, we deduce that:

$$k_{1,z} + k_{2,z} = 0 \qquad (I.31)$$

Nevertheless, the coupling occurs only when the real parts of k_1 and k_2 are positive [35], which is not the case according to (I.31). We can therefore conclude that polaritons do not exist for TE polarization. Consequently, the excitation of polaritons is only possible through P polarization.

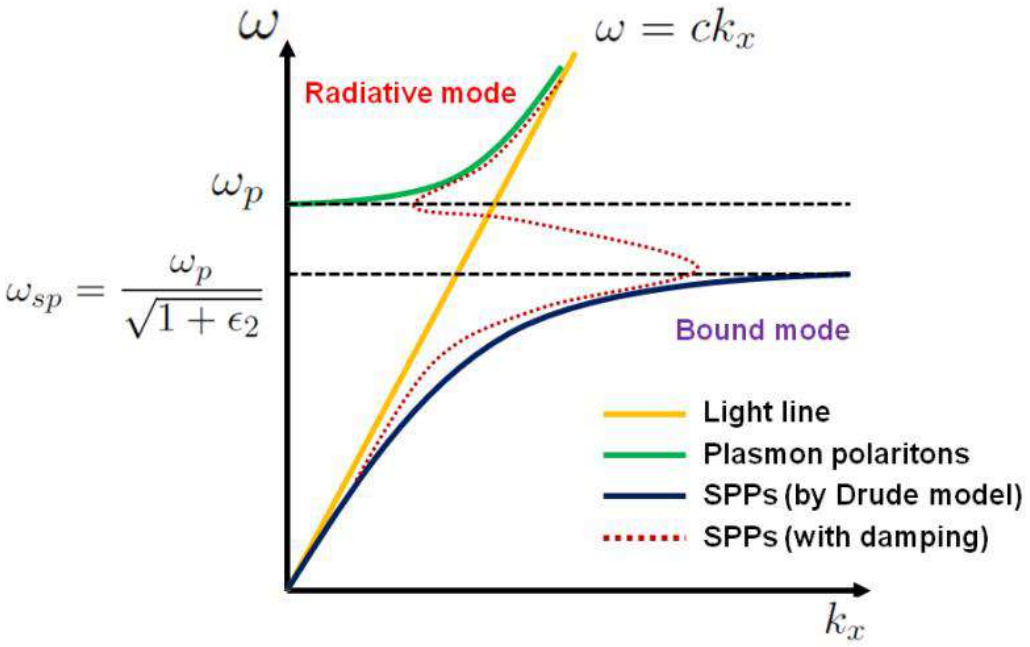

Figure I.4 The dispersion relation of surface plasmon polaritons (SPP) represented relatively to both the undamped Drude model and a real metal exhibiting damping [36].

Figure I.4 shows the dispersion relation of polaritons; the yellow line represents $\omega = ck_x$ and the blue line corresponds to the dispersion curve of surface plasmon polaritons:

$$\epsilon_r(\omega) = 1 - \frac{\omega_p^2}{\omega^2} \qquad (I.32)$$

For low frequencies, the dispersion curve approaches the light line (yellow), and the polaritons exhibit an almost photonic behavior. As the frequency increases, the curve diverges further from the light line until it reaches a frequency (ω_{sp}) known as the "surface plasmon resonant frequency." In the absence of damping, as the frequency increases, the wavevector tends toward infinity, and the mode displays an electrostatic behavior, effectively transforming into surface plasmons (SP).

Conversely, for a real metal, when damping is taken into account in the propagation of polaritons, a bending in the dispersion curve is observed (red lines). In this case, the wavevector reaches a defined value at ω_{sp}, leading to confinement in the wavelength, as described by the wavevector component [37]:

$$k_{z,i} = \sqrt{\epsilon_i \left(\frac{\omega}{c}\right)^2 - k^2} \qquad (I.33)$$

Where ϵ_i represents the relative permittivity of metal and dielectric i = 1.2 respectively.

I.10. propagation Length of Surface Plasmons

Surface plasmons propagate along a metallic surface, gradually attenuating as they lose energy. This lost energy is absorbed by the metal and dissipated as heat. The propagation length is defined as the distance over which the intensity decays to $\frac{1}{e}$ of its initial value.

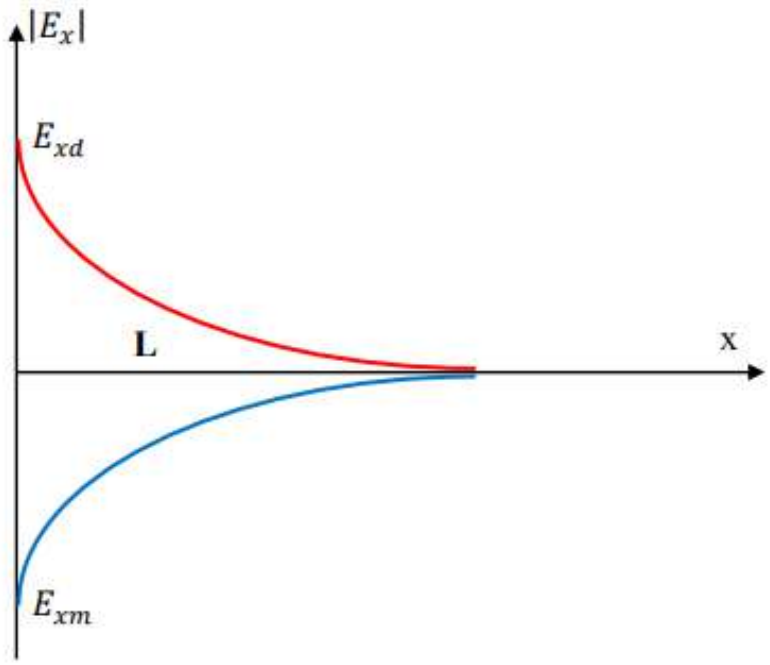

Figure I.5 Representation of the propagation length of surface plasmon [36].

The propagation length L is the distance over which the intensity decreases by a factor of $\frac{1}{e}$:

$$L = \frac{1}{2\beta''}, \beta = \beta' + i\beta'' \qquad (I.34)$$

Using the second formula of the equation (*I*.28):

$$L = \frac{c}{\omega}\frac{\varepsilon_1''}{\varepsilon_1'^2}\left(\frac{\varepsilon_1'\varepsilon_3}{\varepsilon_1' + \varepsilon_3}\right)^{\frac{3}{2}} \qquad (I.35)$$

This decrease is expressed by the attenuation b :

$$b = \beta''\frac{0.2}{\ln 10} \qquad (I.36)$$

Since the energy is lost in the form of heat, it is possible to control the propagation of surface plasmons by modulating the metal's temperature—a challenge that remains in plasmonics. Numerous strategies have been proposed to overcome this issue [36].

I.11. Penetration Depth

The electromagnetic field is maximal at the metal–dielectric interface, after which it decays in both media. This decay, occurring perpendicularly to the interface, is characterized by the distance from the interface to the position (x) where the electromagnetic field diminishes by a factor of $\frac{1}{e}$; this distance is called the penetration depth L_p.

In the metal:

$$x = -\frac{1}{\gamma_1'} \qquad (I.37)$$

In the dielectric:

$$x = \frac{1}{\gamma_3'} \tag{I.38}$$

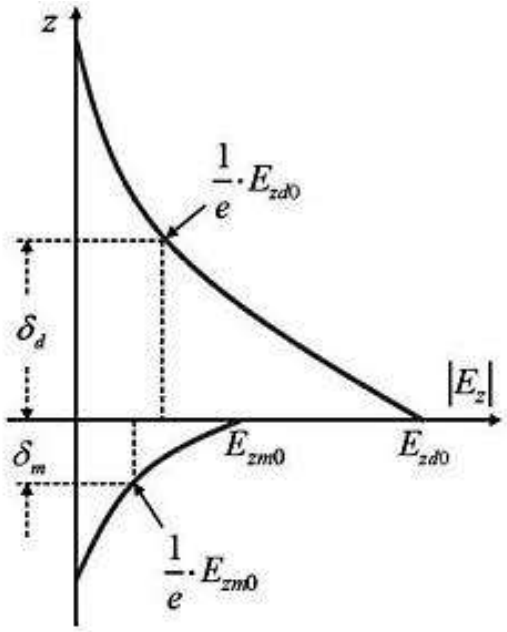

Figure I.6 Penetration depth in a metal and a dielectric [25].

I.12. Surface Plasmon Resonance

When the energy of the incident wave is efficiently transferred to surface plasmons, they exhibit an optical response known as Surface Plasmon Resonance (SPR).

In the case of a metal–dielectric interface, since the real part of the metal's dielectric permittivity is always negative $\varepsilon' < 0$ and the dielectric's permittivity is always positive $\varepsilon_d > 0$:

$$\sqrt{\frac{\varepsilon'}{\varepsilon' + \varepsilon_d}} > 1 \tag{I.39}$$

Therefore

$$\sqrt{\frac{\varepsilon_d \varepsilon'}{\varepsilon' + \varepsilon_d}} > \sqrt{\varepsilon_d} \tag{I.40}$$

If θ is the incident angle of the light beam:

$$\sqrt{\frac{\varepsilon_d \varepsilon'}{\varepsilon' + \varepsilon_d}} > \sqrt{\varepsilon_d} \sin\theta \tag{I.41}$$

meaning:

$$k_0 \sqrt{\frac{\varepsilon_d \varepsilon'}{\varepsilon' + \varepsilon_d}} \neq \sqrt{\varepsilon_d} k_0 \sin\theta \qquad (I.42)$$

Direct excitation of surface plasmons in this case is impossible. However, it can be achieved using an evanescent wave, either through Attenuated Total Reflection (ATR) or via a diffraction grating. To satisfy the wavevector matching condition, an additional momentum term *C* must be introduced to establish equality.

$$k_0 \sqrt{\frac{\varepsilon_d \varepsilon'}{\varepsilon' + \varepsilon_d}} = \sqrt{\varepsilon_d} k_0 \sin\theta + C \qquad (I.43)$$

I.13. Surface Plasmon Excitation

Resonant excitation of surface plasmons is achieved by bombarding them with electrons or a light beam at a matching frequency [38]. This excitation occurs when a highly intense evanescent wave is generated at the interface, decaying exponentially in intensity perpendicular to the interface. This wave results from the optical coupling between the incident light and the surface plasmons.

Among the various coupling methods, the two most commonly used are:

- Diffraction grating coupling
- Prism coupling, based on the principle of Attenuated Total Reflection (ATR).

I.13. 1. Diffraction Grating Coupling

A one-dimensional periodic structure is considered (Figure I.7), where a monochromatic light beam with TM polarization passes through a dielectric medium to reach the metallic surface of the structure.

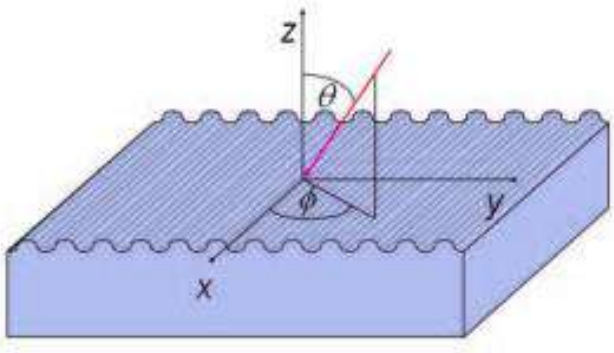

Figure I.7 A luminous incident wave with a polar angle θ and azimuthal angle ϕ [38].

To satisfy the resonance condition, an additional momentum beyond that of the incident photon is required. This additional momentum is provided by the wavevector of diffraction.:

$$\vec{K} = \frac{2\pi m}{d}\vec{j} \qquad (I.44)$$

$\vec{j}$ is the unit vector of the (yy') axis.

d is the period of the grating.

m is an integer, it represents the order of diffraction.

The key point of interest is the tangential component of the wave vector:

$$\overrightarrow{k_\iota} = n_d k_0(\sin\theta\cos\phi\,\vec{\imath} + \sin\theta\sin\phi\,\vec{j}) \qquad (I.45)$$

n_d is the refractive index of the dielectric.

The constant of propagation of surface plasmons equals:

$$\vec{k} = k_0\sqrt{\frac{\varepsilon_d\varepsilon'}{\varepsilon' + \varepsilon_0}}\overrightarrow{k_{sp}} \qquad (I.46)$$

$\overrightarrow{k_{sp}}$ is the unit vector in the direction of SPs.

The impulsion being conserved:

$$\vec{k} = \overrightarrow{k_\iota} + \vec{K} \qquad (I.47)$$

Then:

$$k_0\sqrt{\frac{\varepsilon_d\varepsilon'}{\varepsilon' + \varepsilon_0}}\overrightarrow{k_{sp}} = n_d k_0(\sin\theta\cos\phi\,\vec{\imath} + \sin\theta\sin\phi\,\vec{j}) + \frac{2\pi m}{d}\vec{j} \qquad (I.48)$$

Therefore:

$$\frac{\varepsilon_d \varepsilon'}{\varepsilon' + \varepsilon_0} = (n_d \sin\theta)^2 + \left(\frac{2mn_d\lambda}{d}\sin\theta\sin\phi\right) + \left(\frac{m\lambda}{d}\right)^2 \qquad (I.49)$$

The interesting cases to be studied are: $\phi = 0°, 45°, 90°$.

When $\phi = 0°$:

The incidence plan is parallel to the grooves of the grating, the equation (I.48) becomes:

$$\sin\theta = \sqrt{\frac{\varepsilon_d \varepsilon'}{\varepsilon' + \varepsilon_0} - \left(\frac{m\lambda}{n_d d}\right)^2} \qquad (I.50)$$

A resonance of surface plasmons (SP) is observed under TE polarization, rather than TM polarization (Figure I.6), occurring at a large resonance angle. This result aligns well with the theoretical prediction from equation (I.48). The resonance is deeper and narrower, which is advantageous for sensor performance.

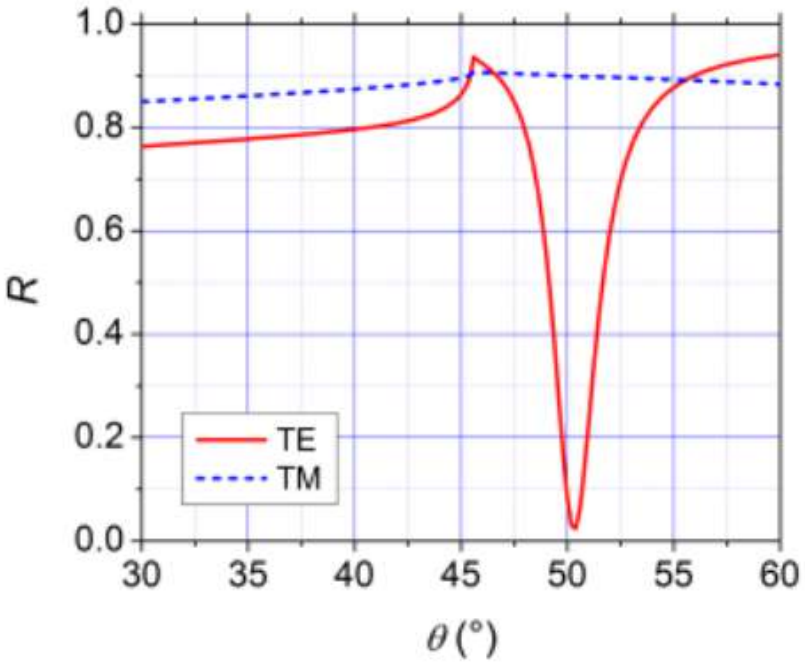

*Figure I.8 Reflectivity as a function of the angle of incidence for a gold grating at wavelength 700 nm for a period of 1*m and grooves with a depth of 70 nm [39].*

When $\phi = 45°$:

The incidence plane makes an angle of 45° with the grooves of the grating, after solving equation (I.48) we obtain the following solutions:

$$\sin\theta = -\frac{m\lambda}{\sqrt{2}n_d d} \pm \sqrt{\frac{\varepsilon_0\varepsilon'}{\varepsilon' + \varepsilon_0} - \frac{1}{2}\left(\frac{m\lambda}{n_d d}\right)^2} \qquad (I.51)$$

For a TM polarization, we observe a surprising result: at the resonance angle, part of the TM polarization is transformed into TE polarization by the diffraction grating (figure I.7), and vice versa for the TE polarization (figure I.8).

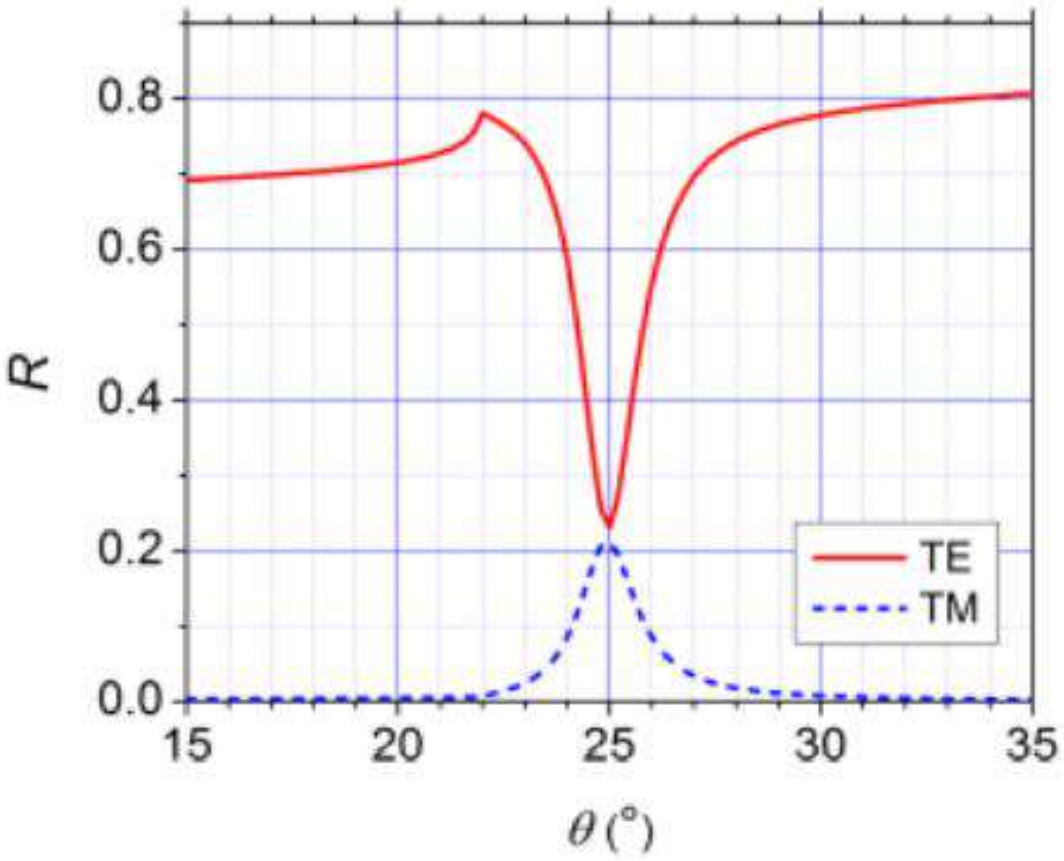

Figure I.9 The reflectivity as a function of the incident angle for a TE polarization [39].

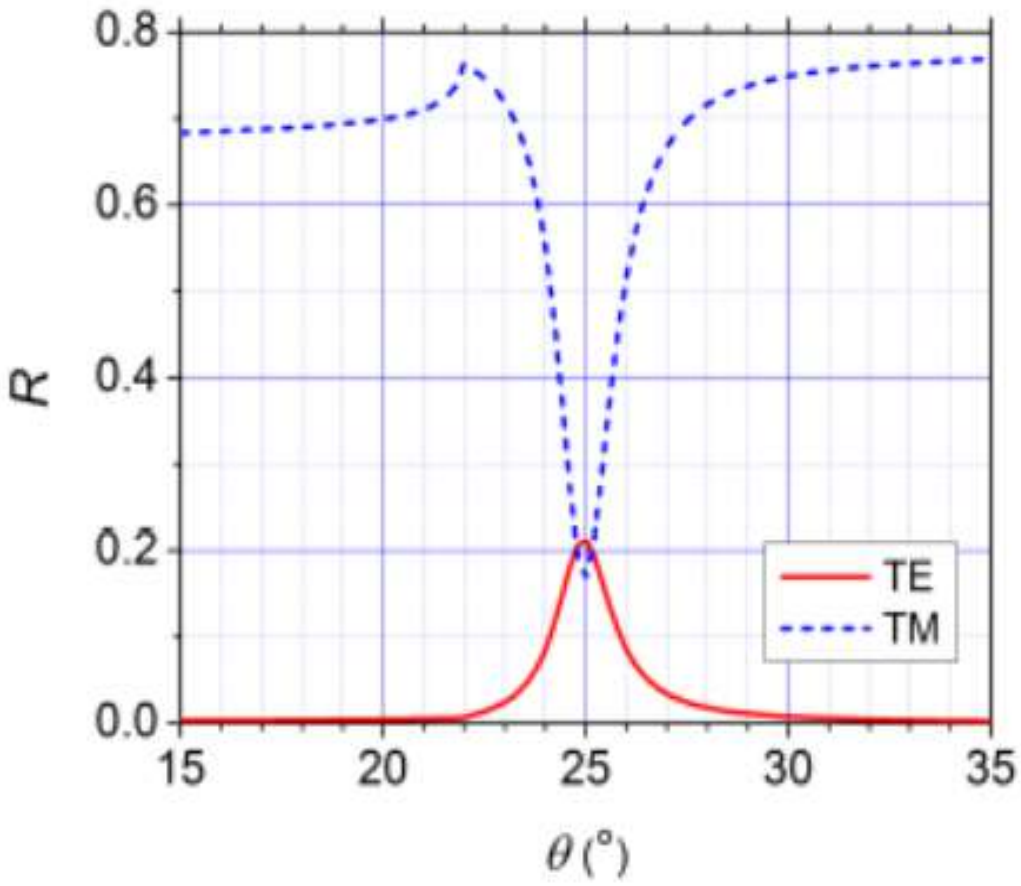

Figure I.10 The reflectivity as a function of the incident angle for a TM polarization [39].

When $\phi = 90°$:

In this case, the plane of incidence is perpendicular to the grooves of the grating, the solutions become:

$$\sin\theta = -\frac{m\lambda}{\sqrt{2}n_d d} \pm \sqrt{\frac{\varepsilon_0\varepsilon'}{\varepsilon' + \varepsilon_0}} \qquad (I.52)$$

For a sinusoidal shape, we have a good resonance only for *m*=1, which is also in good agreement with the experimental results.

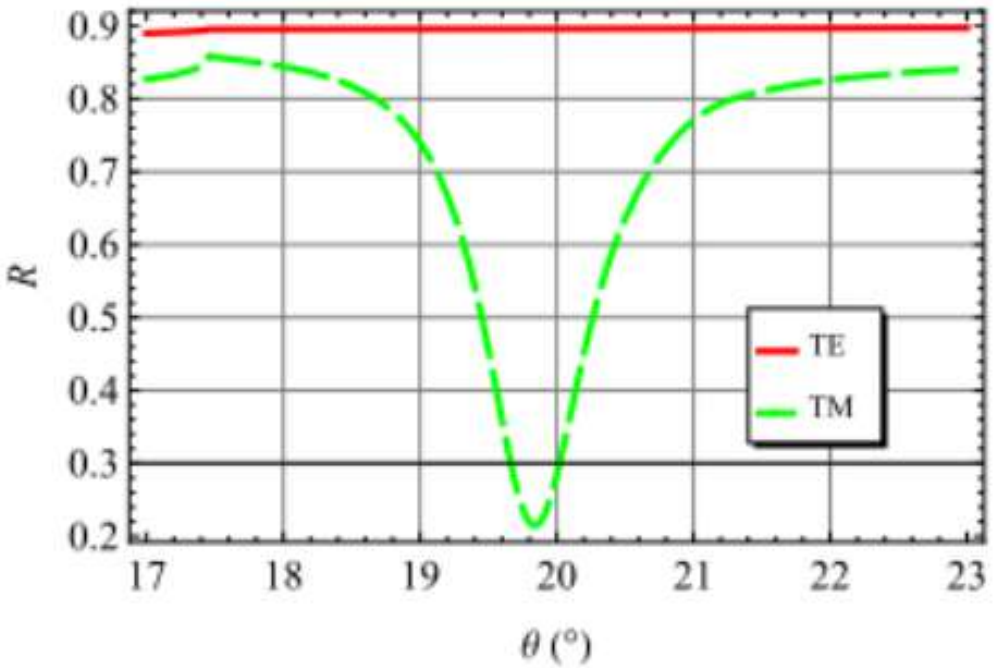

Figure I.11 The reflectivity as a function of the incident angle for a gold grating at wavelength 700 nm [39].

Several parameters influence surface plasmon resonance (SPR):

- Metallic substrate composition (e.g., gold, silver),
- Polarization state of incident light,
- Angle between the plane of incidence and grating grooves,
- Grating period (spacing between grooves),
- Groove depth.

These factors collectively govern the resonance conditions, coupling efficiency, and sensitivity of plasmonic systems.

I.13. 2. Prism Coupling

The objective of this coupling is to generate an evanescent wave through total internal reflection. Two configurations are possible: the Otto configuration and the Kretschmann-Ræther configuration. In both cases, the prism has a higher refractive index. ($n_p > n_d$).

a. Otto Configuration

In this configuration, an infinitesimally thin air gap is created between the prism and the metal surface, while the opposite surface remains in contact with the dielectric. The evanescent wave generated at the interface excites the surface plasmons (SP). Resonance occurs when the tangential component of the incident light's wavevector in the prism matches the propagation

constant of the SP. However, this configuration is rarely used, as achieving such a small air gap experimentally is highly challenging.

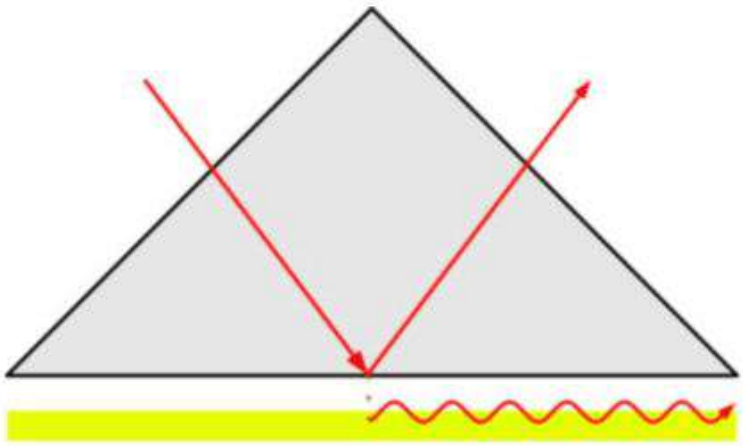

Figure I.12 Coupling of an incident wave with a surface plasmon - Otto configuration [30].

b. Kretschmann-Ræther configuration

In the Kretschmann-Ræther configuration, one side of the metal is in contact with the prism while the other side is in contact with the dielectric. This geometry is commonly employed in sensors. The incident light passes from the prism into the dielectric at an incidence angle exceeding the critical angle with:

$$k_0 \sqrt{\frac{\varepsilon_d \varepsilon'}{\varepsilon' + \varepsilon_d}} = \sqrt{\varepsilon_p} k_0 \sin \alpha_r \qquad (I.53)$$

α_r is the resonance angle, for which the wave is totally transmitted.

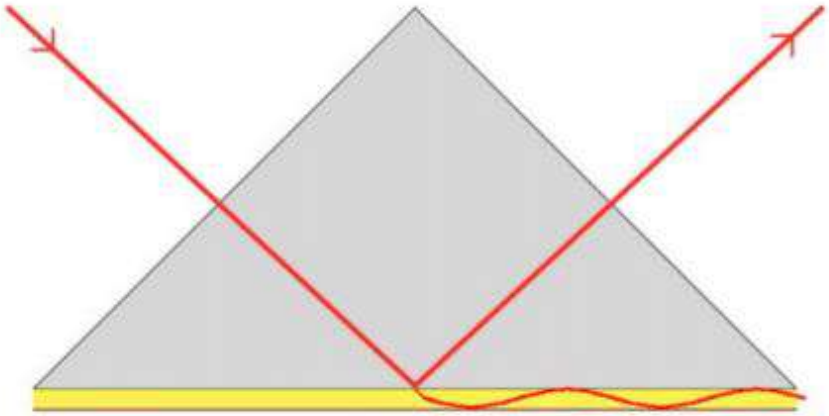

Figure I.13 Coupling of an incident wave with a surface plasmon - Kretschmann-Raether configuration [30].

The incident light couples and transfers all its energy to the SPs.

The real part of the propagation constant becomes:

$$\beta' = \sqrt{\varepsilon_p} k_0 \sin \alpha_r \qquad (I.54)$$

We deduce that regardless of the configuration, a set of parameters influences the efficiency of the resonance: the light's wavelength, the angle of incidence, the nature and thickness of the metal, and the width of the dielectric. All these parameters must therefore be adjusted to achieve optimal—and subsequently effective—coupling, whether it is via diffraction grating or prism coupling.

I.14. Tamm Surface Plasmons

The most popular surface plasmons are those formed at the interface between a metal and a dielectric with Transverse Magnetic (TM) polarization. The essential characteristic of surface plasmons is that they possess a wavevector larger than that of light in vacuum (i.e., they lie outside the light cone), which means that their spontaneous excitation is impossible.

However, A.V. Kavokin et al. [40, 41] demonstrated in 2005 that it is possible to generate surface plasmons inside the light cone using a simple multilayer structure—specifically, at the interface between two Bragg mirrors. The resulting states are called "Tamm optical states," named after the well-known electronic Tamm states [42]. Tamm plasmons were experimentally observed for the first time in 2008 by M. E. Sasin et al. [43].

Unlike conventional surface plasmons, Tamm plasmons can be generated through direct optical excitation (without the use of prisms or diffraction gratings) and can exist in both TM and TE polarizations; they can even be excited at normal incidence.

Thus, the coupling of light with Tamm surface plasmons depends on the parameters of the Bragg mirror [44], the thickness of the metal [45], and its dielectric function [46, 47].

It is important to note that the ability to excite Tamm plasmons directly and in both polarizations offer promising opportunities for developing more versatile plasmonic devices and sensors.

Conclusion

This chapter has introduced the theoretical foundations of our thesis, starting from Maxwell's equations and extending to the excitation and propagation phenomena at the metal–dielectric interface. Surface plasmon resonance has been explored, including its history, excitation mechanisms, and the parameters that influence its sensitivity. Finally, this chapter has presented Tamm surface plasmons as an innovative variant, highlighting their unique

properties such as the possibility of direct optical excitation in both TM and TE polarizations, even at normal incidence.

These concepts provide the necessary groundwork for understanding and harnessing plasmonic phenomena in advanced sensing systems.

Chapter II

Sensors Based on Photonic and Plasmonic Materials

Introduction

This chapter presents an overview of sensors based on photonic and plasmonic materials, with emphasis on the operational principles, interrogation modes, and performance metrics of surface plasmon resonance (SPR) sensors. Both photonic structures—such as photonic crystals and optical fibers—and plasmonic structures relying on SPR or LSPR are discussed. The chapter also highlights the wide range of applications of these technologies in biomedical diagnostics, biochemical analysis, environmental monitoring, and emerging technological fields.

II. Sensors Based on Photonic and Plasmonic Materials

Photonic and plasmonic sensors are essential across many fields, including biology, chemistry, and environmental monitoring. These sensors exploit the unique properties of light and surface plasmons to detect environmental changes, making them extremely sensitive and versatile.

II.1. Photonic Sensors

Photonic sensors use light to measure physical quantities such as temperature, pressure, or chemical composition. They operate based on several principles, including:

- **Interference:** Sensors based on interference patterns can detect changes in the refractive index or material thickness [48].
- **Optical Fibers:** Optical fibers transmit light, and variations in the properties of the transmitted light can indicate environmental changes [49].
- **Photonic Crystals:** These structures manipulate light through periodic dielectric materials, enabling precise control over light propagation and enhancing detection capabilities [50].

Due to their ability to provide high-precision, real-time data, photonic sensors are widely employed in applications such as telecommunications, medical diagnostics, and environmental monitoring.

II.2. Plasmonic Sensors

Plasmonic sensors exploit the phenomena of surface plasmon resonance (SPR) or localized surface plasmon resonance (LSPR). These sensors are particularly renowned for their exceptional sensitivity to refractive index changes near a metal–dielectric interface. They are widely employed to detect variations in the refractive index at the interface using surface plasmon resonance techniques. The evanescent electromagnetic field associated with surface plasmons is extremely sensitive to perturbations at the interface, allowing for the detection of changes in composition, density, or molecular concentration with high sensitivity [51].

The main characteristics include:

- **Surface Plasmon Resonance (SPR):** SPR occurs when the incident light couples with surface plasmons on a metallic surface, leading to a reduction in the intensity of the reflected light at a specific wavelength. This phenomenon is highly sensitive to variations in the refractive index of the surrounding medium [52].
- **Localized Surface Plasmon Resonance (LSPR):** LSPR involves the localized oscillations of electrons in metallic nanoparticles, which can be tuned by modifying the size, shape, or material of the nanoparticles [53].

Plasmonic sensors find applications in biodetection, chemical sensing, and environmental monitoring due to their ability to perform label-free detection and real-time monitoring. Among the various types of plasmonic sensors, those based on surface plasmon resonance (SPR) are particularly prominent because of their widespread use and significant advancements over the years. Furthermore, surface plasmon resonance is also extensively employed in other applications such as plasmonic waveguides, medical diagnostics, cancer cell treatment, and Surface-Enhanced Raman Spectroscopy (SERS).

II.2.1. Plasmonic Guides

The most commonly referenced plasmonic waveguides are fabricated using a thin metallic layer sandwiched between two dielectrics, a configuration that facilitates improved propagation of surface plasmons.

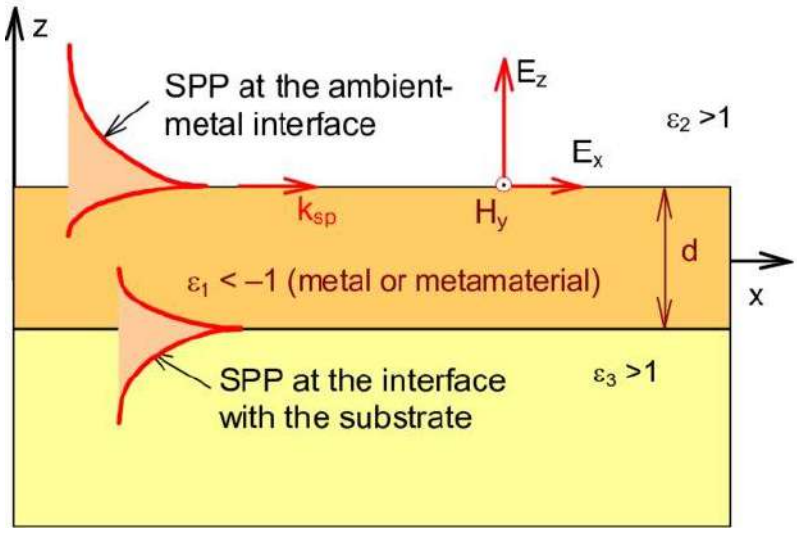

Figure II.1 Basic configuration of a plasmonic guide for the propagation of surface plasmons [54].

When the metallic layer is thicker than the penetration depth of surface plasmons into the metal, there is no overlap, and each plasmon propagates independently. Otherwise, if the metal layer is thinner, the two surface plasmons can couple, giving rise to two modes: a symmetric mode, known as Long-Range Surface Plasmons (LRSP), and an antisymmetric mode, referred to as Short-Range Surface Plasmons (SRSP).

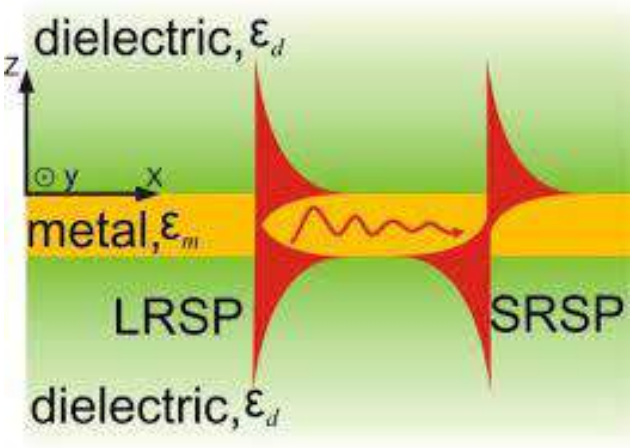

Figure II.2 Schematic of LRSP and SRSP propagation through a metal layer sandwiched between two dielectrics [55].

II.2.2. Spectroscopy

Localized surface plasmons in metallic nanoparticles alter the extinction spectrum of light through absorption and scattering. This property enables their use in spectroscopy, for instance, to detect specific molecules [56,57].

A particularly significant application is Surface-Enhanced Raman Spectroscopy (SERS), a phenomenon first observed by Sir C.V. Raman in 1928 [58]. When monochromatic light illuminates a substance, a portion of the photons is scattered elastically at the same frequency as the incident light—this is called Rayleigh scattering. However, some photons are scattered inelastically at a different frequency, known as Raman scattering. If the scattered frequency is lower than the incident frequency, it is called Stokes Raman scattering; if it is higher, it is referred to as anti-Stokes Raman scattering.

SERS enhances the Raman signal using surface plasmon resonance (SPR) in metallic nanostructures that adsorb molecules, significantly increasing sensitivity even for extremely low analyte concentrations, where conventional Raman spectroscopy would fail to provide a clear signal. This technique is widely applied in fields such as art restoration, for analyzing pigments in historical paintings, and in medicine for detecting diseases like cancer, Parkinson's, and Alzheimer's.

II.2.3. Microscopy and Surface Probes

Surface plasmons are extremely sensitive to surface inhomogeneities due to their shallow penetration depth [56]. This makes them ideal probes for examining the topography and properties of surfaces at the nanometric scale.

II.2.4. Nonlinear Optics

The electromagnetic field of surface plasmons (SPs) can be strongly enhanced at the metal-dielectric interface [57]. This enables the amplification of nonlinear optical effects, such as second-harmonic generation [56].

II.3. SPR Sensors Development

SPR-based sensors primarily rely on changes in the refractive index of the surrounding medium, known as the analyte, which comes into contact with the sensor's surface.

The performance of a sensor is analyzed and evaluated using several key parameters, each of great importance: sensitivity, detection accuracy, figure of merit, limit of detection, detection precision, and signal-to-noise ratio [59-62].

For the excitation of surface plasmons, four types of interrogation methods are possible: angular interrogation [63], spectral interrogation [64], intensity interrogation [65], and phase interrogation [66]. The sensor's sensitivity is determined based on the chosen interrogation method.

II.4. SPR Sensor's Sensitivity

II.4.1. Angular Interrogation (S_θ)

In this type of interrogation, the focus is on reflectance as a function of the resonance angle for a fixed wavelength of incident light. Any slight change in the refractive index of the analyte will cause a shift in the resonance angle toward higher values. This shift is quantified by the angular sensitivity, which is defined as the ratio of the variation in the resonance angle to the variation in the refractive index of the analyte [67].

The angular sensitivity is given by:

$$S_\theta = \frac{\Delta\theta_{SPR}}{\Delta n} \qquad (II.1)$$

$\Delta\theta_{SPR}$ is the shift in the resonance angle.

Δn represents the variation in refractive index.

II.4.2. Spectral Interrogation (S_λ)

In this case, the angle of incidence is fixed at a value exceeding the critical angle, while the wavelength of incident light is varied using a polychromatic source—unlike the previous interrogation method, which employs a monochromatic source. The key advantage of this technique lies in eliminating mechanical movement to adjust the angle of incidence.

The resonance condition is achieved at a specific resonance wavelength, where maximum energy is transferred from the evanescent wave to the surface plasmon, corresponding to the minimum reflectance. In this interrogation mode, the resonance wavelength increases with the analyte's refractive index.

Spectral sensitivity is defined as:

$$S_\lambda = \frac{\Delta\lambda}{\Delta n} \qquad (II.2)$$

$\Delta\lambda$ represents the change in the resonance wavelength.

II.4.3. Intensity Interrogation (S_I)

This method is analogous to angular interrogation, except it focuses on monitoring reflectance variations as a function of the external medium's refractive index at a fixed angle of incidence (always exceeding the critical angle).

Intensity sensitivity is defined as:

$$S_{\mathrm{I}} = \frac{\Delta \mathrm{R}}{\Delta n} \qquad (II.3)$$

ΔR represents the reflectance.

II.4.4. Phase Interrogation (S_ϕ)

In the previously discussed interrogation methods, incident light was TM-polarized. In contrast, phase interrogation involves both TM and TE polarizations of light at a fixed wavelength.

Phase sensitivity is defined as:

$$S_{\phi} = \frac{\Delta \phi_d}{\Delta n} \qquad (II.4)$$

Where ϕ_d is the phase difference between the TM and TE polarizations:

$$\phi_d = |\phi_p - \phi_s| \qquad (II.5)$$

II.5. Figure of Merit (FOM)

A critical parameter for evaluating sensor performance is the **figure of merit (FOM)**, defined as the ratio of sensitivity to the full width at half maximum (FWHM) of the SPR curve.

$$FOM = \frac{S}{FWHM} \qquad (II.6)$$

II.6. Detection Accuracy (DA)

The detection accuracy of an SPR sensor determines its overall precision, defined as the inverse of the full width at half maximum (FWHM) of the SPR curve.:

$$DA = \frac{1}{FWHM} \qquad (II.7)$$

II.7. Limit of Detection (LOD)

Among performance parameters, the **limit of detection (LOD)** is a critical factor in evaluating the capabilities of a surface plasmon resonance (SPR) sensor.

$$LOD = \frac{\Theta_{SPR}}{20 * S * Q} \qquad (II.8)$$

Q is known as the quality factor (Q-factor) of the SPR sensor, it is equal to:

$$Q = \frac{\Theta_{SPR}}{FWHM} \qquad (II.9)$$

II.8. Signal-to-Noise Ratio (SnR)

The **signal-to-noise ratio (SNR)**, derived from the English term, plays a critical role in determining the sensor's precision. It is defined as the ratio of the resonance angle shift ($\delta\Theta_{SPR}$) to the full width at half maximum (FWHM) of the SPR curve:

$$SNR = \frac{\delta\Theta_{SPR}}{FWHM} \qquad (II.10)$$

II.9. SPR Sensors Applications

Surface plasmon resonance (SPR) sensors are a widely used tool across diverse fields due to their ability to detect biomolecular interactions in real time without labels (label-free). Their applications can be categorized into several key domains:

II.9.1. Medical Diagnosis

Surface plasmon resonance (SPR) sensors have garnered significant attention in recent years due to their high sensitivity and capacity for real-time diagnosis of diverse biomarkers, including proteins, nucleic acids, and small molecules. SPR biosensors enable monitoring of molecular interactions without requiring labeling, ensuring unaltered behavior of the analytes [68].

SPR-based biosensors play a pivotal role in disease diagnostics by detecting disease-specific biomarkers in complex biological samples such as blood and serum. They are also instrumental in real-time monitoring of antibody levels or hormonal fluctuations associated with various pathologies.

For instance, in 2022, K. A. Meradi et al. proposed an SPR sensor for cancer cell detection and hemoglobin level monitoring in blood [69]. The sensor, based on the

Kretschmann configuration, comprises a BK7 glass prism layered with titanium (Ti), silver (Ag), and graphene. Under monochromatic light at 633 nm, even minor refractive index variations in the blood sample induce a measurable shift in the resonance angle toward higher values.

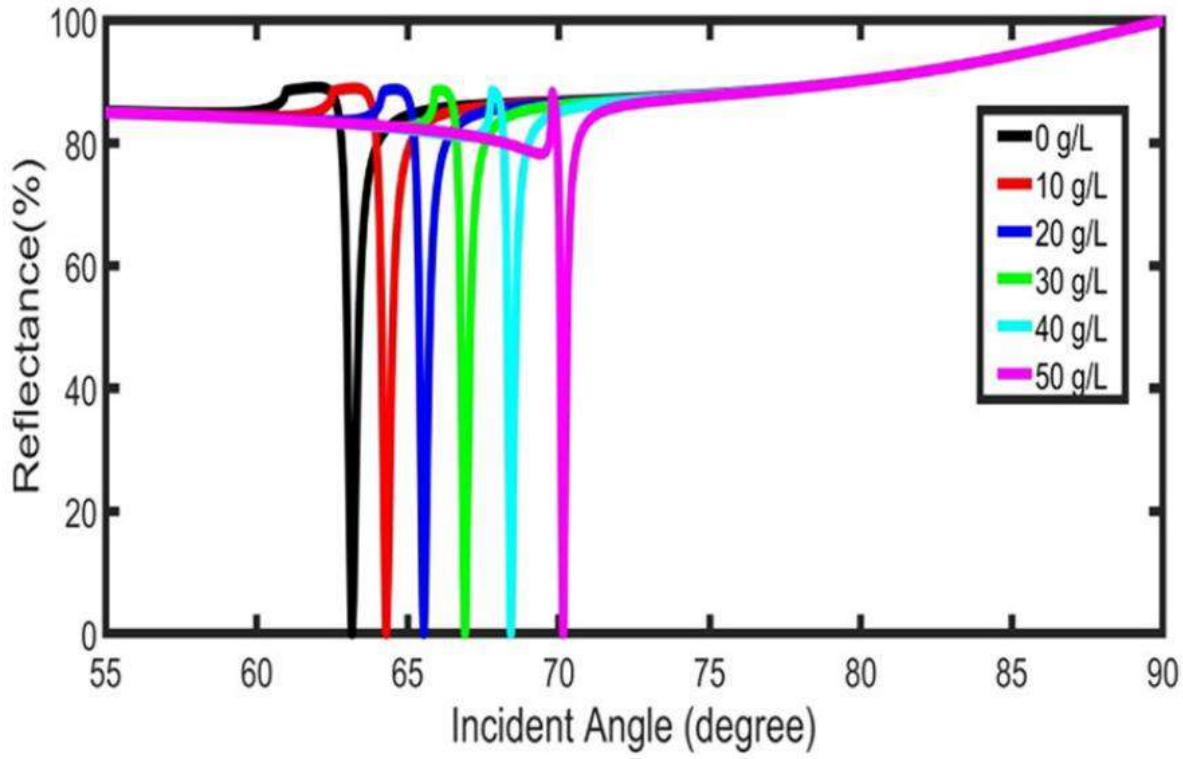

Figure II.3 Reflectance as a function of the incident angle for different hemoglobin concentrations [69].

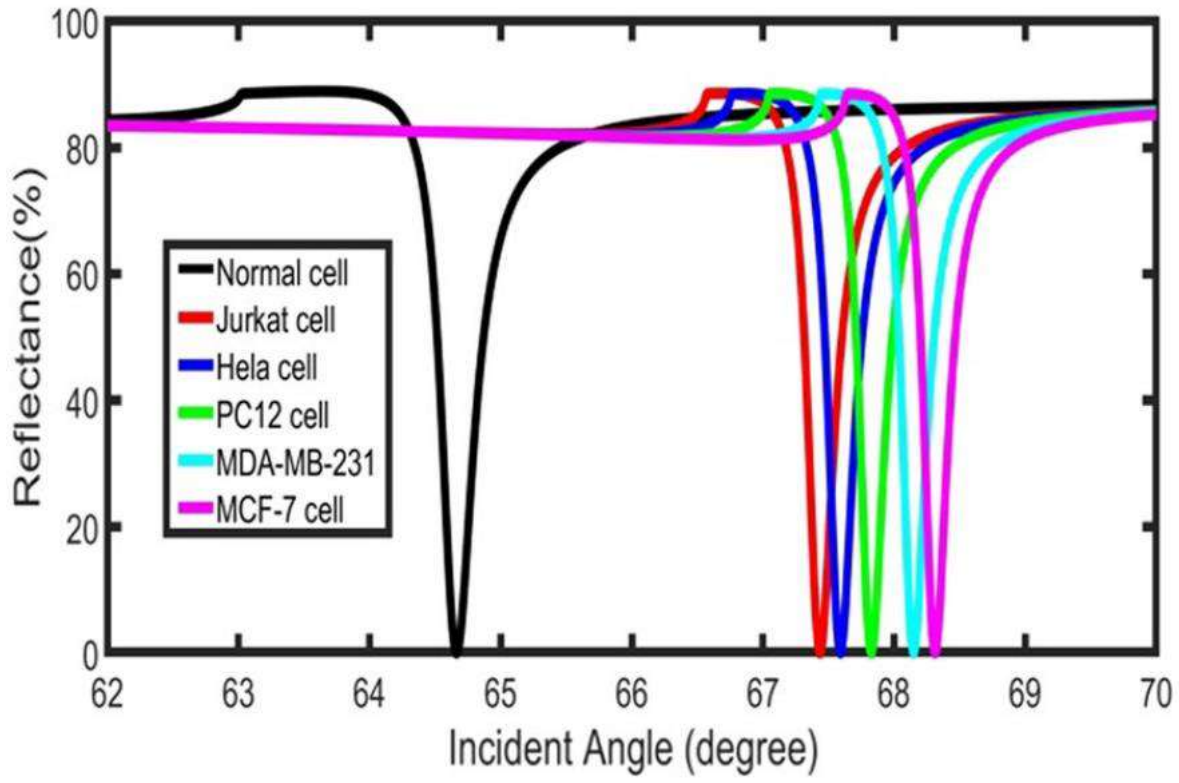

Figure II.4 Reflectance as a function of the incident angle for different cancer cells [69].

Several additional sensors have been developed for medical applications, such as the biosensor proposed by Karki, B.; Jha, A.; Pal, A. et al. [70] for detecting glucose levels in urine. The biosensor is composed of silver (Ag), MXene, zinc oxide (ZnO), and graphene layers, integrated with a BK7 glass prism.

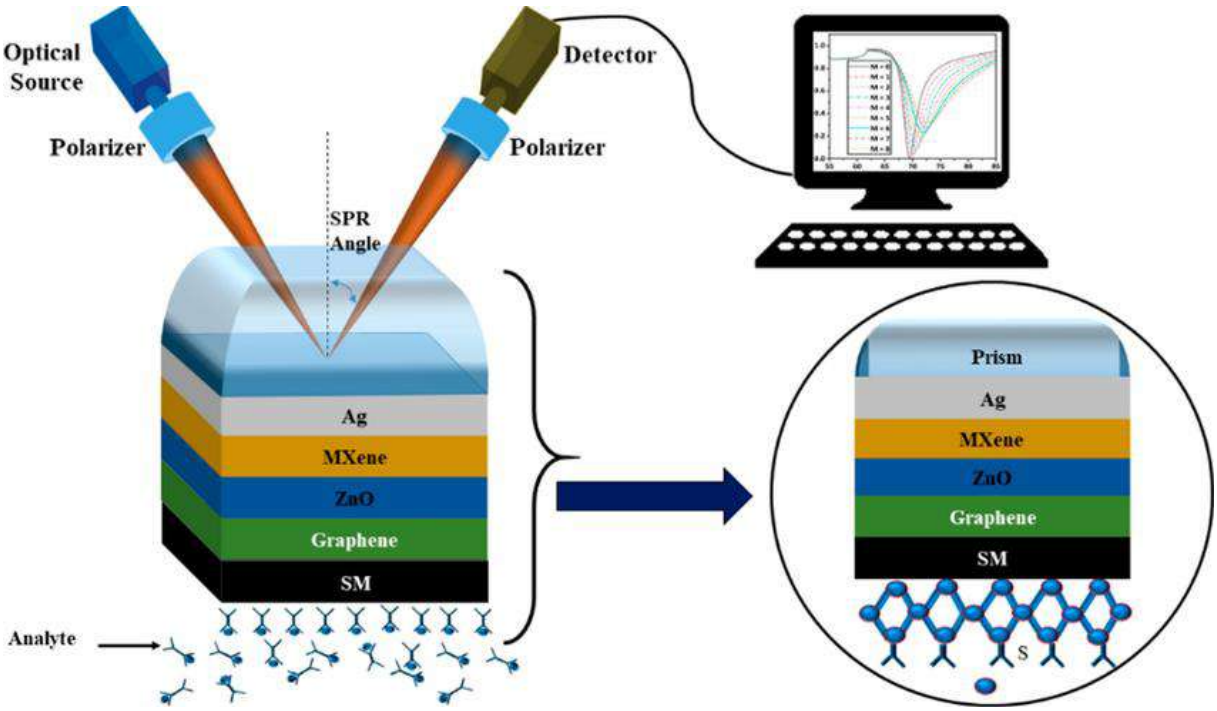

Figure II.5 Schematic representation of the SPR biosensor for monitoring glucose levels in urine [70].

The proposed biosensor manifests a sensibility equal to 123 deg/RIU.

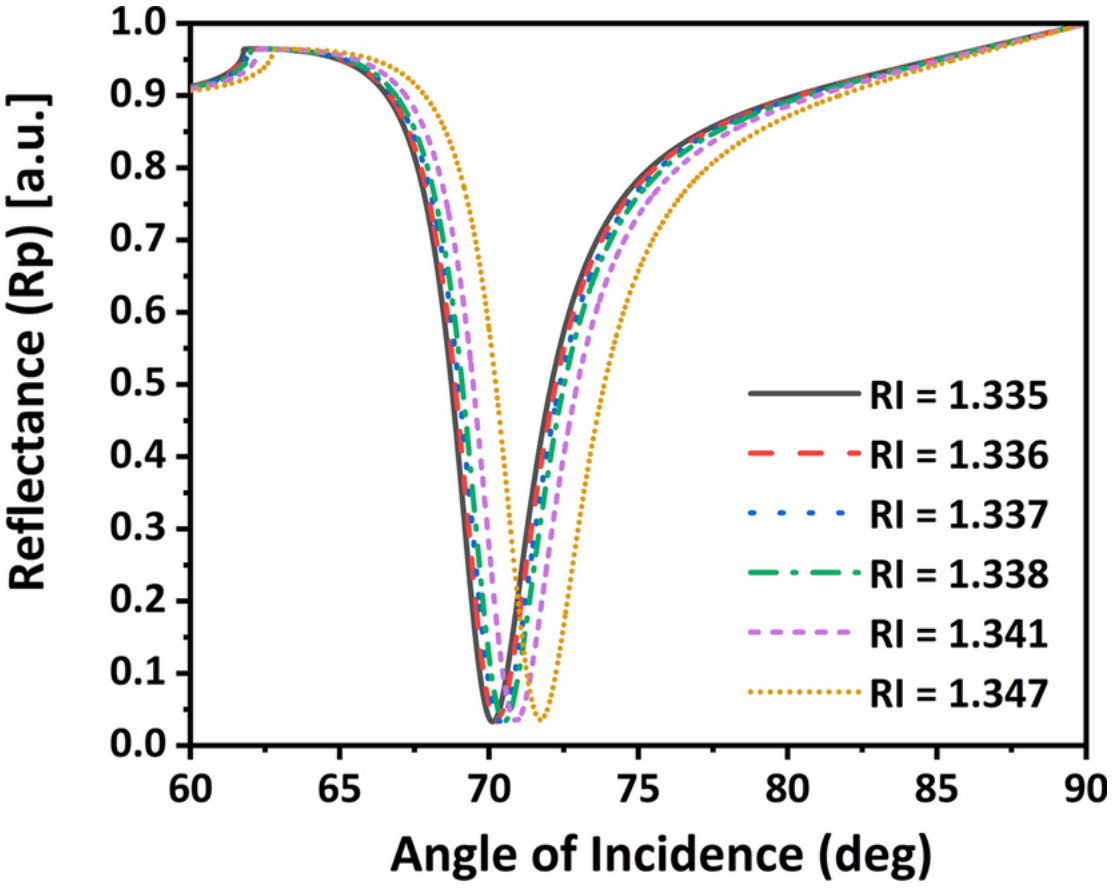

Figure II.6 Reflectance as a function of the incident angle for the biosensor suggested by Karki et al. [70].

In the food industry, SPR sensor technology is employed to ensure food quality and safety by detecting contaminants or specific ingredients that may pose health risks to consumers or compromise product integrity [71].

An experimental example is the SPREETA™ SPR sensor developed by Texas Instruments, which was evaluated by Mohammed et al. for detecting peanut allergens in food samples [72]. The study utilized peanut-specific antibodies immobilized on a gold surface via adsorption, achieving a limit of detection (LOD) of 0.7 mg/mL. The term "SPREETA" is derived from "SPR-ITA," combining Surface Plasmon Resonance (SPR) with the Spanish suffix "-ita" (denoting "small" or "compact"), reflecting the device's miniaturized design.

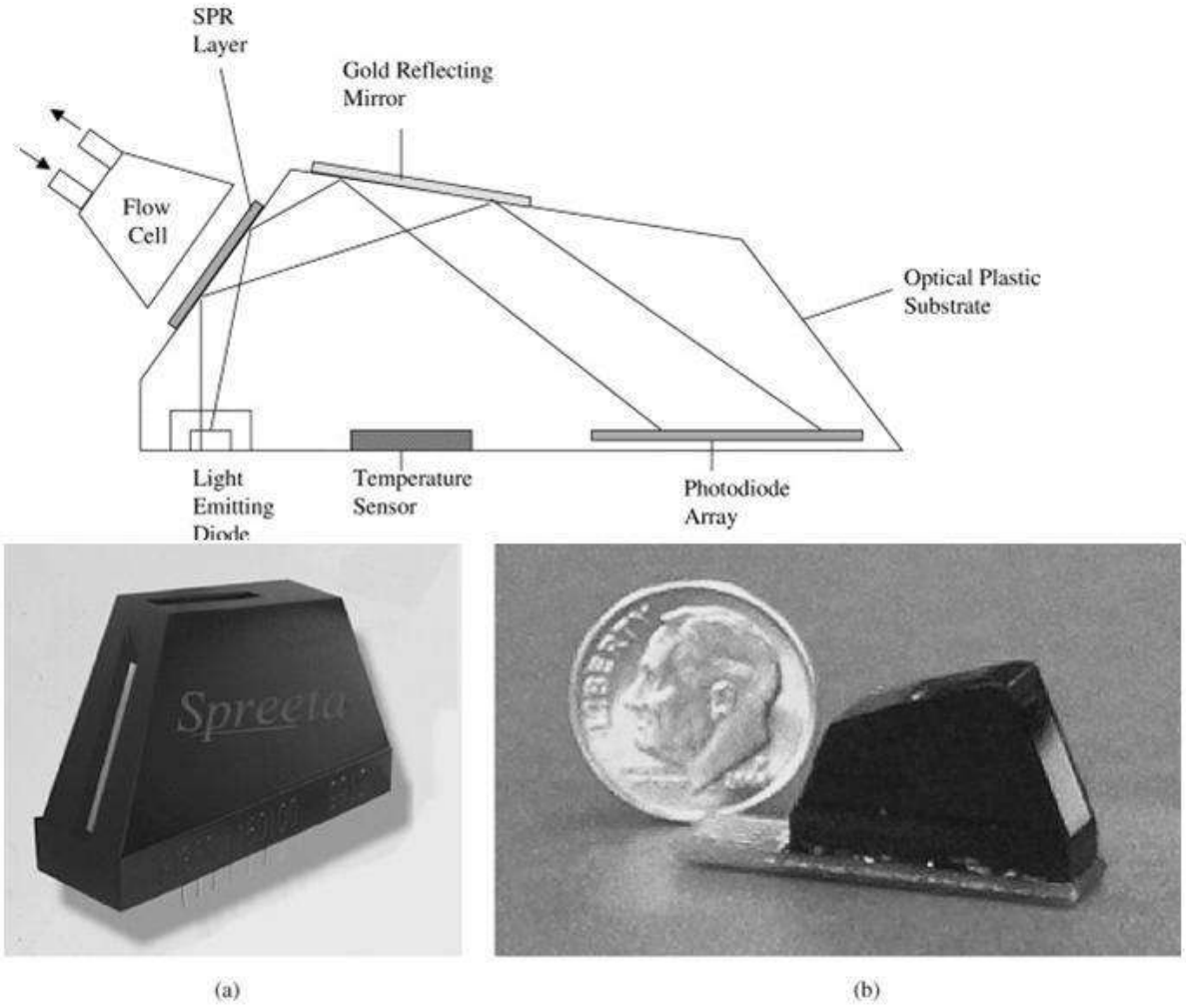

Figure II.7 Upper: optical representation of the SPREETA™ sensor. (a) the original sensor and (b) a miniaturized version of the SPR sensor [72].

In 2023, Meng Sun et al. [73] investigated an SPR sensor for alcohol detection by integrating **$Ni(OH)_2$ nanoflowers** onto a gold layer to enhance detection performance. This design leverages the catalytic properties of $Ni(OH)_2$ nanostructures synergistically combined with the high sensitivity of gold layers in surface plasmon resonance (SPR). The sensor demonstrated exceptional sensitivity and rapid response times for trace alcohol detection, marking a promising advancement for applications in chemical analysis and quality control.

II.9.2. Biochemical Analysis

In the biochemical domain, surface plasmon resonance (SPR)—and more specifically, SPR-based sensors—plays a pivotal role. These sensors are particularly valuable for studying affinity-driven interactions, such as **antibody-antigen binding** [74], **enzyme-substrate**

interactions, and **receptor-ligand kinetics** [75]. This capability is indispensable for unraveling biological processes and advancing therapeutic development strategies [76].

II.9.3. Environmental Monitoring

From pollutant detection to water and air quality monitoring, surface plasmon resonance (SPR) sensors have emerged as critical tools due to their exceptional sensitivity and precision.

In 2017, SPR sensors were developed for detecting explosives such as **RDX (1,3,5-trinitroperhydro-1,3,5-triazine)** in environmental water systems. These sensors operate effectively in field-deployable conditions, enabling rapid analysis of water samples for explosive residues at **parts-per-billion (ppb)** concentrations. Their accuracy has been validated against standard methods like high-performance liquid chromatography (HPLC) [77].

SPR is also instrumental in detecting heavy metals and toxic substances in water sources, including **lead (Pb), mercury (Hg), and cadmium (Cd)**, which is vital for safeguarding drinking water safety and protecting aquatic ecosystems [78]. Furthermore, SPR sensors can be adapted for monitoring gaseous pollutants such as **nitrogen oxides (NOx)** and **sulfur oxides (SOx)**, essential for air quality assessment and compliance with environmental regulations.

II.9.4. Other Emerging Applications

Surface plasmon resonance (SPR) is increasingly utilized in emerging fields such as nanoparticle research, particularly for real-time monitoring of nanoparticle synthesis and surface modifications. This capability is critical for optimizing nanoparticles' properties in drug delivery systems and imaging applications. By evaluating nanoparticle-biomolecule interactions, researchers can refine nanomaterial design and functionality, enhancing their efficacy in targeted therapies.

In the realm of neurodegenerative diseases, SPR sensors are employed to detect and characterize biomarkers associated with conditions like Alzheimer's and Parkinson's diseases. The ability to measure real-time binding kinetics enables researchers to identify diagnostic markers and potential therapeutic targets, offering a pathway to early intervention and improved patient outcomes.

Among emerging technologies, advanced SPR sensors represent a rapidly evolving frontier, driven by the integration of novel materials such as two-dimensional (2D) materials (e.g., graphene, transition metal dichalcogenides) and tailored dielectrics. These materials

enhance sensor sensitivity and performance, enabling detection of analytes at ultralow concentrations. Such advancements unlock new possibilities for applications in precision medicine, environmental monitoring, and beyond.

Conclusion

This chapter has been dedicated to exploring the diverse applications of surface plasmons, underscoring their pivotal role across varied domains such as sensing, plasmonic waveguides, spectroscopy, microscopy, nonlinear optics, and the development of surface plasmon resonance (SPR) sensors. These plasmon resonance-based technologies offer exceptional sensitivity to refractive index variations, driving significant advancements in medical diagnostics, biochemical analysis, environmental monitoring, and food safety. The integration of novel materials—particularly metallic and two-dimensional nanostructures—has further amplified SPR sensor performance, enabling emerging applications in biomarker detection, nanoscale imaging and quality control.

Chapter III

Numerical Methods and Materials Used

Introduction

This chapter introduces the numerical and computational tools used in the design and optimization of SPR-based sensors. It presents the main numerical techniques—Transfer Matrix Method (TMM), Finite Element Method (FEM), and Finite-Difference Time-Domain (FDTD)—and explains why TMM is adopted as the primary method in this work. The chapter also describes the materials employed in the sensor structures, including metals, dielectrics, photonic crystals, and advanced 2D materials. Finally, it outlines the simulation environment and design considerations required to model plasmonic sensor architectures accurately.

III. Numerical Methods and Materials.

The various numerical methods frequently used for the study of surface plasmons and SPR sensors are:

III.1. The Transfer Matrix Method

The Transfer Matrix Method (TMM), derived from its English nomenclature, is a computational technique used to calculate the reflection and transmission coefficients of electromagnetic waves propagating through multilayer thin-film structures. This numerical approach is particularly valuable in the design and analysis of surface plasmon resonance (SPR) sensors, where precise modeling of light-matter interactions at metal-dielectric interfaces is critical.

In TMM, each layer of a stratified medium (e.g., a prism, metallic film, and analyte in an SPR sensor) is represented by a transfer matrix that mathematically encodes the layer's optical properties (e.g., refractive index, thickness) and its interaction with incident electromagnetic fields. By sequentially multiplying the matrices corresponding to each layer, the total response of the system—such as the resonant angle or wavelength—can be computed. This enables researchers to predict sensor performance metrics like sensitivity, figure of merit (FOM), and resonance linewidth under varying design parameters (e.g., metal thickness, material composition) [79].

Key Advantages of TMM:

- Multilayer Handling: Efficiently models complex, stratified structures (e.g., hybrid SPR configurations with graphene, oxides, or 2D materials).

- Computational Efficiency: Reduces the need for resource-intensive simulations (e.g., finite element analysis) in preliminary sensor optimization.
- Versatility: Applicable to both angular and wavelength interrogation modes in SPR sensing.

For instance, TMM has been instrumental in optimizing Kretschmann-configuration SPR sensors by simulating the effect of adhesion layers (e.g., chromium, titanium) on plasmon excitation efficiency. Such simulations guide experimentalists in selecting materials and layer thicknesses to maximize sensitivity to refractive index changes in the analyte.

III.1.1. Principle of the Method

The Transfer Matrix Method (TMM) is grounded in the mathematical representation of electric (*E*) and magnetic (*H*) fields through transfer matrices, which describe the interaction between electromagnetic waves and the multilayer structure of a surface plasmon resonance (SPR) sensor. Each layer within the sensor's stratified architecture—such as the prism, metallic film, dielectric coating, and analyte—is characterized by a transfer matrix derived from its optical properties, including refractive index, thickness, and the excitation frequency of surface plasmons. This frequency governs the resonance conditions critical for efficient plasmon coupling.

Central to TMM is the expression of *E* and *H* fields as vectors at each interface between layers, with transfer matrices modeling their propagation through adjacent materials. These matrices account for phase shifts and amplitude modulation experienced by electromagnetic waves as they traverse each layer, determined by the material's permittivity, permeability, and geometric dimensions. The method inherently satisfies the boundary conditions at layer interfaces, ensuring continuity of *E* and *H* fields and yielding physically consistent solutions. A key dependency in SPR applications is the alignment of the excitation frequency with the surface plasmon resonance frequency, which dictates the efficiency of light-plasmon coupling and is rigorously modeled through TMM.

By cascading layer-specific matrices, TMM computes the total electromagnetic response of the multilayer system, such as reflectance, transmittance, or resonance angle shifts. This capability is pivotal for predicting SPR sensor behavior under varying geometric configurations and material compositions, enabling optimization of sensitivity and resolution without the need for costly experimental iterations. For instance, in a Kretschmann-configuration SPR sensor, TMM can simulate how subtle changes in metallic layer

thickness—such as a 50 nm gold film versus a 60 nm layer—alter resonance angle shifts, guiding experimental design to maximize plasmon excitation efficiency. Similarly, the integration of advanced materials like graphene or dielectric oxides into SPR sensors can be computationally explored to assess their impact on performance metrics such as sensitivity and figure of merit (FOM).

The versatility of TMM extends to both angular and wavelength interrogation modes, making it indispensable for advancing SPR sensor technology in applications ranging from biomedical diagnostics to environmental monitoring. By bridging theoretical modeling and practical design, TMM accelerates the development of next-generation plasmonic devices with enhanced precision and functionality.

III.1.2. Method Steps

The Transfer Matrix Method (TMM) involves the following steps:

1. Mode Decomposition: Electromagnetic fields are decomposed into two propagation modes—TE (Transverse Electric) and TM (Transverse Magnetic). Each mode is represented by a field function.
2. Transfer Matrix Calculation: For each layer, a transfer matrix is computed based on the layer's optical properties (e.g., refractive index, thickness) and the excitation frequency.
3. Matrix Assembly: The individual transfer matrices of all layers are combined to form a global transfer matrix, which describes the interaction between electromagnetic fields and the sensor.
4. Transfer Equation Solving: The assembled global matrix is used to solve the transfer equation, modeling how fields propagate through the sensor.
5. Result Analysis: The solution is analyzed to determine key sensor properties, such as resonance angle, sensitivity, or reflectance profiles.

III.2. Finite Elements Method

The Finite Element Method (FEM) involves dividing the computational domain into small finite elements and establishing a variational formulation of the electromagnetic field within each element. This method is particularly well-suited for solving the complex differential equations governing surface plasmon resonance (SPR)-based sensors, enabling precise modeling of their optical and electromagnetic behavior [80].

III.2.1. Principle of the Method

The Finite Element Method (FEM) is a powerful numerical approach for solving complex physical problems, including those inherent to surface plasmon resonance (SPR) sensors. At its core, FEM involves discretizing the computational domain into a mesh of small, interconnected finite elements. Within each element, the governing differential equations—such as Maxwell's equations for electromagnetic phenomena—are approximated using variational formulations or weighted residual techniques. This discretization transforms the original partial differential equations into a system of algebraic equations, which can be solved computationally to model the behavior of the system.

For SPR sensors, FEM enables precise simulation of light-matter interactions at the metal-dielectric interface, accounting for intricate geometries, material anisotropies, and boundary conditions. By iteratively refining the mesh and solving the discretized equations, researchers can predict resonance conditions, field distributions, and sensitivity metrics critical to sensor design. Its flexibility in handling irregular geometries and complex material properties makes FEM indispensable for optimizing plasmonic structures, such as nanostructured gratings or hybrid sensor configurations, while maintaining rigorous adherence to physical laws [80].

III.2.2. Method Steps

1. Geometry Definition & Meshing: Discretize the SPR sensor's physical structure into finite elements (e.g., triangles, tetrahedrons) to represent complex geometries (metallic layers, dielectric interfaces).
2. Variational Formulation: Reformulate Maxwell's equations (governing electromagnetic wave propagation) into a weak form to simplify boundary conditions and enable numerical approximation.
3. Finite Element Approximation: Approximate electromagnetic fields within each element using polynomial basis functions and transform the continuous problem into a linear system of algebraic equations.
4. Linear System Solving: Solve the system numerically (e.g., Gaussian elimination, iterative solvers) to compute electric/magnetic field distributions.
5. Post-Processing: Extract sensor performance metrics (sensitivity, resolution, resonance shifts) from the computed fields.

III.3. Finite-Difference Time-Domain

The Finite-Difference Time-Domain (FDTD) method is a numerical technique that solves Maxwell's equations in the time domain by discretizing spatial and temporal derivatives using finite differences.

III.3.1. Principle of the Method

The Finite-Difference Time-Domain (FDTD) method involves discretizing the spatial and temporal derivatives of Maxwell's equations using finite differences. The electric (E) and magnetic (H) fields are represented as finite-sized matrices, and Maxwell's equations are iteratively solved at each discrete time step.

III.3.2. Method Steps

1. Spatial Discretization: The computational domain is divided into a grid of discrete points called nodes, where electromagnetic fields (E and H) are represented as discrete values.
2. Temporal Discretization: Time is discretized into a sequence of time steps, with field values updated iteratively at each step.
3. Discretized Maxwell's Equations: Maxwell's equations are approximated using finite differences for spatial and temporal derivatives, converting them into algebraic equations solvable at each time step.
4. Field Updates: Electromagnetic fields are iteratively updated using the discretized equations, propagating waves through the grid over successive time steps.
5. Result Analysis: Simulated field distributions are analyzed to extract sensor properties (e.g., sensitivity, resonance angle, reflectance profiles).

III.4. Numerical Method Used in This Study

The Transfer Matrix Method (TMM) is the primary approach in our studies due to its widespread applicability and advantages:

1. It enables precise determination of reflection and transmission coefficients for the layered components of SPR sensors, essential for understanding sensor behavior.
2. It incorporates the frequency-dependent dielectric constants of materials, allowing realistic modeling of optical properties [80].

3. Its mathematical implementation is relatively straightforward, making it accessible for analyzing SPR-based sensors.

4. Open-source programs and tools (e.g., MATLAB, Python libraries) based on TMM are readily available, facilitating its adoption by researchers [81]

We can therefore detail this method in order to better understand how it works.

We consider a system of N layers (N-1 interfaces), where each layer (k) has a thickness noted (d_k).

Each layer of the N-layer system is characterized by two parameters: the dielectric constant ε_k and the magnetic permeability μ_k. For each layer, the complex refractive index n_k is defined by:

$$n_k^2 = \varepsilon_k = (n_k + ik_k)^2 \qquad (III.1)$$

where n_k is the real part of the complex refractive index and k_k is the extinction coefficient; the imaginary part of the complex RI.

The relationship between the first (k=1) and the last (k=n-1) interfaces is governed by:

$$\begin{bmatrix} U_1 \\ V_1 \end{bmatrix} = M \begin{bmatrix} U_{N-1} \\ V_{N-1} \end{bmatrix} \qquad (III.2)$$

Here, *M* is the characteristic matrix, calculated as:

$$M = \prod_{k=1}^{N-1} M_k = \begin{pmatrix} M_{11} & M_{12} \\ M_{21} & M_{22} \end{pmatrix} \qquad (III.3)$$

$$M_k = \begin{bmatrix} \cos\beta_k & -i\sin\beta_k / q_k \\ -iq_k \sin\beta_k & \cos\beta_k \end{bmatrix} \qquad (III.4)$$

q_k represents the optical admittance and β_k the phase shift between every medium:

$$q_k = \left(\frac{\mu_k}{\varepsilon_k}\right)^{\frac{1}{2}} \cos\theta_k = \frac{\left(\varepsilon_k - n_{pr}^2 \sin^2\theta_1\right)^{\frac{1}{2}}}{\varepsilon_k} \qquad (III.5)$$

$$\beta_k = d_k \frac{2\pi}{\lambda} \left(\varepsilon_k - n_{pr} \sin^2\theta_1\right)^{\frac{1}{2}} \qquad (III.6)$$

n_{pr} represents the prism's refractive index and θ_k the angle in layer *k*.

The reflectance R_p for p-polarized light is derived from the Fresnel reflection coefficients [82]:

$$R_p = \left|r_p\right|^2 = \left|\frac{(M_{11} + M_{12}q_N)q_1 - (M_{21} + M_{22}q_N)}{(M_{11} + M_{12}q_N)q_1 + (M_{21} + M_{22}q_N)}\right|^2 \qquad (III.7)$$

TMM is extensively used to optimize structural components (e.g., layer thicknesses, materials) to minimize reflectance at the SPR angle and maximize sensitivity. Enhancements involve tuning these parameters to amplify the sensor's response to refractive index changes in the analyte [83].

III.4.1. Advantages of TMM

- The TMM offers accurate modeling of the reflectance and sensitivity of SPR sensors.
- It allows for detailed analysis and optimization of sensor performance.
- It can be applied to various SPR sensor configurations, including hybrid structures, making TMM a versatile tool for the design and optimization of new sensors.
- The transfer matrix method enables the enhancement of performance indices for surface plasmon resonance sensors by optimizing their structural parameters and material compositions.
- Additional advantages include its computational efficiency, the capability to handle complex multilayer structures, and its flexibility in simulating both TE and TM polarization modes.
- TMM is also widely used in the design of optical coatings and photonic devices, offering valuable insights for both theoretical studies and practical implementations.

III.5. Programming and simulation

In order to use the transfer matrix method (TMM), we must choose a working environment. Among the different programming and simulation softwares, we cite as examples:

- COMSOL Multiphysics [84].

- MATLAB [85].
- OptiFDTD [86].

Our choice was to use MATLAB. With a robust program, MATLAB allows for a precise and straightforward study of different sensor types. It provides a versatile platform for the modeling, simulation, and optimization of SPR sensors, enabling a deeper exploration of various sensor configurations and material compositions to enhance sensor performance.

Additionally, MATLAB offers a wide range of built-in functions and specialized toolboxes for numerical analysis, data visualization, and algorithm development, which facilitate rapid prototyping and iterative optimization. While COMSOL Multiphysics provides powerful multiphysics simulation capabilities and OptiFDTD offers precise electromagnetic simulations, MATLAB's flexibility and ease of integration with custom scripts make it especially well-suited for our needs. Its lower computational overhead for the types of simulations required in our study further contributed to our decision, making MATLAB the optimal choice for our sensor design and analysis.

III.5.1. MATLAB

Named "*Matrix Laboratory*" and created by Cleve Moler, MATLAB is a programming environment dedicated to scientists for data analysis, algorithm development, and model creation. It is a high-level programming language in which operations are performed on matrices and arrays rather than on individual numbers, making MATLAB the ideal tool for complex mathematical operations [85].

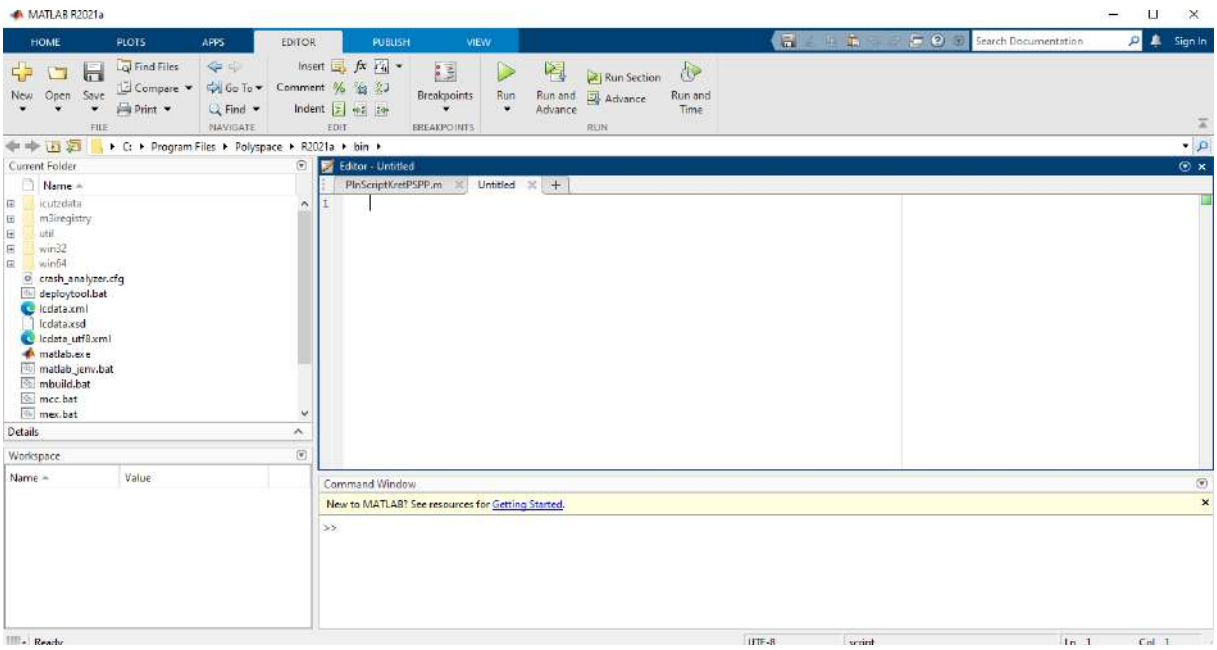

Figure III.1 MATLAB R2021a interface.

III.5.2. Key Characteristics of MATLAB

MATLAB is considered an excellent programming language for studying complex physical phenomena for several reasons:

- Matrix-Based Language: MATLAB is a matrix language designed for the natural expression of computational mathematics [87].
- High-Level Scientific Computing: It is a high-level language for scientific calculations, enabling the straightforward execution of algorithms.
- Interactive Environment: It offers an interactive environment that supports iterative exploration, leading to better solutions for complex mathematical problems. It also facilitates the development of custom interactive applications and programs.
- Graphical Capabilities: Its advanced graphical capabilities aid in the modeling and visualization of data, which simplifies data analysis and comprehension.
- Extensive Libraries: MATLAB comes with a vast library of pre-installed functions and toolboxes for various applications, including linear algebra, statistics, Fourier analysis, and the solving of ordinary differential equations.

All these features make MATLAB the preferred tool for scientists across all disciplines.

III.5.3. History

- **In the 1960s:** Cleve Moler begins developing interactive matrix computing environments, laying the groundwork for MATLAB's future.
- **In the 1970s:** Key software libraries such as LINPACK and EISPACK are developed, providing robust tools for numerical linear algebra.
- **In 1979:** MATLAB is first unveiled at the Naval Postgraduate School (NPS), offering an innovative tool for data analysis and algorithm development.
- **In 1984:** MATLAB is commercially released by MathWorks, marking its transition from an academic tool to a widely used software platform.
- **Late 1980s:** Early versions start incorporating graphical user interfaces, enhancing usability and paving the way for broader adoption in both academia and industry.
- **In the 1990s:** MATLAB gains widespread recognition and use. In 1993, MATLAB 4 is released with significant improvements, and by 1997, MATLAB 6 introduces enhanced performance, a more robust feature set, and deeper integration of toolboxes.
- **In year 2000:** The introduction of the LAPACK library for advanced linear algebra further extends MATLAB’s computational capabilities.
- **In 2008:** Major updates are made to Simulink and various toolboxes, expanding MATLAB's utility in modeling and simulation applications.
- **In 2010:** Support for GPU computing is added, allowing users to harness the parallel processing power of modern graphics processing units for computationally intensive tasks.
- **In 2012:** A major overhaul of the user interface, along with significant expansions in Simulink’s functionality, is introduced—improving the user experience and enabling more sophisticated simulations.
- **2021 to the present day:** MATLAB continues to evolve with ongoing enhancements in data analytics, machine learning, deep learning, and cloud computing support. These improvements, along with regular updates and the expansion of its extensive toolbox ecosystem, solidify MATLAB's status as an indispensable tool for both research and industrial applications.

III.6. Design Considerations for SPR Sensors

Designing effective surface plasmon resonance (SPR) sensors involves a variety of factors to achieve optimum sensitivity, resolution, and overall performance. Among the key considerations are:

a. Material Selection

The materials used in fabricating SPR sensors are fundamental to a successful design. Starting with the metallic layer, gold offers high sensitivity but lower resolution, in addition to being costly. Conversely, silver provides higher resolution at the expense of sensitivity, making it a more economical choice for commercial sensor designs [88]. Employing a bimetallic layer can balance these properties, delivering both good sensitivity and relatively high resolution [89].

The incorporation of two-dimensional nanomaterials such as graphene or transition metal dichalcogenides (TMDC) can significantly boost sensitivity. However, adding extra layers tends to increase the full width at half maximum (FWHM) of the SPR response, which may potentially reduce resolution [89].

b. Optical Configuration of the SPR Sensor

The choice of optical configuration is crucial for creating an effective SPR sensor:

- Kretschmann Configuration: This widely used configuration involves placing the metallic film at the interface of a high-refractive-index prism. It allows for efficient coupling of the incident light to excite surface plasmons. Detection is performed by monitoring variations in the resonance angle or wavelength, which directly influence both the sensor's resolution and sensitivity.

- Fiber Optic Configuration: SPR sensors can also be integrated into fiber optic systems, which offer the benefits of miniaturization and flexibility. In this design, it is critical to ensure that the refractive index of the fiber core matches that of the dielectric layer to maximize sensitivity [90].

c. Geometrical Properties

The geometrical properties—particularly the thickness of each layer in the SPR sensor—play a crucial role in determining sensor performance. Numerical simulations are often

used to optimize these thicknesses, enabling the evaluation of how variations affect the SPR response and helping to determine the ideal operating conditions [91].

d. Environmental and System Integration Considerations

Additional factors such as temperature control are important, as fluctuations can introduce noise into the measurements [88]. Other key considerations include proper sensor calibration, minimization of optical losses, and optimizing surface functionalization to ensure selective analyte binding. Moreover, integrating the sensor into a robust system—considering aspects like alignment, packaging, and reproducibility—further enhances overall performance and reliability.

III.7. SPR Sensor Manufacturing Techniques

Experimentally, the fabrication of SPR sensors involves precise techniques for creating structures that support surface plasmon waves, which are essential for detecting refractive index changes near the sensor surface. The main fabrication methods include [92]:

- Physical Vapor Deposition (PVD): This method includes thermal evaporation or sputtering, which allows for precise control over the thickness and uniformity of the metallic layer.
- Chemical Vapor Deposition (CVD): This technique can also be used to deposit thin films, offering high purity and excellent adhesion properties.
- Self-Assembled Monolayers (SAM): Functionalizing the metallic surface with SAMs can enhance the binding of target analytes, thereby improving the sensor's selectivity and sensitivity.
- Atomic Layer Deposition (ALD): ALD provides sub-nanometer control over film thickness, ensuring high uniformity and excellent conformity even on complex geometries. This precision is critical for optimizing the metal and dielectric layers in SPR sensors.
- Electrodeposition: This electrochemical process allows for the deposition of metals with controlled morphology and composition. Electrodeposition can be particularly useful for creating nanopatterned surfaces that enhance the plasmonic response.
- Nanoimprint Lithography (NIL): NIL is a high-throughput, cost-effective patterning technique used to create nanoscale features or gratings. These patterned structures can significantly improve the coupling efficiency and sensitivity of SPR sensors.

- Spin Coating and Dip Coating: These methods are widely employed for depositing uniform thin films, especially in the fabrication of polymer layers or nanoparticle films that can later be functionalized with metallic coatings to enhance SPR performance.
- Pulsed Laser Deposition (PLD): PLD is a versatile technique that enables the deposition of thin films with precise control over composition and microstructure, which can be tailored to improve sensor characteristics.

III.8. Characterization Methods of SPR Sensors

Characterization of surface plasmon resonance (SPR) sensors is crucial for evaluating their performance, sensitivity, and reliability. It provides a deeper understanding of the sensor's behavior, guiding optimization for each specific application and ensuring reliable detection of molecular interactions [93]. Several methods are employed to evaluate the optical properties and response characteristics of these sensors:

III.8.1. Optical Characterization

This method involves analyzing SPR curves—that is, measuring the reflectance as a function of the incident angle or wavelength—to determine the resonance conditions, which are highly sensitive to variations in the refractive index near the sensor surface. This analysis provides critical insights into the sensor's sensitivity and its detection limits.

In addition, a more advanced technique called multiparametric SPR (MP-SPR) measures complete SPR curves at several wavelengths simultaneously. This approach enables the extraction of kinetic parameters and structural information about the analyte layer, such as binding constants and layer thickness [94].

Additional optical characterization methods further enhance our understanding of SPR sensor performance. Together, these optical characterization techniques form a comprehensive toolkit for evaluating and optimizing SPR sensors, ensuring they deliver high performance in various applications:

- Ellipsometry: By analyzing changes in the polarization state of reflected light, ellipsometry provides precise measurements of film thickness and refractive index profiles, which are crucial for sensor calibration and optimization.

- Phase-Sensitive Techniques: These methods measure the phase shift of the reflected light, offering enhanced resolution and sensitivity beyond what intensity-based measurements can achieve.
- Imaging-Based SPR: Spatially-resolved SPR imaging systems allow for the visualization of binding events across the sensor surface, facilitating the study of heterogeneous samples and localized interactions.
- Reflectometry: This technique complements SPR by providing detailed data on the optical properties of thin films, further aiding in the optimization of sensor design.

III.8.2. Surface Characterization

Surface characterization plays a crucial role in evaluating the quality and performance of SPR sensors, as surface properties directly impact plasmon resonance conditions and sensor sensitivity. Beyond ellipsometry and atomic force microscopy (AFM), several other advanced techniques can be used to assess the morphology, composition, and uniformity of sensor surfaces. Combining these surface characterization techniques ensures that SPR sensors are manufactured with high precision, leading to improved reliability, sensitivity, and reproducibility in various sensing applications:

- Scanning Electron Microscopy (SEM): This technique provides high-resolution imaging of the sensor surface, allowing the visualization of nanostructures, surface roughness, and deposition quality. SEM can also be coupled with energy-dispersive X-ray spectroscopy (EDS) to analyze the elemental composition of the surface.
- Transmission Electron Microscopy (TEM): TEM enables the analysis of ultra-thin sensor layers, revealing structural characteristics at the atomic level. This is particularly useful for studying the interface between the metal layer and dielectric materials.
- X-ray Photoelectron Spectroscopy (XPS): XPS is a powerful technique for determining the chemical composition and oxidation states of surface elements. It provides insights into surface functionalization and contamination, which can affect sensor performance.
- Atomic Layer Deposition (ALD) Monitoring: ALD is used to deposit ultra-thin layers with high precision. Real-time monitoring of ALD processes ensures uniformity and optimal thickness for SPR sensor coatings.

- Contact Angle Measurements: By assessing the wettability of the sensor surface, this method helps evaluate the effectiveness of surface functionalization and the ability of the sensor to interact with analytes.
- Raman Spectroscopy and Surface-Enhanced Raman Spectroscopy (SERS): These techniques provide molecular-level insights into surface functionalization, particularly for sensors using nanostructured plasmonic surfaces.

III.8.3. Functional Characterization

Functional characterization of SPR sensors is essential to evaluate their real-world performance, ensuring specificity, sensitivity, and reproducibility [95]. Various techniques are employed to assess the sensor's ability to detect target analytes accurately under different conditions:

- Binding Kinetics Analysis: This involves monitoring the real-time interaction between the sensor surface and analytes to determine association and dissociation rates. Techniques such as MP-SPR (Multi-Parametric SPR) enable the extraction of kinetic constants, helping to understand molecular interactions.
- Limit of Detection (LOD) and Sensitivity Tests: By introducing analytes at varying concentrations, the lowest detectable concentration can be determined. The sensitivity is evaluated based on the sensor's ability to detect minimal changes in refractive index.
- Selectivity and Specificity Studies: Functional characterization involves testing the sensor with structurally similar but non-target molecules to assess its specificity. This step ensures that the sensor provides accurate detection without cross-reactivity.
- Regeneration and Reusability Tests: The ability of an SPR sensor to be regenerated for multiple uses is crucial for cost-effectiveness. This is tested by introducing regeneration agents to remove bound analytes without damaging the sensor surface.
- Temperature and pH Stability: Environmental conditions, such as temperature fluctuations and pH variations, can impact SPR sensor performance. Functional characterization under different conditions ensures stability and reliability.
- Real-Sample Testing: To validate the sensor's practical application, it is tested with real biological, environmental, or industrial samples rather than just standard solutions. This helps assess matrix effects and potential interference from complex sample compositions.

- Multiplex Detection Capability: In advanced SPR platforms, functional characterization may involve testing the sensor's ability to detect multiple analytes simultaneously, improving efficiency in diagnostic or environmental monitoring applications.

These functional characterization methods help optimize sensor performance, ensuring accurate, reproducible, and robust results for real-world applications.

III.8.4. Environmental Stability

Evaluating the stability and robustness of SPR sensors is crucial to ensuring their long-term reliability and functionality in real-world applications. Several key techniques are used for this purpose:

- Environmental Stress Testing: SPR sensors are subjected to repeated cycles of temperature variations and humidity exposure. By monitoring their performance before, during, and after these cycles, their stability under extreme or fluctuating conditions can be assessed.
- Thermal Stability Assessment: Sensors are tested at different temperatures to determine their resistance to thermal degradation. This helps identify temperature thresholds beyond which sensor performance deteriorates.
- Humidity and Moisture Resistance: Exposure to high humidity levels allows for the evaluation of potential material degradation, oxidation (especially in metallic layers), or loss of sensitivity due to water adsorption on the sensor surface.
- Long-Term Stability Studies: The sensor's response is monitored over extended periods to determine if there is any drift in its baseline signal or reduction in sensitivity over time.
- Mechanical Durability Tests: Repeated mechanical stress, such as bending (for flexible SPR sensors) or exposure to vibrations, helps assess the mechanical integrity of the sensor and its resistance to wear.
- Chemical Stability Testing: The sensor is exposed to different pH levels, solvents, or aggressive chemical environments to evaluate its resistance to corrosion or surface degradation.
- Storage Stability Tests: Sensors are stored under different conditions (e.g., vacuum-sealed, refrigerated, or exposed to air) to determine the best preservation methods and ensure they remain functional over time.

- Repeatability and Reproducibility Assessments: By subjecting sensors to identical test conditions multiple times, the consistency of their response is analyzed. A stable sensor should exhibit minimal variability across multiple test cycles.

III.9. Used Materials

III.9.1. Prism

Among the most commonly used glasses for prisms in Surface Plasmon Resonance (SPR) sensors:

- **BK7 Glass:** The most widely used in the literature due to its excellent optical properties and high sensitivity in SPR applications. It is a borosilicate glass that offers a well-balanced refractive index and good transmission characteristics, making it a reliable choice for various applications.
- **SF11 Glass:** A dense flint glass with a relatively high refractive index, which can enhance SPR sensor sensitivity. It is often used in applications that require improved detection capabilities.
- **Fused Silica:** Known for its chemical resistance, low absorption, and high transmission from ultraviolet (UV) to infrared (IR) wavelengths. It is particularly useful in applications requiring specific interactions with certain media.

The refractive indices of these materials at **λ = 633 nm** are summarized in Table III.1.

Table III.1 Refractive indices for different glass materials used as prisms.

Material	**Refractive index (RIU)**	**Reference**
BK7	1.5151	[96]
SF11	1.7786	[96]
Fused Silica	1.4570	[97]

III.9.2. Photonic crystals

Photonic crystals are crystals that have a periodic optical index; there are three types of photonic crystals:

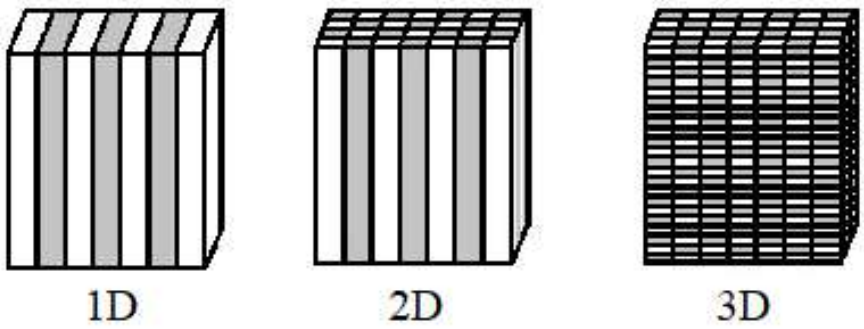

Figure III.2 Schematic representation of the different photonic crystal types [97].

- One-dimensional photonic crystal

A one-dimensional photonic crystal has periodicity in a single spatial direction. Each layer satisfies the **Bragg condition** $n.d = \lambda/4$ where:

n is the refractive index.

d represents the layer thickness.

λ is the incident light wavelength.

- Two-dimensional photonic crystal

In two-dimensional photonic crystals, periodicity occurs in two spatial directions, influencing light propagation accordingly.

- Tridimensional photonic crystal

Three-dimensional photonic crystals exhibit periodicity in all three spatial directions. The representation of the three PC types is illustrated in Figure III.2.

III.9.3. Metal

The two most commonly used metals in Surface Plasmon Resonance (SPR) are gold (Au) and silver (Ag).

Gold (Au) is widely favored due to its chemical stability and resistance to oxidation, making it an ideal choice for long-term applications in SPR-based sensors. Additionally, gold provides a consistent plasmonic response across a broad spectral range, which enhances sensor reliability [98]. Silver (Ag), on the other hand, is preferred for its superior optical properties, leading to sharper resonance peaks and higher sensitivity in SPR sensors [98]. However, silver is highly susceptible to oxidation and surface degradation, which can impact its performance over time.

To mitigate this issue, protective layers such as dielectric coatings (e.g., SiO_2, Al_2O_3) or alloying strategies are often employed to enhance its stability.

Other metals, such as Platinum (Pt) and Palladium (Pd), have been explored for specific applications, particularly in gas sensing due to their unique catalytic properties. However, their high optical absorption limits their efficiency in standard SPR configurations [99, 100].

Since the permittivity of metals is highly dependent on the incident wavelength, accurate modeling is crucial for predicting SPR behavior. Several theoretical models exist to describe metal permittivity, including:

- Drude Model: This model considers free electron movement in a metal and is widely used to approximate permittivity at longer wavelengths.
- Drude-Lorentz Model: Extends the Drude model by incorporating the effects of bound electrons, improving accuracy, particularly at shorter wavelengths.

- Drude Model

The Drude model, proposed by Paul Drude in 1900, is a classical approach to understanding the electrical and thermal conductivity of metals. It is based on the idea that conduction electrons can be treated as a free electron gas, moving within a lattice of fixed atoms. Although this approximation neglects quantum effects, it provides a fundamental understanding of the transport properties of metals.

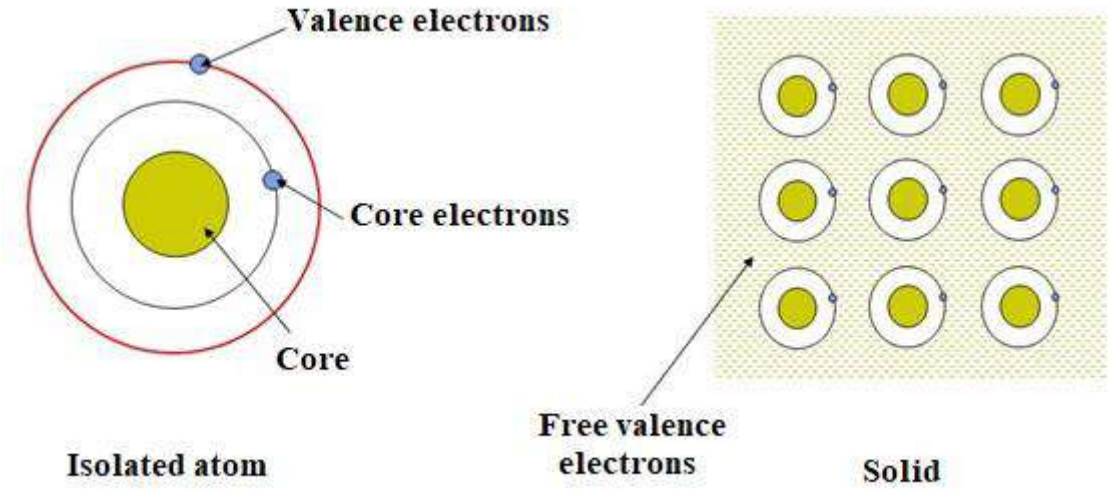

Figure III.3 The Drude model represented [99].

The model relies on the following assumptions:

- Free-electron approximation: Conduction electrons are treated as free particles moving within the metal without being bound to individual atoms.
- Scattering events: Electrons undergo random collisions with atomic cores, leading to a diffusive motion. These collisions are responsible for electrical resistance.
- Response to an external field: When an electric field E is applied, electrons acquire a drift velocity v_d, superimposed on their random thermal motion.

In the presence of an external electric field *E*, the motion of an electron of charge *e* and mass *m* is governed by the equation:

$$m\frac{dv}{dt} = -eE - \frac{m}{\tau}v \qquad (III.8)$$

where τ is the mean free time (the average time between two successive collisions). At steady state ($dv/dt = 0$), the drift velocity is given by:

$$v_d = -\frac{e\tau}{m}E \qquad (III.9)$$

The current density J is then given by Ohm's law:

$$J = \sigma E \qquad (III.10)$$

where the electrical conductivity σ is expressed as:

$$\sigma = \frac{ne^2\tau}{m} \qquad (III.11)$$

with n being the electron density.

The Drude model successfully explains several fundamental properties of metals, such as:

- Electrical conductivity: The model predicts that conductivity is proportional to the number of free electrons and their mobility.
- Thermal conductivity: It establishes a relationship between thermal and electrical conductivity, known as the Wiedemann-Franz law:

$$\frac{\kappa}{\sigma T} = \frac{\pi^2 k_B^2}{3e^2} \qquad (III.12)$$

where κ is the thermal conductivity, k_B is the Boltzmann constant, and T is the absolute temperature.

However, the Drude model is based on classical physics and fails to incorporate quantum mechanical effects, such as the wave nature of electrons and the Pauli exclusion principle. These limitations led to refinements, such as the Drude-Lorentz model, which incorporates elements of quantum mechanics to improve accuracy.

- The Drude-Lorentz Model

The Drude-Lorentz model is an extension of the classical Drude model, incorporating quantum mechanical principles to provide a more accurate description of electron behavior in metals. This refinement improves the understanding of electron-lattice interactions, energy dissipation, and the response of metals to electromagnetic waves.

Some of the key improvements of the Drude-Lorentz model include:

1- Quantum Nature of Electrons: Unlike the classical Drude model, which treats electrons as classical particles, the Drude-Lorentz model considers them as quantum entities that exhibit wave-particle duality, as described by de Broglie's hypothesis:

$$\lambda = \frac{h}{p} \qquad (III.13)$$

Where:

λ is the de Broglie wavelength.

h is the Planck's constant.

p is the electron momentum.

The modification makes the model more consistent with experimental observations, as it accounts for quantum mechanical effects.

2- Electron-Phonon and Electron-Impurity Scattering: In the Drude model, electron scattering was only considered as a result of random collisions with atomic cores. The Drude-Lorentz model refines this by incorporating:
   - Electron-phonon interactions (scattering with lattice vibrations),

- Electron-impurity interactions (scattering with structural defects or impurities).

To account for these interactions, a damping force (opposing motion) is introduced in the equation of motion:

$$m\frac{dv}{dt} = -eE - \gamma mv \qquad (III.14)$$

where γ represents the damping coefficient, which depends on the material's phonon structure and impurity density. The mean free time τ is now influenced by these additional scattering mechanisms:

$$\tau^{-1} = \tau_{phonon}^{-1} + \tau_{impurity}^{-1} \qquad (III.15)$$

where τ_{phonon} and $\tau_{impurity}$ are the mean free times for phonon and impurity scattering, respectively.

3- The Complex Permittivity and Electromagnetic Response: The Drude-Lorentz model improves the description of a metal's response to electromagnetic waves by refining the permittivity function. The Drude model describes the metal's dielectric function as:

$$\varepsilon(\omega) = \varepsilon_\infty - \frac{\omega_p^2}{\omega^2 + i\gamma\omega} \qquad (III.16)$$

where:

- $\varepsilon(\omega)$ is the frequency-dependent dielectric function,
- ε_∞ is the high-frequency permittivity (accounting for interband transitions),
- ω_p is the plasma frequency,
- γ is the damping factor (electron scattering rate),
- ω is the angular frequency of the incident wave.

This model predicts plasmonic resonances, which are critical for applications such as Surface Plasmon Resonance (SPR) sensors.

4- The Anomalous Skin Effect: One of the major advancements of the Drude-Lorentz model is its ability to explain the anomalous skin effect, which occurs when an electromagnetic wave penetrates a metal.

According to classical electrodynamics, the skin depth (δ) of a metal is given by:

$$\delta = \frac{c}{\sqrt{2\pi\sigma\mu\omega}} \qquad (III.17)$$

where:

- c is the speed of light,
- σ is the electrical conductivity,
- μ is the magnetic permeability,
- ω is the frequency of the electromagnetic wave.

In the Drude-Lorentz model, at high frequencies (THz to optical range), the electron mean free path becomes comparable to the skin depth. This causes a deviation from classical predictions, as the electron collisions no longer behave like a simple resistive medium, leading to the anomalous skin effect where:

$$\delta \propto \frac{1}{\omega^q}, q > 1 \qquad (III.18)$$

This effect is crucial in plasmonic applications and high-frequency metal optics.

III.9.4. Other Employed Materials

- Silicon Dioxide

Silicon dioxide (SiO_2), found in crystalline or amorphous forms, is widely utilized in surface plasmon resonance (SPR) sensors due to its ability to provide a functionalizable surface, enhance sensitivity and stability, and enable precise tuning of optical properties. These attributes establish SiO_2 as a critical material for advancing SPR sensor technology [101].

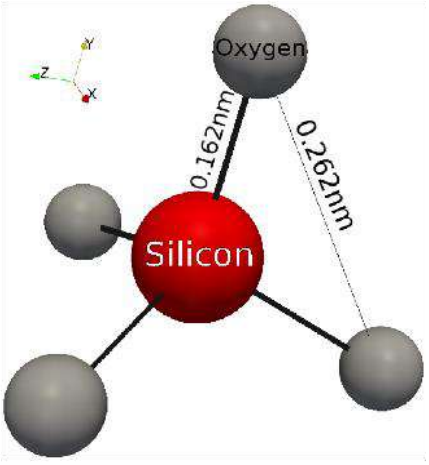

Figure III.4 Silicon dioxide structure [102].

The dispersion relation [102] gives the refractive index of silicon dioxide:

$$n^2 = 1 + \frac{0.6961663\lambda^2}{\lambda^2 - 0.0684043^2} + \frac{0.4079426\lambda^2}{\lambda^2 - 0.1162414^2} + \frac{0.8974794\lambda^2}{\lambda^2 - 9.896161^2} \quad (III.19)$$

- Transition Metal Dichalcogenides

Transition Metal Dichalcogenides (TMDCs) are increasingly employed in surface plasmon resonance (SPR) sensors owing to their compelling properties, including ease of fabrication and the ability to tune their electronic and optical characteristics by controlling the number of layers [103]. The integration of these materials has facilitated the development of ultra-sensitive SPR sensors, significantly enhancing detection capabilities [104].

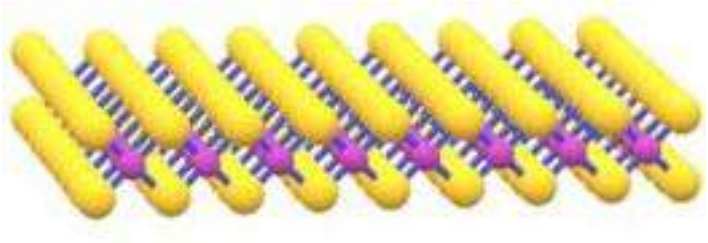

Figure III.5 Structure of a TMDC [103].

Among the TMDCs, our focus has primarily been on platinum diselenide ($PtSe_2$), which is utilized in SPR sensors. It can be combined with other materials, such as silicon dioxide or black phosphorus, to design highly sensitive hybrid sensors. Its complex refractive index at λ = 633 nm is given as [105]:

$$n = 3.4473 + 1.9113 * i \quad (III.20)$$

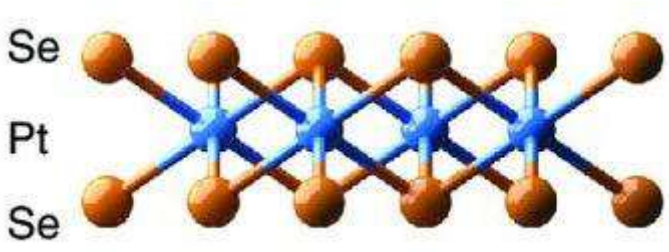

Figure III.6 Platinum diselenide structure [106].

- Black Phosphorus

Black Phosphorus (BP) is a two-dimensional material that has attracted considerable attention across various scientific fields due to its remarkable electrical properties, notably its layer-dependent bandgap, which varies from approximately 2 eV to 0.3 eV. Its refractive index is reported as 3.5 + 0.01i for a layer thickness of 0.53 nm per layer [107].

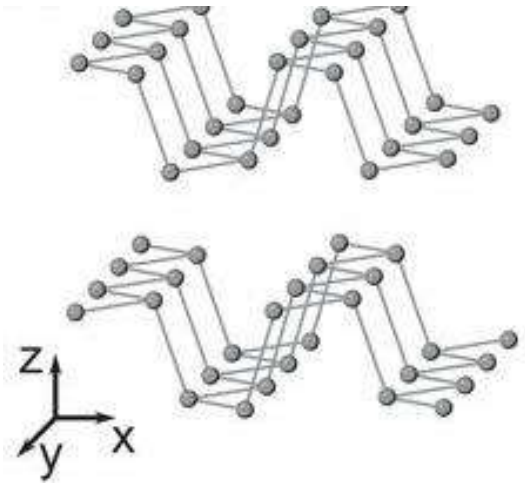

Figure III.7 Structure of two layers of BP [108].

- Rhodium

Rhodium (Rh) is an excellent choice for use in bimetallic layers in combination with silver, a configuration that can enhance the sensitivity of SPR sensors, particularly in gas sensing applications. Rhodium exhibits favorable optical properties for the desired interactions, is chemically stable, and is sufficiently robust to ensure high sensor performance even under extreme conditions.

The complex refractive index of rhodium at λ = 633 nm is given as:

$$n = 2.1520 + 5.6102 * i \qquad (III.21)$$

- Gallium Arsenide

Gallium Arsenide (GaAs) is a semiconductor renowned for its high-frequency performance and optoelectronic properties. It is employed in SPR sensors due to its high sensitivity, direct bandgap characteristics, versatility in coating processes, compatibility with photonic devices, and ongoing research advancements that continue to expand its applications in detection technologies.

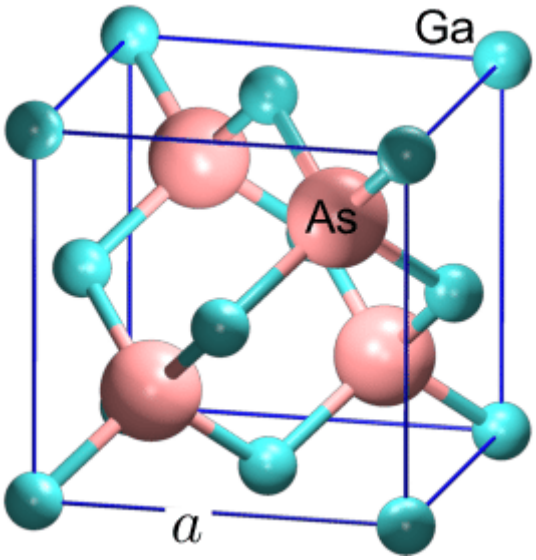

Figure III.8 Representation of gallium arsenide structure [109].

For incident light at a wavelength of 633 nm, the refractive index of GaAs is given by [109]:

$$n = 3.8571 + 0.19814 * \mathrm{i} \qquad (III.22)$$

- Magnesium Fluoride

Magnesium Fluoride (MgF_2) is a crystalline inorganic material widely used in optics. It is typically available in the form of transparent crystals and exhibits excellent light transmission throughout the ultraviolet-visible spectrum. Its superior optical properties and robustness make it particularly suitable for various applications, including SPR sensors.

In these devices, MgF_2 ensures optimal light transmission essential for the detection of biomolecules while minimizing losses due to reflection or absorption. The refractive index of MgF_2 is 1.4212 [110].

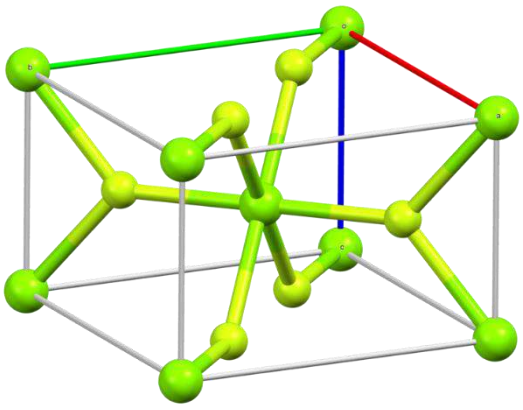

Figure III.9 Structure of MgF_2[110].

- Zinc Monoxide

Zinc Oxide (ZnO) is an inorganic compound with a range of properties that make it highly valuable for multiple applications. Commonly encountered as a white powder, ZnO is known for its high transparency, elevated electron mobility, and wide bandgap (~3.3 eV), which renders it a material of choice for researchers and engineers in many fields [111].

ZnO crystallizes primarily in two forms: hexagonal wurtzite and cubic zinc blende. Due to its optical and electronic properties, ZnO is extensively used in SPR sensors for biomolecule detection, where its wide bandgap and strong light-matter interactions contribute to improved precision and sensitivity in these devices.

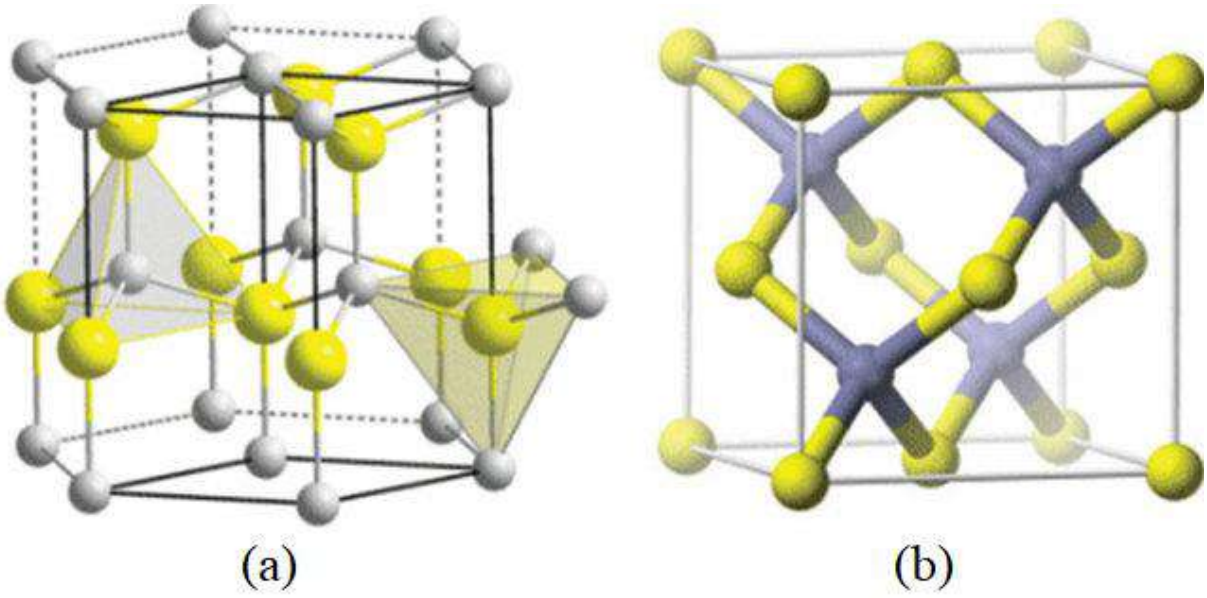

Figure III.10 The two main ZnO structures (a) hexagonal wurtzite and (b) cubic zinc blende [111].

III.10. SPR Sensors Optimization

Optimizing Surface Plasmon Resonance (SPR) sensors is a critical challenge for enhancing their sensitivity, precision, and selectivity. Numerous approaches have been proposed, including the integration of novel materials and modifications to the sensor structure. For example, Taya et al. investigated the effect of incorporating a layer of $BiFeO_3$ and graphene into an SPR sensor and demonstrated that this configuration significantly enhances the device's sensitivity [112]. Recent research has focused on selecting the appropriate materials for the

desired application, as the choice of metal and dielectric directly influences sensor performance. Moreover, fine-tuning the thickness of the various layers is essential to optimize the sensor structure and deliver improved results.

In addition to material and structural optimization, enhancing the stability and reproducibility of SPR sensors is crucial for ensuring consistent and precise performance under varying environmental conditions. Strategies to achieve this include optimizing the hardware design by integrating optical filters, error-correction mechanisms, and signal amplification techniques, all of which contribute to a reduction in noise [113]. Improvements in circuit design further strengthen sensor stability, while the careful selection of robust casings and materials minimizes mechanical stress and sensitivity to environmental fluctuations, thereby extending the sensor's longevity.

Furthermore, optimization efforts also encompass the development of advanced optical interrogation techniques—whether angular, spectral, intensity, or phase-based—that enable high-resolution detection and real-time monitoring. The integration of microfluidic technology into sensor designs plays a vital role by providing controlled sample delivery and reducing measurement variability. Collectively, these strategies pave the way for next-generation SPR sensors with enhanced sensitivity, stability, and functionality, making them highly effective for applications in biosensing, environmental monitoring, and chemical detection.

Conclusion

This chapter underscored the importance of numerical methods—particularly the transfer matrix method (TMM)—in the optimization of surface plasmon resonance (SPR) sensors. The application of TMM, especially within the MATLAB programming environment, provides a powerful tool for analyzing, designing, and enhancing the performance of SPR sensors. This method enables precise modeling of electromagnetic interactions and facilitates the optimization of structural parameters, which is essential for improving sensor sensitivity, resolution, and overall efficiency.

In addition, the selection of materials, the optical configuration, and the fabrication techniques play crucial roles in advancing SPR sensor performance. The integration of advanced nanomaterials and the use of high-precision manufacturing methods lead to more effective SPR sensors that are suitable for a wide array of applications, including biomedicine, chemistry, physics, and the agri-food sector. In summary, this chapter highlights the synergies between numerical methodologies and material innovations, which are vital for the development of advanced SPR sensors. These advancements pave the way for broader applications in molecular

detection, thereby reinforcing the importance of SPR sensors in scientific fields such as biotechnology and environmental monitoring.

Chapter IV

Design and Optimization of Biosensors Based on Photonic and Plasmonic Materials

Introduction

Biological sensors based on SPR are designed to measure (detect) a single parameter, such as the presence of a specific molecule in a sample or its concentration. These sensors are widely used across various fields. Consequently, it is important to design an SPR sensor for different applications in any given domain. This chapter examines several SPR sensors, both single-function and dual-function. To achieve this, the various components of the sensor are studied and modified to meet the requirements of the desired application.

IV. Design and Optimization of Biosensors Based on Photonic and Plasmonic Materials

IV.1. First Sensor: Application for Water Quality Control

IV.1.1. Schematic of the SPR Sensor

The proposed sensor [114] is schematically represented in Figure IV.1. In this sensor structure, several types of glass were used as the prism to study the effect of the prism material on the overall sensor behavior, thereby determining the optimal configuration. The chosen configuration consists of a BK7 glass prism overlaid with a 50 nm thick gold (Au) layer, a thin 0.7 nm layer of silicon dioxide (SiO_2), 2 nm of $PtSe_2$, and three layers (3 × 0.53 nm) of black phosphorus (BP).

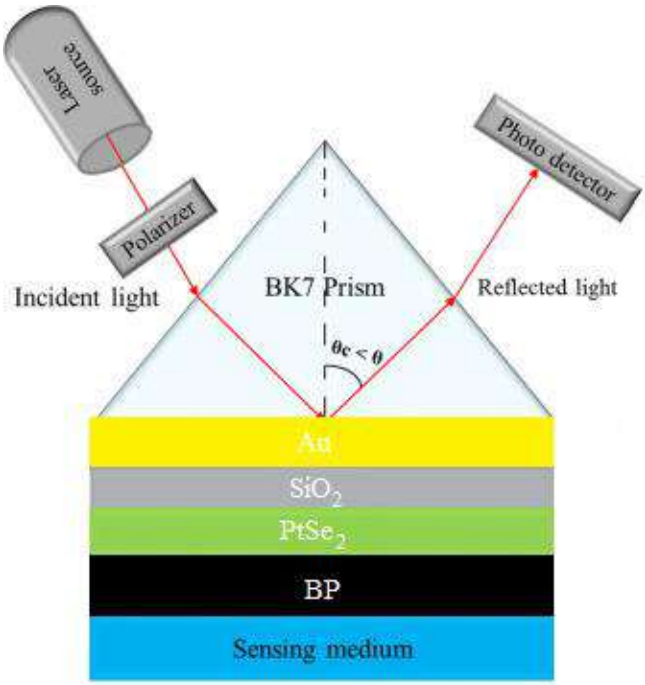

Figure IV.1 Design of the proposed SPR sensor (Ouardi et Al. [114]).

The variation in the thickness of the $PtSe_2$ layer led to an improvement in angular sensitivity by approximately 35% and over 70% compared to a conventional SPR sensor (BK7/gold). The comparison between the proposed sensor and the conventional gold sensor is shown in Figure IV.2.

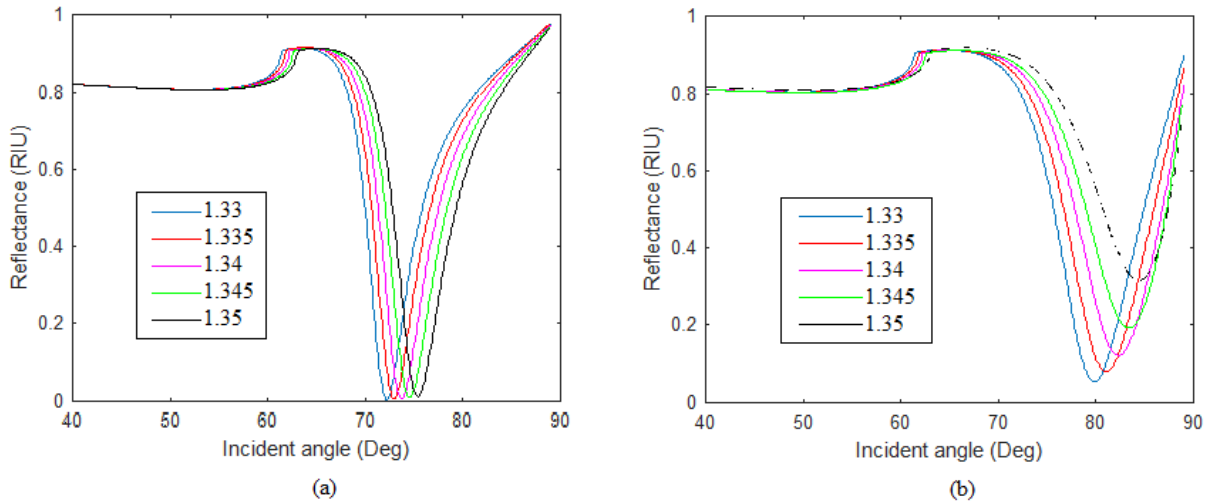

Figure IV.2 Variation of reflectance as a function of incidence angle for (a) the conventional gold-based sensor; and (b) the proposed sensor (Ouardi et Al. [114]).

IV.1.2. $PtSe_2$ Layer Thickness Effect

The thickness of each layer—whether metallic or dielectric—significantly affects the sensor's performance parameters. For example, the platinum diselenide layer is examined in detail in Figures IV.3 and IV.4.

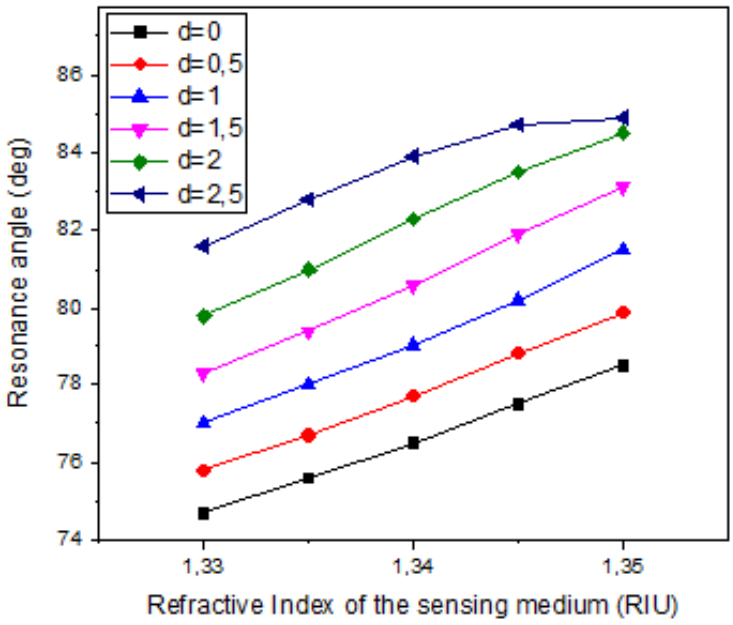

Figure IV.3 Change in resonance angle as a function of refractive index of the medium for different thicknesses of PtSe2 (in nm) (Ouardi et Al. [114]).

Figure IV.3 illustrates that the resonance angle shifts to higher values as a function of the refractive index, except for d = 2.5 nm.

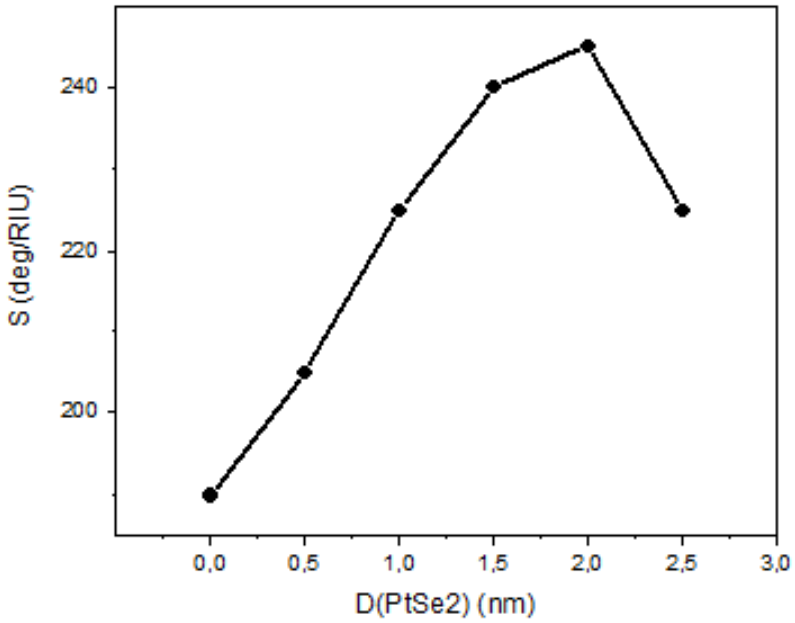

Figure IV.4 Variation of sensitivity (S) of the proposed sensor for different thicknesses of PtSe2 (Ouardi et Al. [114]).

The maximum sensitivity is achieved for a $PtSe_2$ thickness of 2 nm.

Angular sensitivity is not the only performance metric influenced by the thickness of the sensor layers; Table IV.1 details the effect of $PtSe_2$ thickness on the other performance parameters of the sensor.

Table IV.1 Performances of the SPR sensor relative to the PtSe2 layer thickness (Ouardi et Al. [114]).

$PtSe_2$ thickness (nm)	Resonance angle (deg)	Angular sensitivity (deg/RIU)	FWHM (deg)	Figure of Merit (RIU^{-1})
0	74.7	180	7.03	25.6
0.5	75.8	180	7.44	24.2
1	77	200	7.95	25.2
1.5	78.3	220	9.77	22.5
2	79.8	240	8.91	26.9
2.5	81.6	165	10.4	15.86

Based on the data provided by Figures IV.2 to IV.4 and Table IV.1, the best result is obtained with BK7 as the prism, 50 nm of gold, 0.7 nm of SiO_2, 2 nm of $PtSe_2$, and three layers of BP (3 × 0.53 nm). This configuration offers a maximum sensitivity of 240 deg/RIU with a figure of merit of 26.9 RIU^{-1}.

Thus, according to the results provided by this structure, the SPR-based sensor is capable of measuring water purity (potable or otherwise). It can detect changes in the ambient refractive index on the order of 0.005. A change in the refractive index implies a change in the composition of the medium, meaning that an SPR-based device can serve as a healthy water sensor for various applications. (This study was presented at the 10th National Seminar on Lasers and Their Applications (SENALAP'10) organized at the University of Science and Technology Houari Boumediene in Algiers [114]).

IV.2. Second Sensor: Detection of Alcohol Content in Water by Surface Plasmon Resonance

In this section, a new configuration of an SPR-based sensor is investigated. Based on key elements of surface plasmon resonance and its sensors—namely, silver, black phosphorus, and silicon dioxide—this sensor is designed as a tool to measure the alcohol concentration in water. This application is particularly relevant for quality control purposes, and it also holds potential for medical use in the context of allergies [115].

IV.2.1. Schematic of the SPR Sensor

The configuration of the proposed sensor is illustrated in Figure IV.5. In this structure, a simple configuration is employed (BK7/Ag/BP/SiO_2).

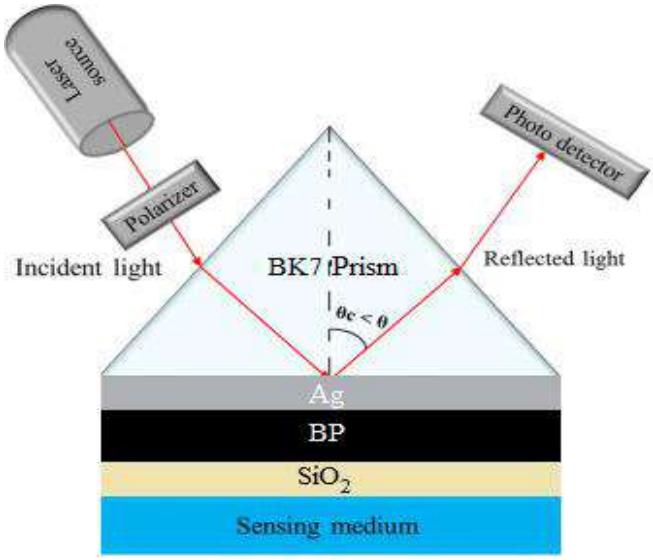

Figure IV.5 Representation of the proposed SPR sensor (Ouardi et Al. [123]).

The selection of the materials constituting the SPR biosensor was strategic and based on several considerations. Regarding the choice of silver, it offers a cost-effective option compared to gold for such applications [116], despite its chemical instability—a problem that must be addressed. Furthermore, sensors incorporating silver have demonstrated higher sensitivity in the literature compared to those based on gold, across various wavelengths in the visible spectrum.

For silicon dioxide, its inclusion serves primarily as a protective layer; by applying a SiO_2 layer, the risk of silver oxidation is mitigated, with the dielectric acting as a shield against external factors. Additionally, silicon dioxide has a relatively low refractive index (1.4721 for an incident light wavelength of 633 nm), which helps optimize the conditions for plasmon resonance and thereby improves sensitivity to changes in the ambient refractive index. Its versatility is also notable, as SiO_2 can be utilized in various forms—such as thin films, nanospheres, or nanorods—providing flexibility in selecting the optimal structural configuration.

The use of black phosphorus (BP) is equally strategic. BP can be applied in layers as thin as 0.53 nm, allowing for the stacking of multiple layers to achieve enhanced performance. Numerous studies have demonstrated that BP significantly optimizes the sensitivity of SPR sensors when compared to other two-dimensional nanomaterials, making it a material of choice for improving the response of SPR-based biosensors [117]. In addition, its mechanical

flexibility makes BP an excellent option for applications involving contact with irregular surfaces, such as biological tissues.

After testing various combinations of the materials, it was concluded that the optimal configuration for achieving the best SPR sensor response for the desired application consisted of 50 nm of silver, eight layers of black phosphorus (8 × 0.53 nm) deposited over 25 nm of silicon dioxide. The different combinations tested are shown in Tables IV.2, IV.3, and IV.4.

Table IV.2 The variation in sensitivity as a function of the number of BP layers (Ouardi et Al. [123]).

Number of BP layers	6	7	8	9
Sensitivity (Deg/RIU)	233	300	400	133

Table IV.3 Effect of the SiO_2 layer thickness on sensor sensitivity (Ouardi et Al. [123]).

SiO_2 layer thickness (nm)	15	20	25	30
Sensitivity (Deg/RIU)	300	366	400	100

Table IV.4 The impact of the silver layer thickness on the SPR sensor response (Ouardi et Al. [123]).

Silver layer thickness (nm)	40	45	50	55
Sensitivity (Deg/RIU)	266	333	400	233

The performance of the proposed biosensor was initially evaluated using water as the analyte (n = 1.33) to assess its capabilities. The SPR curve obtained for water is presented in

Figure IV.6. The sensor exhibited a sensitivity of 186 deg/RIU, a significant value that renders the proposed biosensor an interesting subject of study.

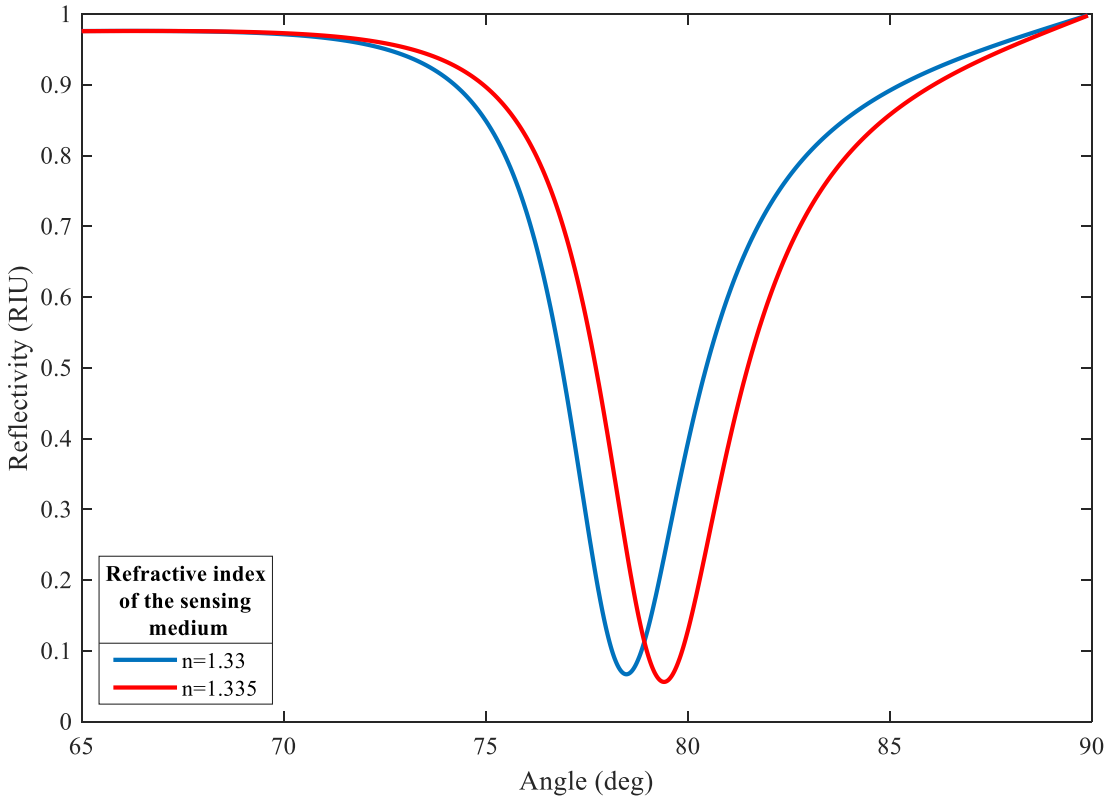

Figure IV.6 SPR curve of the proposed sensor with water as a sensing medium (Ouardi et Al. [123]).

The alcohol content in water was then investigated as a percentage; changes in alcohol concentration induce a variation in the refractive index of the water–alcohol mixture, as shown in Table IV.5 [118].

Table IV.5 Refractive index of the different concentrations of alcohol in water [118].

Alcohol-water content (%)	**Refractive index at 30°C**
0	1.333
10	1.3384
20	1.3450
30	1.3510
40	1.3550
50	1.3578
60	1.3597
70	1.3608
80	1.3611
90	1.3603
100	1.3573

Analyzing the SPR curves for each value listed in the table required calculating several performance factors, as described in Chapter II. The overall results for the studied biosensor are detailed in Table IV.6.

Table IV.6 Different performance parameters of the proposed SPR sensor (Ouardi et Al. [123]).

Alcohol percentage in water (%)	10	20	30	40	50	60	70	80	90	100
Sensitivity (Deg/RIU)	191	218	256	302	350	384	400	400	400	386
Figure of Merit	46.67	50.05	54.83	61.33	68.70	73.84	76.68	76.70	76.70	76.19
Q-factor	19.57	18.71	17.79	17.11	16.73	16.53	16.57	16.59	16.53	16.79
Signal-to-noise ratio	0.39	0.33	0.32	0.24	0.19	0.14	0.08	0.02	0.06	0.22
Limit of detection (RIU)	$10e^{-4}$	$9.9\ e^{-4}$	$9.1\ e^{-4}$	$8.1\ e^{-4}$	$7.2\ e^{-4}$	$6.7\ e^{-4}$	$6.5\ e^{-4}$	$6.5\ e^{-4}$	$6.5\ e^{-4}$	$6.5\ e^{-4}$

As can be observed, the SPR biosensor displays a remarkable response for the intended application, with a high sensitivity reaching up to 400 deg/RIU for concentrations above 70%. The SPR curves of the proposed sensor further elucidate its behavior, as illustrated in Figure IV.7.

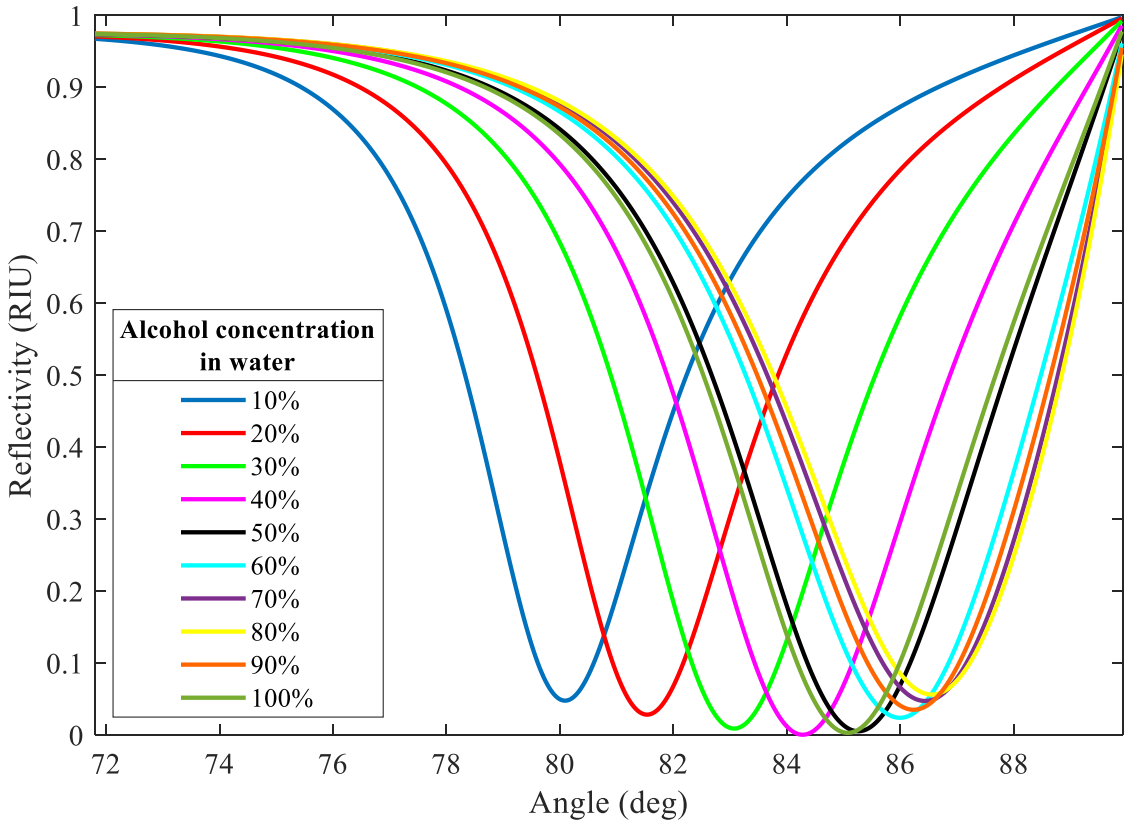

Figure IV.7 SPR curves for different alcohol concentrations in water (Ouardi et Al. [123]).

With an angular sensitivity of 400 deg/RIU and a figure of merit of 76.7 RIU^{-1}, the proposed SPR biosensor stands out compared to several previously reported sensors, which exhibited considerably lower sensitivity values, as summarized in Table IV.7.

Table IV.7 Comparison of the SPR sensor's sensitivity with anterior works.

Configuration	Sensitivity (Deg/RIU)	Reference
BK7/Ti/Ag/SiO_2/TiO_2	72	[119]
SF10/ZnO/Au/MoS_2/Graphene	101.6	[120]
SF10/Au/Si/MoS_2	126	[121]
BAK1/Ag/$BiFeO_3$/BPS	358	[122]
BK7/Ag/BP/SiO_2	400	Proposed work

This study culminated in an article published in *Plasmonics* (Springer) [123].

IV.3. Third sensor: Cancer Cell Detection

For this popular application of surface plasmon resonance, the transfer matrix method is employed to design a simple and cost-effective structure without compromising the efficiency of the SPR sensor or its ability to detect the presence of cancer cells in a given sample.

IV.3.1. Schematic of the SPR Sensor

The structure, based on the Kretschmann configuration, comprises a BK7 glass prism, a silver layer deposited atop a gallium arsenide (GaAs) layer. The key to achieving a high-performance sensor is to optimize the structural parameters of the configuration, such as the thicknesses of both layers, until a satisfactory result is obtained. Figure IV.8 illustrates a schematic representation of the proposed sensor.

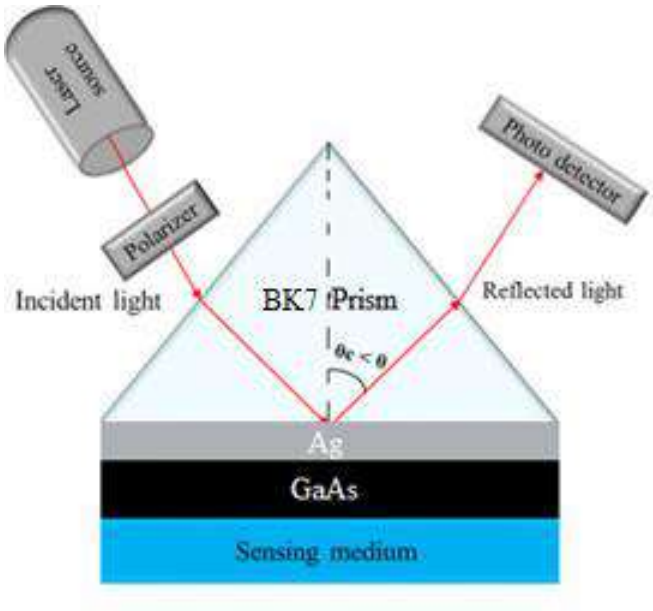

Figure IV.8 Structure of the proposed SPR sensor (Ouardi et Al. [127]).

Gallium arsenide appears to be a promising candidate for the intended application; this semiconductor exhibits a high refractive index, remarkable chemical stability, and excellent compatibility with optical detection [124]. The primary objective behind the design of this sensor is to detect various types of cancer cells using a single detector that is simple to fabricate, compact, highly efficient, and cost-effective.

The selection of the most effective SPR sensor is primarily based on its angular sensitivity and figure of merit. In pursuit of high values for these parameters, several configuration combinations were tested and analyzed—particularly by varying the thickness of

the GaAs layer while keeping the noble metal layer thickness fixed at 45 nm, a value that demonstrated a favorable response (see Figure IV.9).

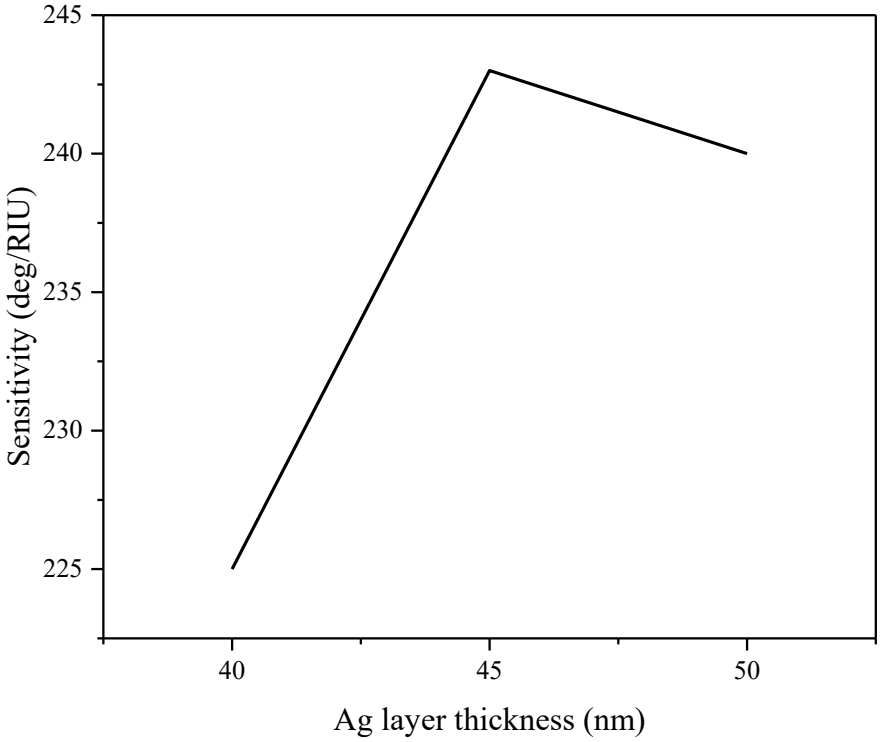

Figure IV.9 Sensitivity as a function of Ag layer thickness for the proposed sensor (Ouardi et Al. [127]).

It was observed that performance reaches its maximum for 45 nm of silver; this value was fixed for the metal layer thickness while the sensor's response was evaluated for various thicknesses of the semiconductor layer.

Table IV.8 Sensitivity according to the thickness of the GaAs layer (Ouardi et Al. [127]).

GaAs layer thickness (nm)	**1**	**2**	**3**	**4**
Sensitivity (deg/RIU)	169	196	243	189

According to the results of this study, the proposed SPR biosensor achieves optimal performance with 45 nm of silver and 3 nm of gallium arsenide, yielding a sensitivity of 243 deg/RIU and a figure of merit of 39.5 RIU^{-1}. Its behavior can then be further examined by plotting the SPR curve for different refractive index values corresponding to each type of cancer cell.

Table IV.9 Performance parameters of the suggested SPR sensor for different types of cancer cells (Ouardi et Al. [127]).

Cancer cell type	**Refractive index**	**Sensitivity (deg/RIU)**	**Figure of merit (RIU^{-1})**
Zero (healthy cell)	1.35	/	/
Jurkat (T-cell leukemia)	1.39	211	36.0
HeLa (cervical cancer)	1.392	216	36.1
PC12 (pheochromocytoma)	1.395	226	36.7
MDA-MB-231 (breast cancer)	1.399	239	38.3
MCF-7 (breast cancer)	1.401	243	39.5

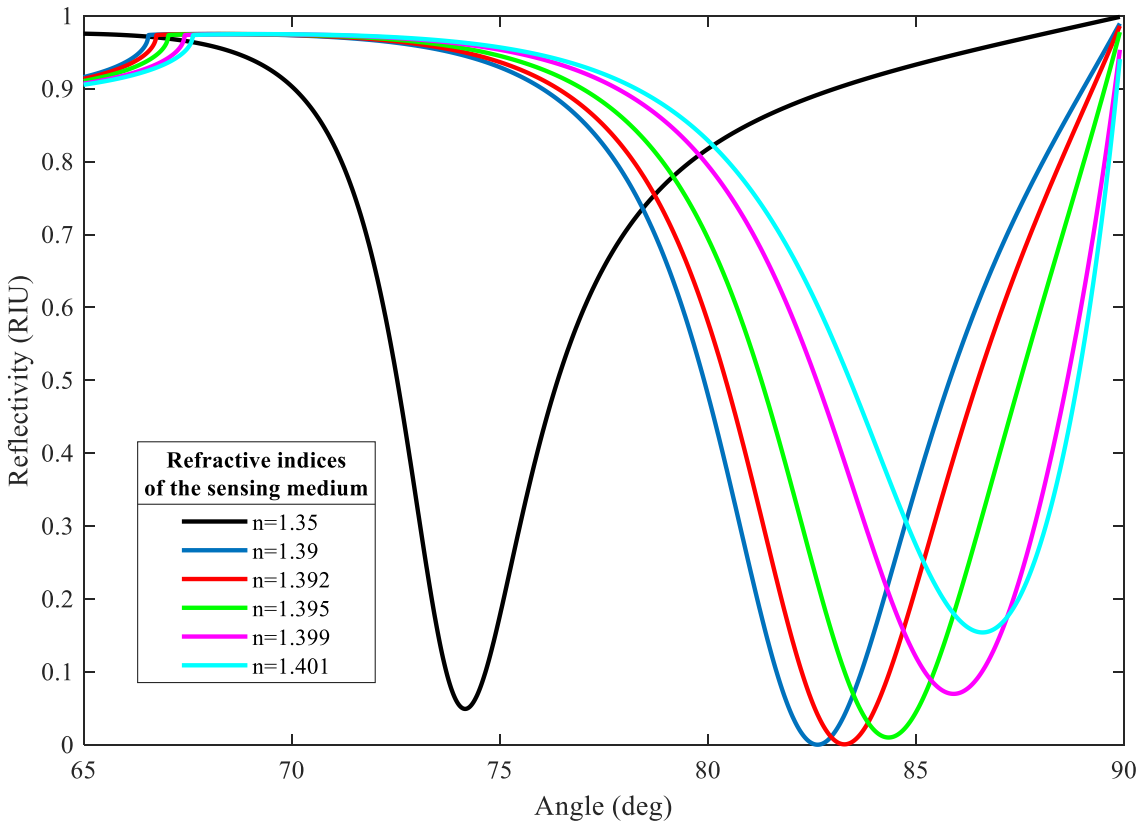

Figure IV.10 SPR curves of the proposed sensor for different cancer cell types (Ouardi et Al. [127]).

The results obtained with the SPR biosensor designed for cancer cell detection distinguish it from other sensors; a comparison between our sensor and those reported in previous studies is provided in Table IV.10. Notably, the proposed sensor exhibits superior sensitivity while maintaining a much simpler configuration.

Table IV.10 Comparison of the proposed SPR sensor with other works.

Configuration	**Sensitivity (Deg/RIU)**	**FoM (RIU^{-1})**	**Reference**
SF10/Au/Si/MoS_2	126	6.4	[121]
BK7/Ag/ MoS_2/Graphene	64.4	184	[126]
SF10/ZnO/Au/MoS_2/Graphene	101.6	15.1	[120]
BK7/Ti/Ag/SiO_2/TiO_2	72	346	[119]
BK7/Ag/GaAs	243	39.5	**Proposed sensor**

This SPR-based biosensor was the subject of a study presented at the third edition of the International Conference on Material Science and Engineering and Their Impact on the Environment (ICMSE'2024) at Djillali Liabès University in Sidi-bel-Abbes [127].

IV.4. Fourth Sensor: Blood Sugar Level Monitoring

For this fourth model, the detection of diabetes was the focus of our research, and designing an SPR sensor with high sensitivity is essential to ensure the device's practical utility.

IV.4.1. Schematic of the SPR Sensor

The proposed sensor, following the renowned Kretschmann-Raether configuration, is composed of a BK7 glass prism, two silver layers (0.5 nm and 45 nm, respectively) that sandwich a 0.5 nm rhodium layer, as well as six layers of black phosphorus (6 × 0.53 nm). The incident light (P-polarized) is set at a wavelength of 633 nm.

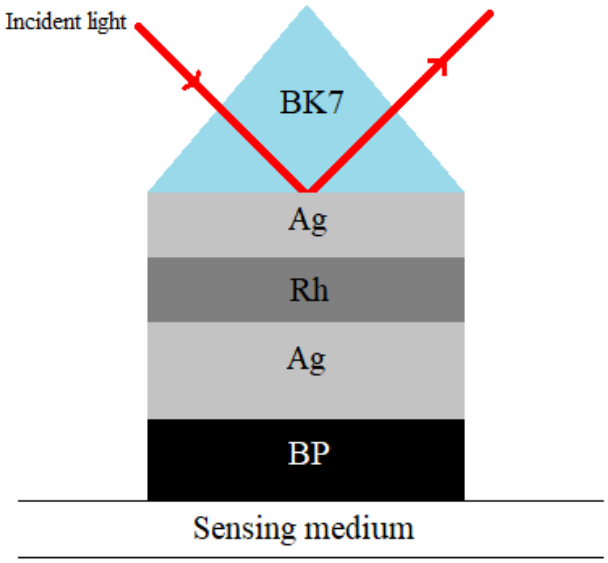

Figure IV.11 Representation of the proposed sensor (Ouardi et Al. [131]).

The sensor's reactivity to variations in blood glucose levels is studied, as the refractive index of the analyte is highly sensitive to changes in glucose concentration. Table IV.11 reports the statistical data from diabetic patients along with the refractive indices corresponding to each glucose concentration [128].

Table IV.11 Refractive indices relative to glucose concentrations in blood samples [128].

Glucose concentration		**Refractive index**
%	mM	
0	0	1.3391
0.13	7	1.3481
0.22	12	1.3572
0.31	17	1.3671
0.4	22	1.3765
1	55.5	1.3853
2	111	1.3940
3	166.6	1.4014

Using 0 mM glucose as the baseline for our study, any shift in the resonance angle is calculated relative to this reference. Figure IV.12 illustrates the SPR curve for 0 nM glucose, which reveals a resonance angle of 72.18°, a minimum reflectivity of 0.197 RIU, and a FWHM of 1.60°.

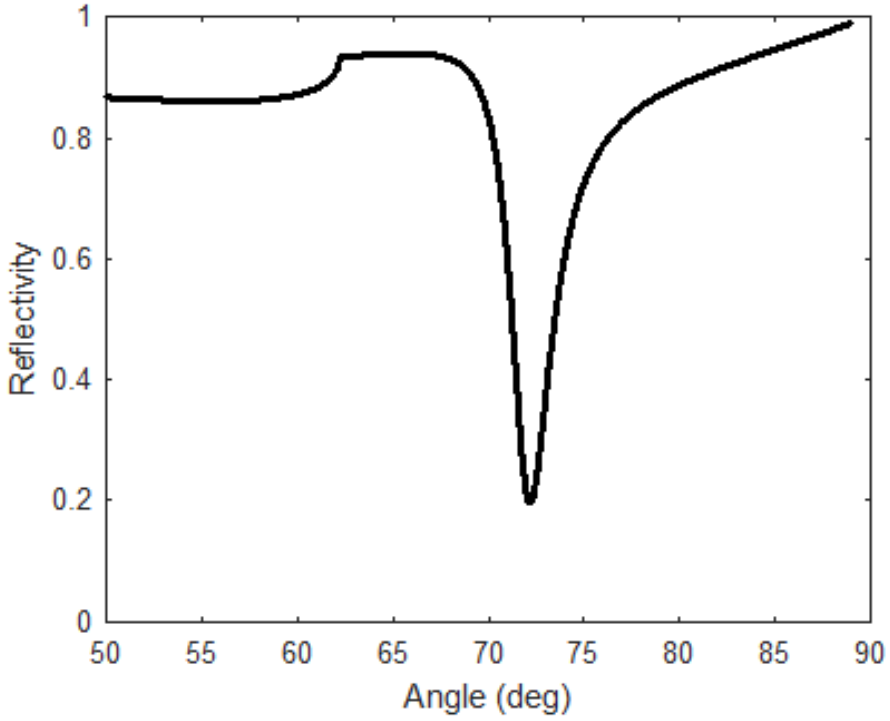

Figure IV.12 SPR curve of the studied sensor for a glucose concentration of 0% (Ouardi et Al. [131]).

The biosensor's ability to monitor blood glucose is determined by the shift in the resonance angle resulting from even minute changes in the target concentration.

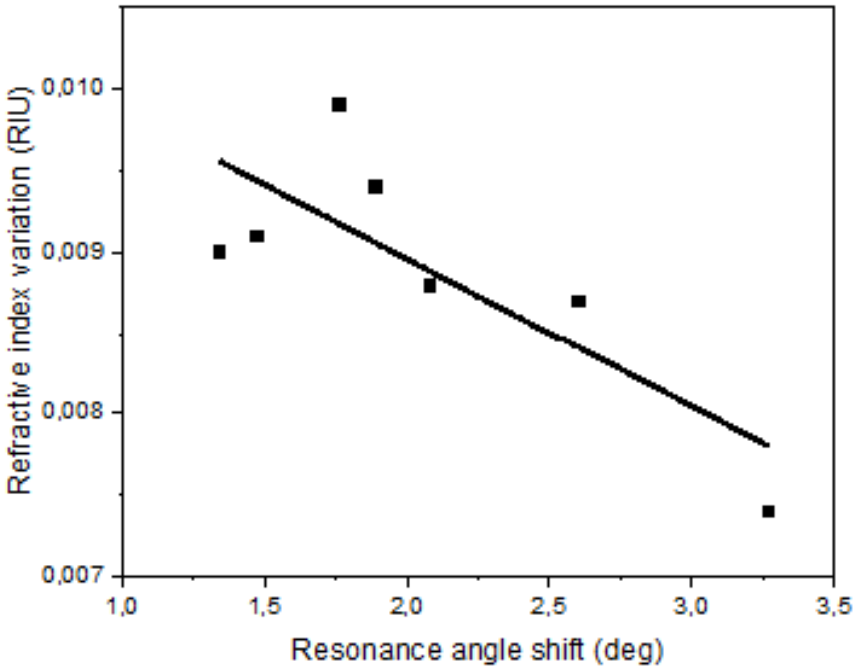

Figure IV.13 Resonance angle shift from 0% with respect to refractive index variation (Ouardi et Al. [131]).

The SPR sensor demonstrates a maximum sensitivity of 238 deg/RIU, a detection precision of 0.26, and a FWHM of 3.813°, resulting in a figure of merit of 62.4 RIU^{-1}. These performance metrics render the biosensor a reliable tool for capturing subtle variations in blood glucose levels.

Moreover, with a detection limit ranging from 0 to 7 mM, the proposed sensor is well-suited for monitoring normal blood glucose levels (i.e., less than 8 mM postprandially and less than 6 mM during fasting).

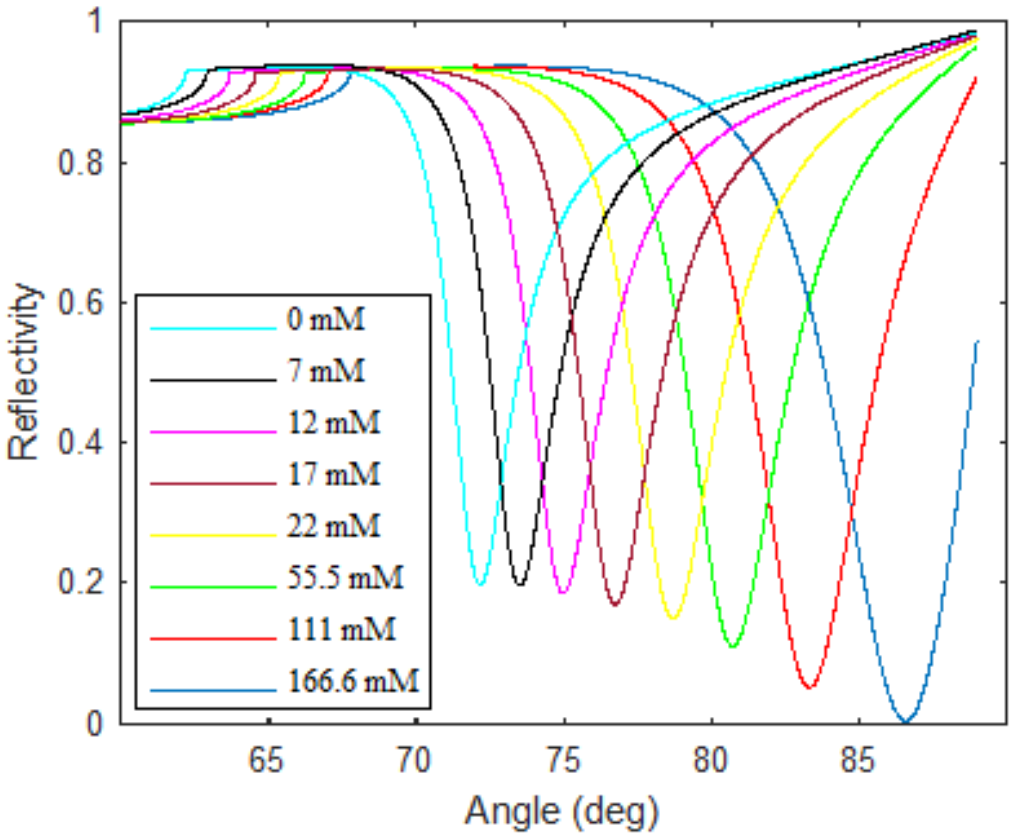

Figure IV.14 SPR curves of the proposed sensor for different glucose concentrations in blood samples (Ouardi et Al. [131]).

This sensor was the subject of a study presented at the International Conference on Engineering, Natural Sciences, and Technological Developments (ICENSTED 2024) in Erdek, Turkey [129].

IV.5. Fifth Sensor: Pregnancy Detection

The detection of the pregnancy hormone (HCG) in a urine sample enables the determination of whether a woman is pregnant, and SPR-based detection is indeed capable of achieving this. This capability arises from the fact that the refractive index of urine differs between pregnant and non-pregnant women. Although this difference is extremely small—on the order of 1/1000—it can be exploited to design an SPR-based biosensor for pregnancy detection.

IV.5.1. Schematic of the SPR Sensor

A 630 nm wavelength laser is used to direct a beam of light through a BK7 glass prism, beneath which are superimposed a layer of silver, a layer of magnesium fluoride (MgF_2), and multiple layers of black phosphorus (BP).

The inclusion of MgF_2 in this sensor is intended to enhance sensitivity and minimize the detrimental impact of the metallic layer on sensor performance. It acts as a stabilizing agent and has demonstrated excellent performance in other sensor configurations [130].

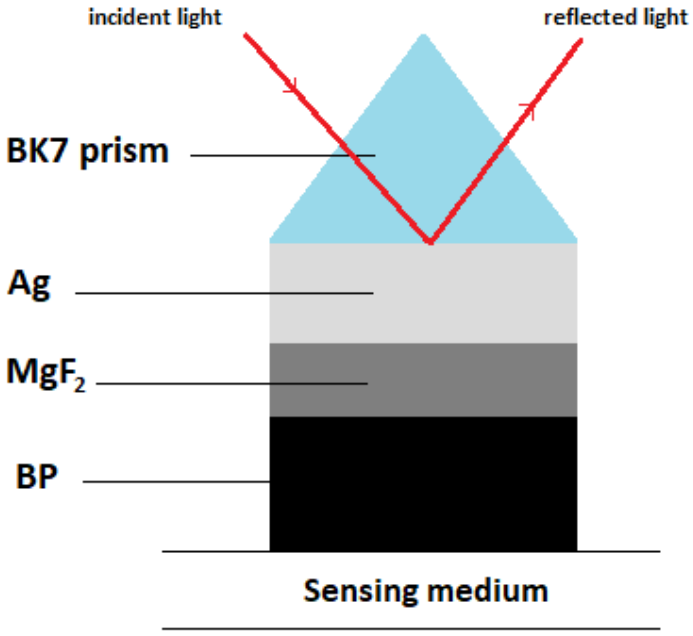

Figure IV.15 Representation of the SPR design (Ouardi et Al. [131]).

To determine the optimal thickness for each layer and the ideal number of BP layers needed to achieve the highest possible sensitivity, each parameter was studied individually by isolating one layer at a time, as illustrated in Figures IV.16 to IV.18.

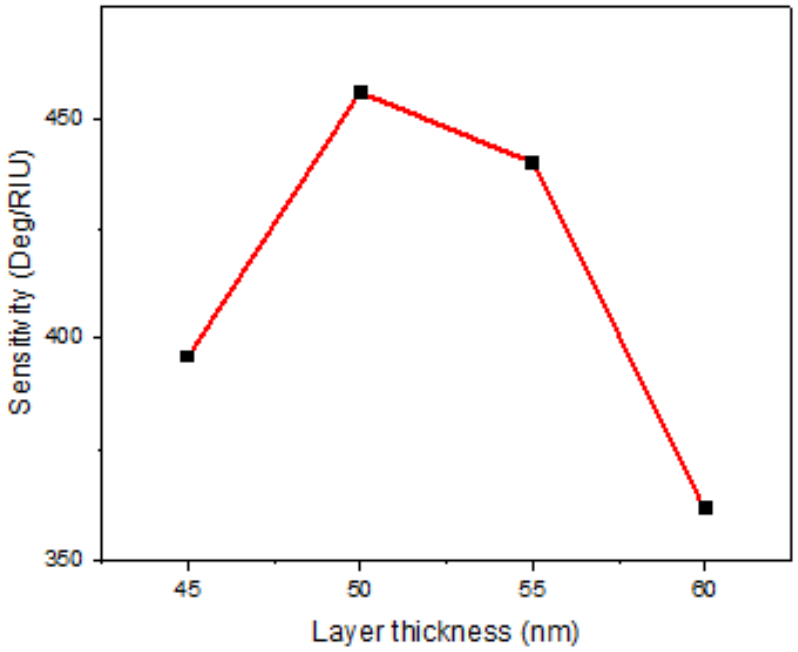

Figure IV.16 Sensitivity relative to Ag layer thicknesses (Ouardi et Al. [131]).

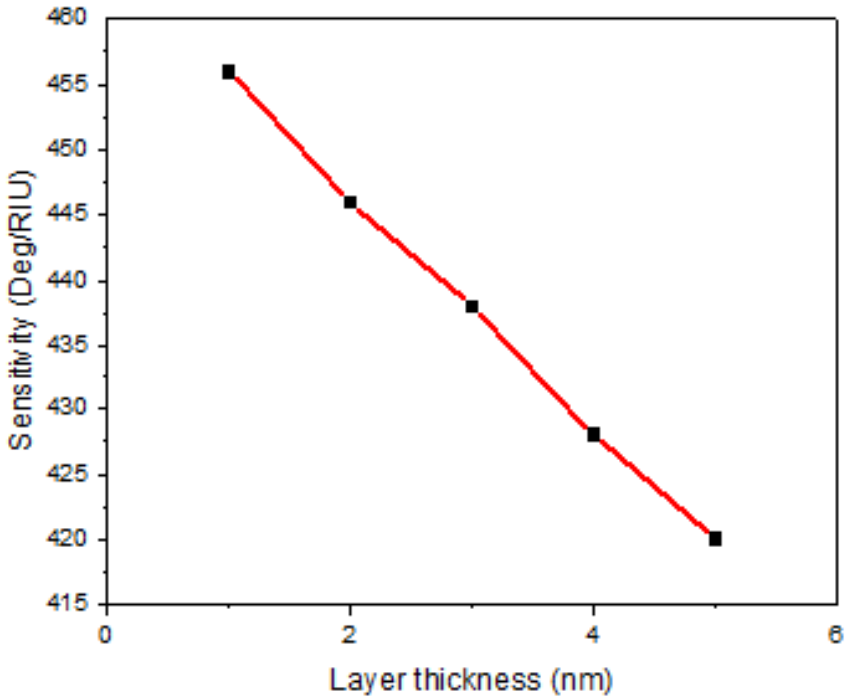

Figure IV.17 Sensitivity of the SPR sensor according to MgF_2 layer thickness (Ouardi et Al. [131]).

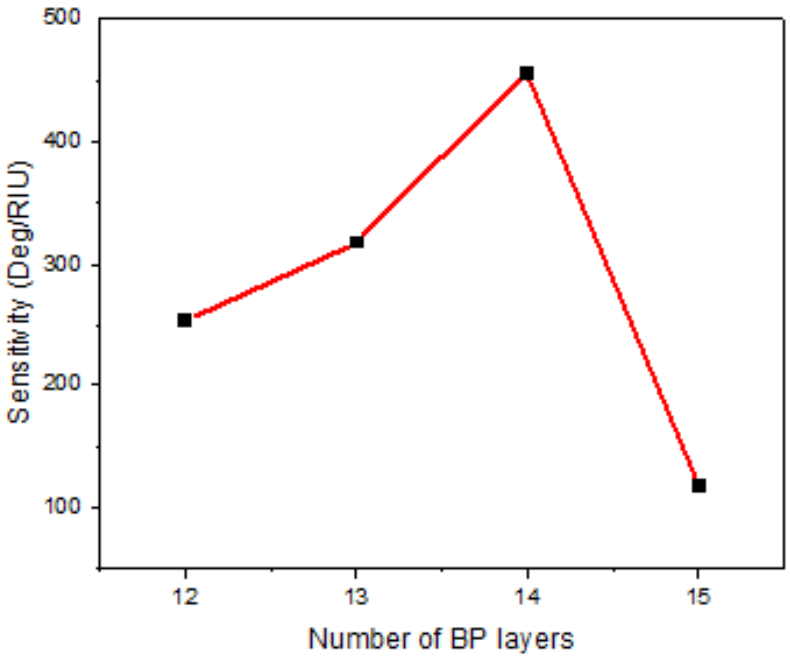

Figure IV.18 Sensitivity of the SPR sensor relative to the number of BP layers (Ouardi et Al. [131]).

The results indicate that the optimal Kretschmann-Raether configuration for pregnancy detection is: BK7/Ag (50 nm)/MgF_2 (1 nm)/BP (14 × 0.53 nm).

The refractive index of urine varies from 1.335 for non-pregnant women to approximately 1.342–1.343 for pregnant women. SPR curves were plotted for these refractive index values to graphically represent the sensor's response to such subtle changes (Figure IV.19).

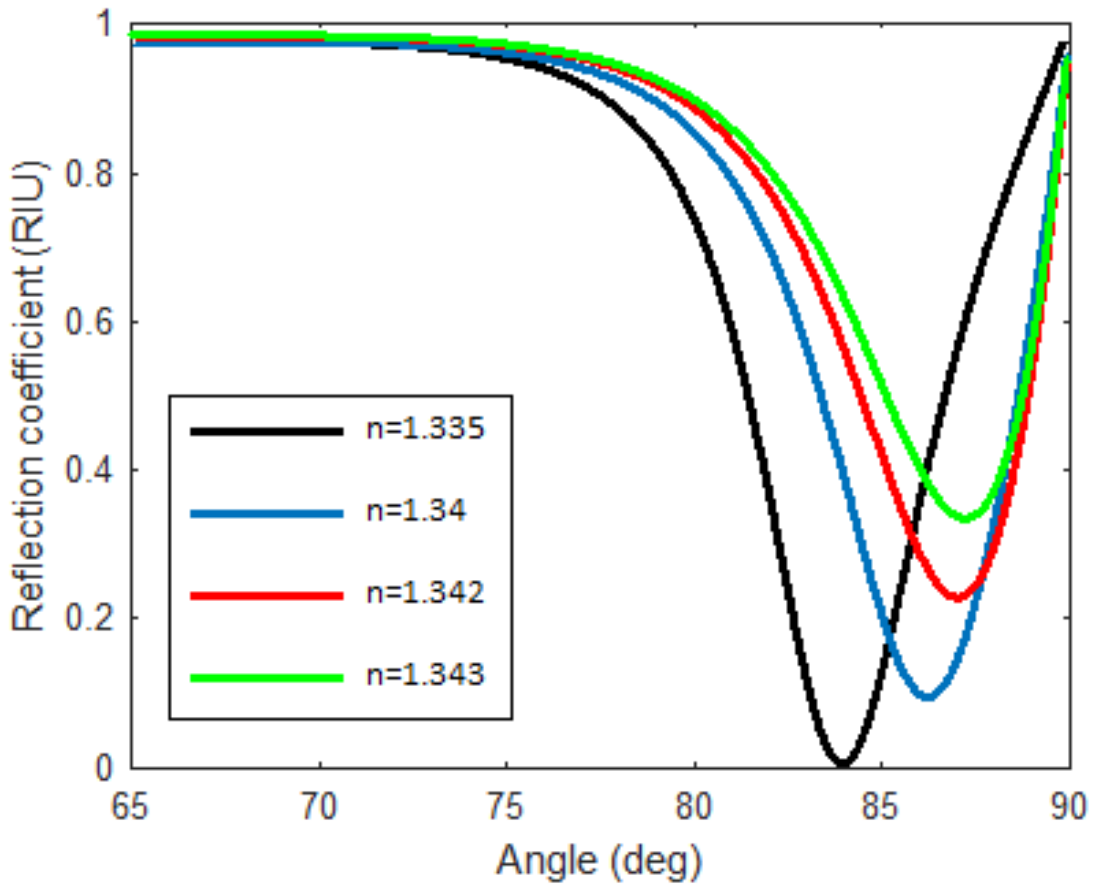

Figure IV.19 SPR curve of the studied biosensor (Ouardi et Al. [131]).

The SPR-based pregnancy test exhibits a maximum sensitivity of 456 deg/RIU, a detection precision of 0.18, and a figure of merit of 81.54 RIU^{-1}. In addition, the quality factor is measured at 15.48, the detection limit of the sensor is 6.13 RIU, and the signal-to-noise ratio is 0.41. These performance metrics are among the most impressive results achieved in our project, particularly for an application as critical as pregnancy detection. The exceptional sensitivity and reliability of the sensor have led to the publication of our work in the *Sensing and Imaging* journal [131].

IV.6. Sixth Sensor: Simultaneous Detection of Anemia and Diabetes

The study is now evolving to develop a dual-purpose sensor capable of analyzing two different samples: human blood and urine. Monitoring the hemoglobin levels in blood and the glucose levels in urine is crucial for detecting anemia and diabetes, respectively.

IV.6.1. Schematic of the SPR Sensor

For this application, a sensor based on the Kretschmann configuration has been proposed, comprising a BK7 glass prism, silver, silicon dioxide (SiO_2), zinc oxide (ZnO), and black phosphorus (BP). This sensor is designed to detect both chemical entities by utilizing their respective refractive indices [132].

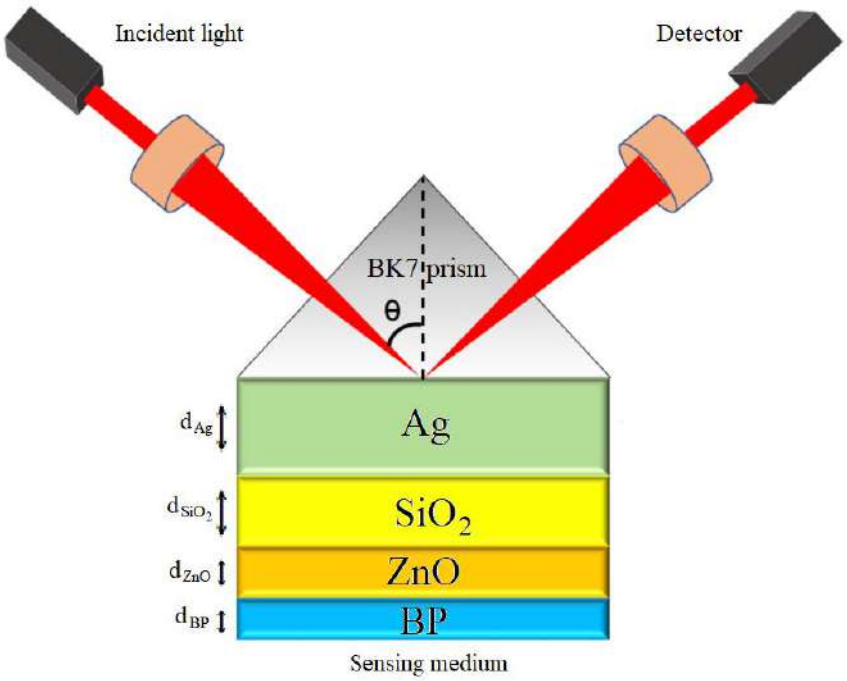

Figure IV.20 Schematic representation of the SPR sensor structure (Ouardi et Al. [135]).

According to R. S. Riley, the concentration of glucose in urine should range between 0 and 0.015 g/dl in a healthy individual; values above this threshold indicate diabetes [133].

Table IV.12 Refractive indices of different glucose concentrations in urine samples [133].

Glucose concentration in urine (g/dl)	Refractive index	Patient health
0-0.015	1.335	Healthy
0.625	1.336	Diabetic
1.25	1.337	
2.5	1.338	
5	1.341	
10	1.347	

For blood hemoglobin levels, Zhernovaya et al. have measured the refractive index values corresponding to each concentration [134].

Table IV.13 Refractive index corresponding to hemoglobin concentrations in blood samples (Ouardi et Al. [135]).

Hemoglobin concentration (g/l)	70	80	90	100	110	120	130	140
Refractive index	1.344	1.346	1.347	1.349	1.350	1.352	1.353	1.354

As shown in Tables IV.12 and IV.13, the refractive indices of both samples vary slightly with the concentration changes of the target biomolecules. This subtle variation necessitates the design of an optimized sensor that is highly sensitive and offers precise detection.

This study adopts a different perspective by focusing on the fact that the sensitivity of an SPR sensor is primarily associated with a maximal shift in the resonance angle while maintaining minimal reflectance. Therefore, optimizing the proposed sensor requires a thorough investigation of the thickness of each layer and its effect on these two critical parameters. Figures IV.21 and IV.22 illustrate this process by comparing configurations with a 1 nm thick ZnO layer against those without ZnO. Figure IV.21 examines the effect of varying the thickness of the silver layer while keeping the SiO_2 layer fixed at 6 nm, whereas Figure IV.22 investigates the reverse scenario, with the SiO_2 thickness varied and the silver layer fixed at 55 nm.

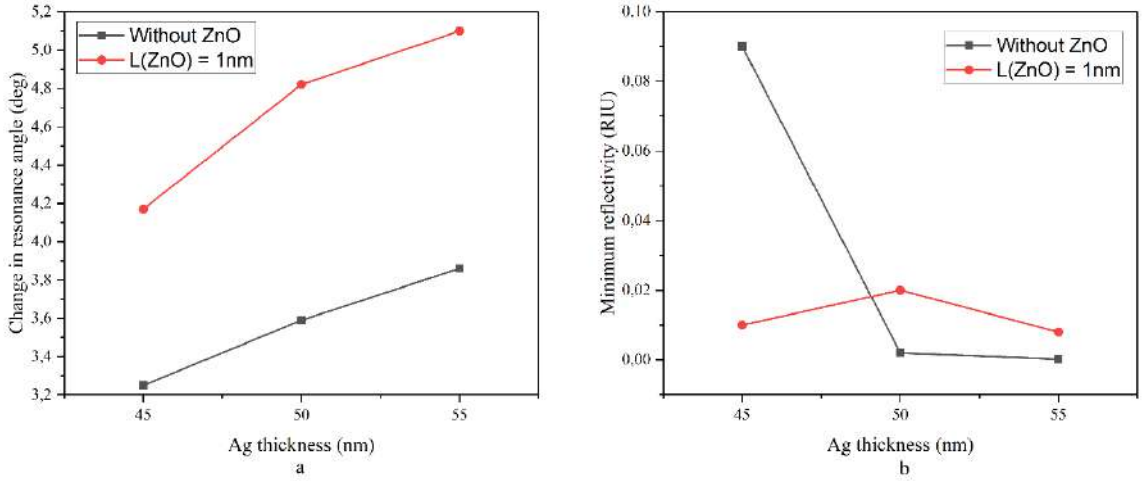

Figure IV.21 (a) Resonance angle and (b) minimum reflectance variations for different silver layer thicknesses (Ouardi et Al. [135]).

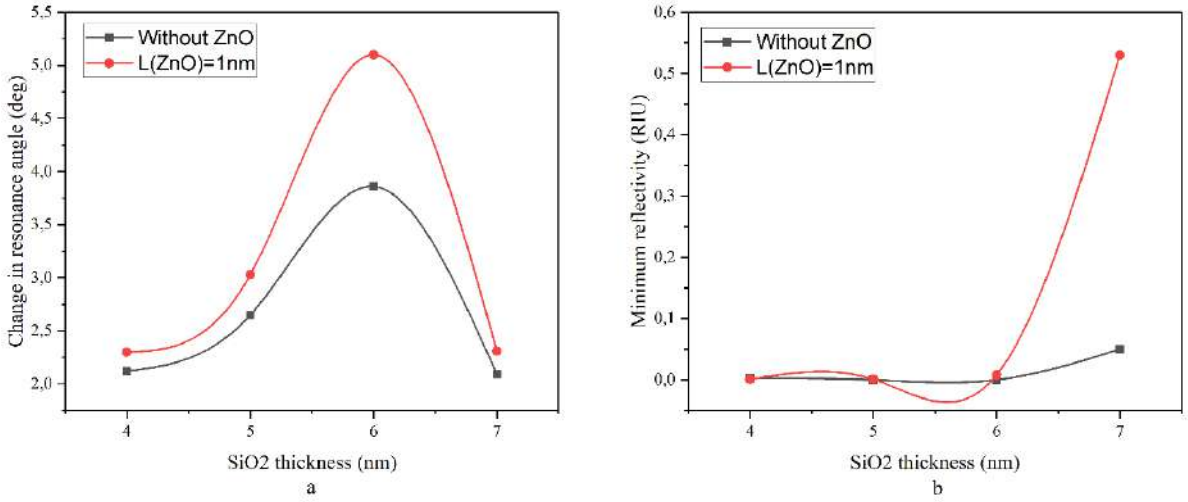

Figure IV.22 (a) Resonance angle and (b) minimum reflectance variations for different silicon dioxide layer thicknesses (Ouardi et Al. [135]).

The optimal configuration for this dual-purpose sensor was found to be 55 nm of silver, 1 nm of ZnO, and 6 nm of SiO_2. For the BP layer, a single layer (0.53 nm) is sufficient to enhance the sensor's sensitivity by over 60% compared to a sensor without BP; additional BP layers actually deteriorate performance. The SPR curve for this optimal configuration is presented in Figure IV.23.

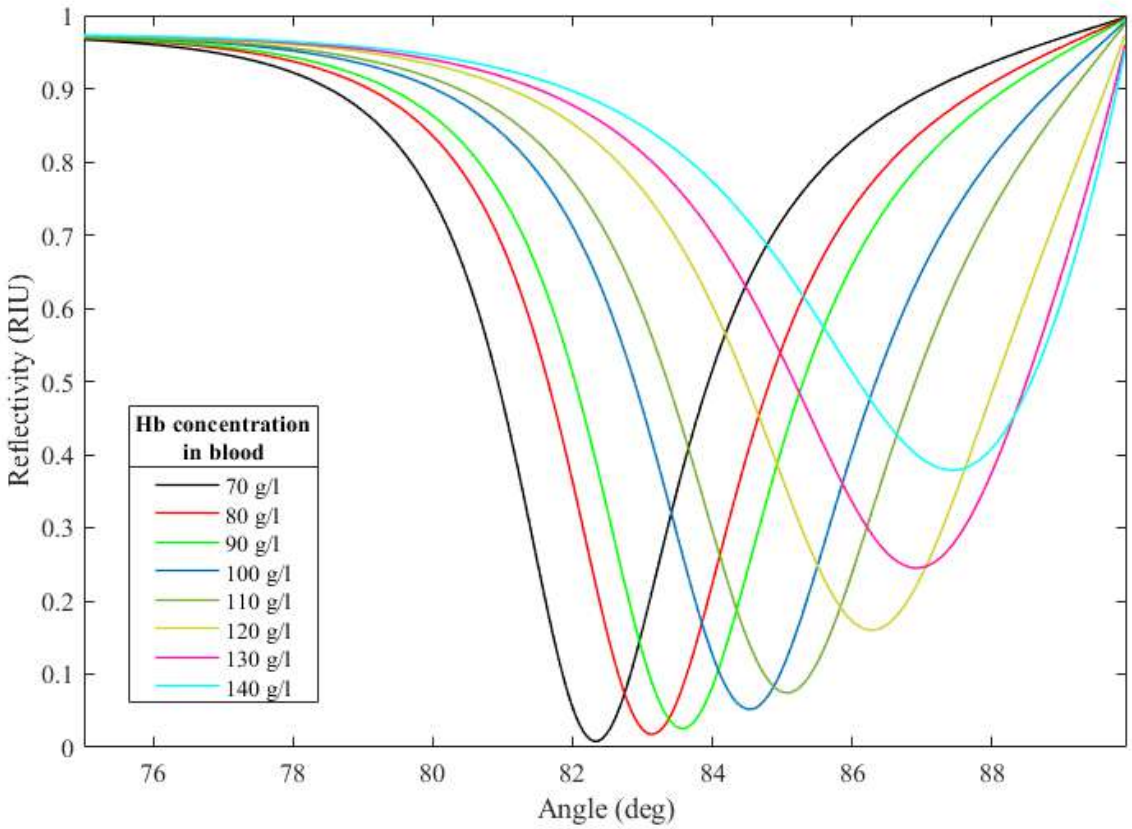

Figure IV.23 SPR curves of the proposed biosensor for hemoglobin level monitoring application (Ouardi et Al. [135]).

For the detection of anemia, the sensor exhibited excellent results, achieving a sensitivity of 640 deg/RIU and a figure of merit of 183.2 RIU^{-1}, with the remaining performance parameters summarized in Table IV.14 below.

Table IV.14 Performance parameters of the SPR sensor for different hemoglobin concentrations (Ouardi et Al. [135]).

Hemoglobin concentration (g/l)	**Sensitivity (deg/RIU)**	**Figure of Merit (RIU^{-1})**	**Q-factor**	**Limit of detection (deg)**
70	/	/	/	/
80	405	125.7	25.8	3.97 E-04
90	430	128.9	25.1	3.87 E-04
100	480	132.9	23.4	3.76 E-04
110	540	142.8	22.5	3.5 E-04
120	605	146.3	20.87	3.41 E-04
130	640	149.4	20.3	3.34 E-04
140	510	183.2	31.41	2.72 E-04

The same SPR sensor configuration provides acceptable results regarding the diabetes monitoring, SPR curves of the proposed sensor for glucose concentrations in urine samples are plotted in figure IV.24.

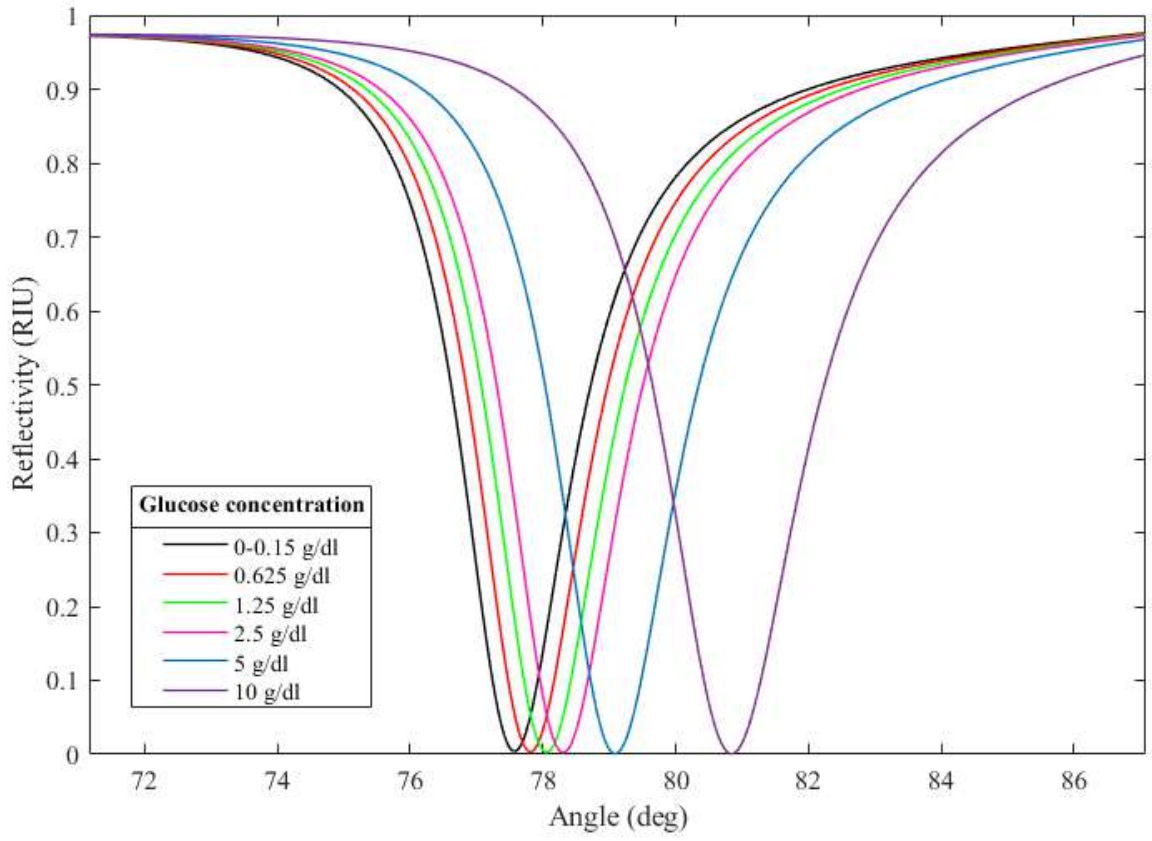

Figure IV.24 SPR curves of the SPR biosensor for glucose concentrations in urine application (Ouardi et Al. [135]).

Additionally, the sensor demonstrated very low minimum reflectance, a strong indicator of overall performance quality. When used for glucose detection in urine, the biosensor achieved a sensitivity of 291 deg/RIU and a high figure of merit (114.9 RIU^{-1}), with additional performance parameters for varying glucose concentrations detailed in Table IV.15.

Table IV.15 Performance parameters of the SPR sensor for different glucose concentrations in urine (Ouardi et Al. [135]).

Glucose concentration (g/dl)	**Sensitivity (deg/RIU)**	**Figure of Merit (RIU^{-1})**	**Q-factor**	**Limit of detection (deg)**
> 0.015	/	/	/	/
6.25	240	111.9	36.28	4.46 E-04
1.25	250	114.9	35.88	4.35 E-0.4
2.5	250	113.2	35.46	4.41 E-0.4
5	260	112.3	34.17	4.45 E-0.4
10	291	112.4	31.24	4.44 E-0.4

The exceptional performance of our sensor has been recognized through a publication in the journal *Plasmonics* [135], underscoring its potential impact in the fields of medical diagnostics and environmental monitoring. Moreover, the dual-use capability of this sensor not only broadens its applicability but also exemplifies how careful material selection and layer optimization can lead to multifunctional devices capable of addressing complex biomedical challenges.

IV.7. Seventh Sensor: Pesticide Detection

Moving into a field distinct from the medical sector, we now address agro-food, a domain critical to daily life and ecological balance. Pesticide detection is essential in agriculture and environmental protection since pesticides are primary tools for controlling pests and viral diseases. Their use is instrumental in increasing food production on limited land, thereby contributing to a more sustainable ecological equilibrium [136]. However, despite their advantages, pesticides can pose significant hazards to the environment and human health if misused, making strict adherence to safety protocols indispensable.

We propose, simulate, and study an SPR sensor specifically designed for pesticide detection, focusing on deltamethrin—a pyrethroid widely used to control various insects and worms [137]. The sensor is evaluated at the maximum permissible concentration of deltamethrin, defined as 25 mL of deltamethrin diluted in 10 liters of m-Xylene for up to three treatments [138–140]. The refractive index of the pesticide solution has been estimated using

the Gladstone-Dale approximation [141], a formula that allows one to estimate the refractive index of a mixture based on the refractive indices and volume fractions of its components:

$$n = \frac{\varphi_1 n_1 + \varphi_2 n_2}{\varphi_1 + \varphi_2} \qquad (IV.1)$$

Where n, n_1 and n_2 represent the refractive indices of the mixture, the first substance, and the second substance respectively, and φ_1 and φ_2 are their respective volume fractions.

IV.7.1. QSchematic of SPR sensor

For this study, the proposed sensor relies solely on the number of BP layers, as its structure consists only of a BK7 glass prism, a 50 nm silver layer, and layers of black phosphorus (BP), as shown in Figure IV.25.

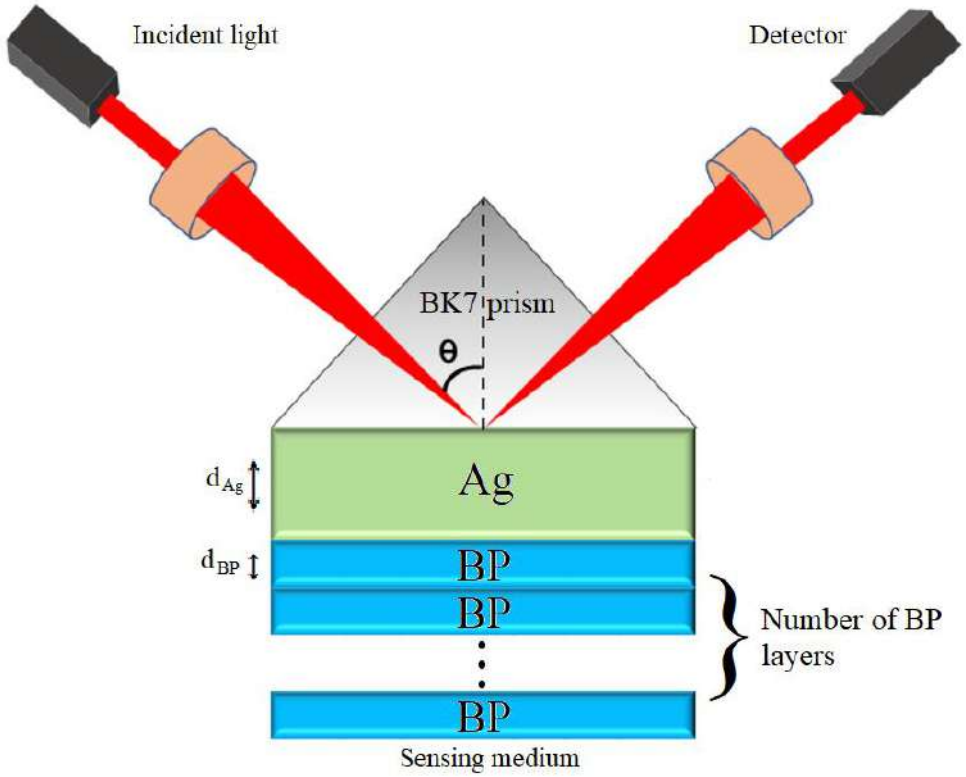

Figure IV.25 Schematic representation of the proposed SPR sensor (Ouardi et Al. [143]).

The baseline for our study is water (with n=1.333), representing a solvent with 0% deltamethrin. The corresponding SPR curve is plotted in Figure IV.26.

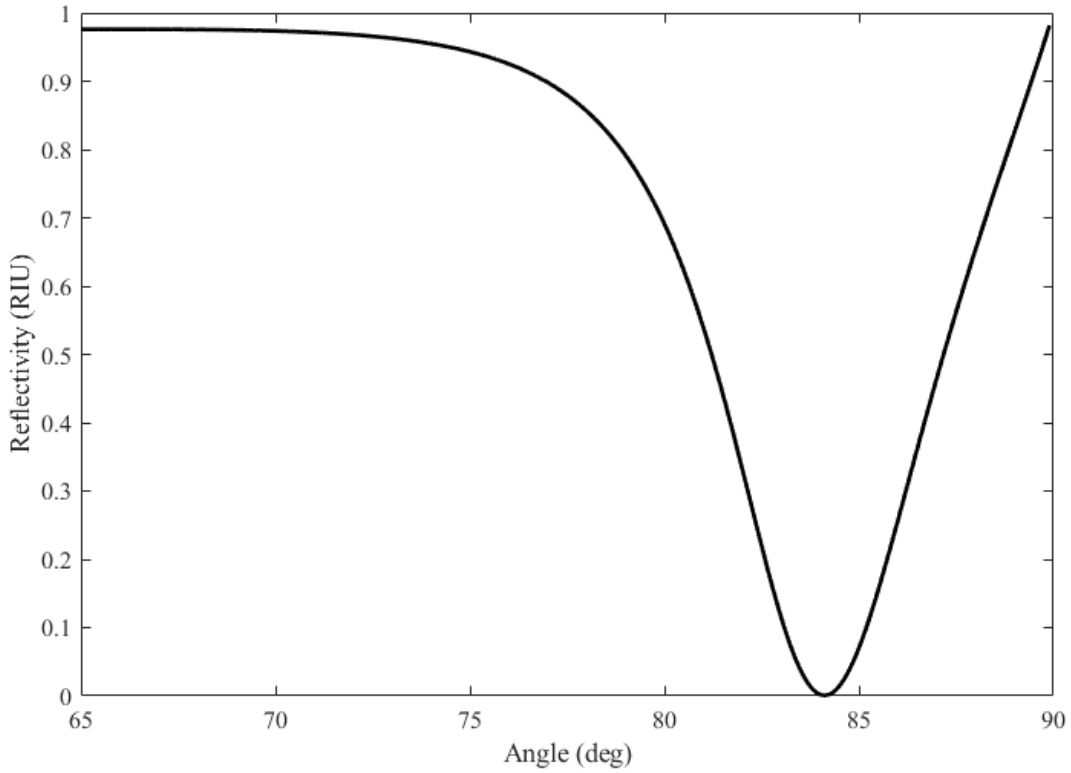

Figure IV.26 SPR curve of the SPR sensor with water as analyte (Ouardi et Al. [143]).

As noted, the number of BP layers is critical to determining the optimal sensor configuration for detecting deltamethrin concentration. Figure IV.27 summarizes the test results obtained by simulating the sensor with various numbers of BP layers for the same application.

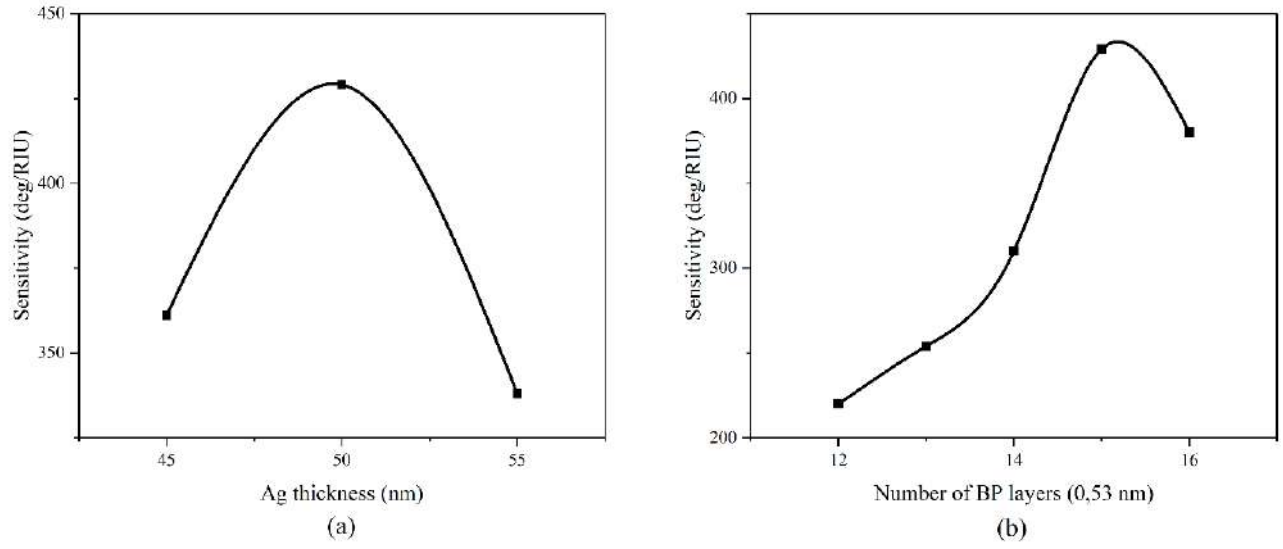

Figure IV.27 Sensitivity of the sensor for different values of (a) Ag thickness and (b) number of BP layers (Ouardi et Al. [143]).

The data reveal that the optimal configuration consists of 50 nm of silver and 15 BP layers (15 × 0.53 nm), which yields a sensitivity of 499 deg/RIU. This result validates our approach and provides a green light to simulate the sensor across a range of deltamethrin concentrations up to the maximum permitted level.

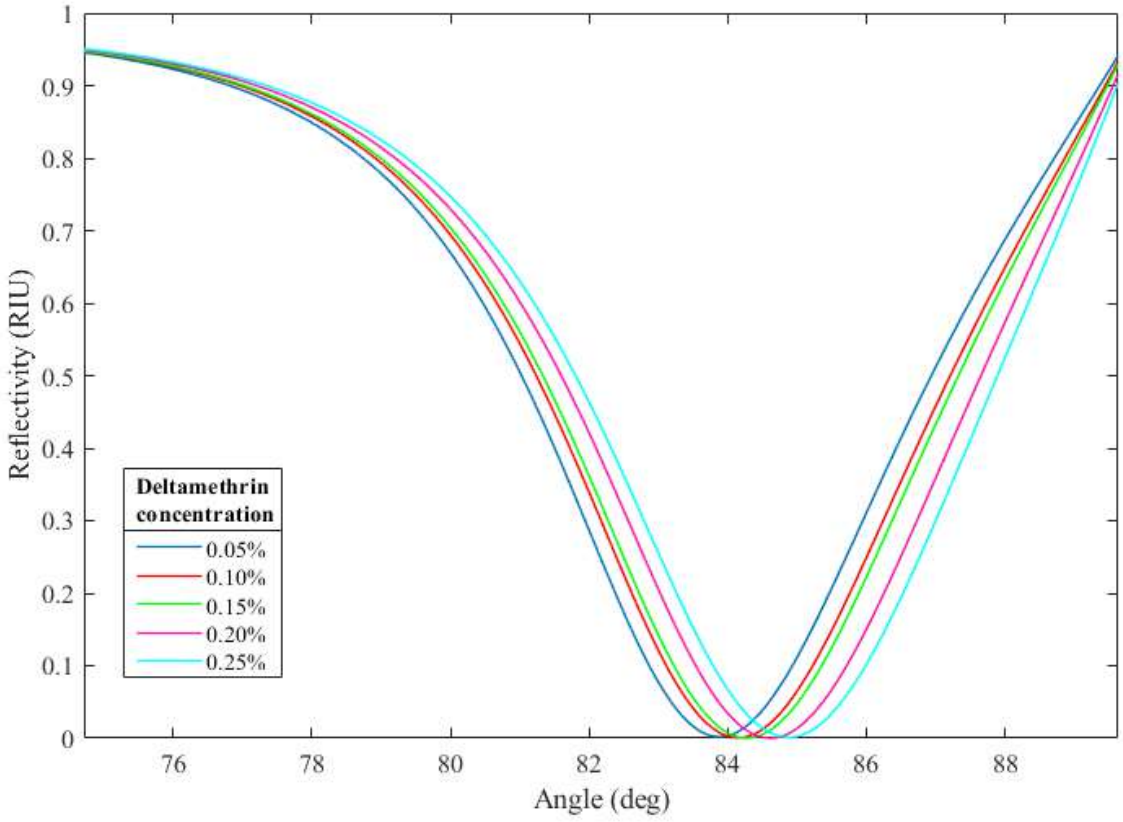

Figure IV.28 SPR curves of the SPR sensor for different values of deltamethrin concentrations (Ouardi et Al. [143]).

The resonance angle shifts toward higher incidence angles as the deltamethrin concentration increases, even though the variation in the refractive index is extremely small (on the order of 0.001). This capability to detect such minute changes in refractive index underscores the sensor's potential for addressing the challenging task of pesticide detection.

Table IV.16 summarizes the performance factors of the SPR sensor for pesticide detection.

Table IV.16 performance parameters of the proposed sensor for deltamethrin detection (Ouardi et Al. [143]).

Deltamethrin concentration (%)	**0.05**	**0.1**	**0.15**	**0.2**	**0.25**
Sensitivity (deg/RIU)	412	405	415	426	449
Figure of Merit (RIU^{-1})	70.58	68.87	70.37	71.74	75.13
Limit of detection (RIU)	$7.08e^{-4}$	$7.26\ e^{-4}$	$7.1\ e^{-4}$	$6.9\ e^{-4}$	$6.6\ e^{-4}$
Q-Factor	14.37	14.31	14.29	14.25	14.2
Signal-to-noise ratio	0.041	0.045	0.02	0.05	0.045

In summary, the proposed sensor—comprising a high refractive index BK7 prism with a 50 nm silver layer overlaid by fifteen BP layers—enables effective detection and monitoring of deltamethrin levels in water, even at concentrations up to 0.25%. Achieving a sensitivity of 499 deg/RIU, this SPR sensor stands out as an exceptional tool for this application. The promising results of this study have led to the publication of a scientific article on pesticide detection using this sensor in the *Sensing and Imaging* journal [143].

IV.8. Eighth Sensor: Early HIV Detection

Another study focuses on the early detection of viruses, with the proposed and optimized sensor designed specifically for detecting the human immunodeficiency virus (HIV), which causes AIDS.

The capability of SPR sensors to detect very low concentrations of analytes enables effective management of HIV infections. HIV is a virus that attacks the body's immune system, potentially leading to acquired immunodeficiency syndrome (AIDS) if left untreated, as the immune system becomes severely compromised and the body becomes vulnerable to infections. SPR sensors can provide highly sensitive and real-time detection of HIV-related biomolecules, thereby facilitating early diagnosis and treatment.

IV.8.1. Schematic of SPR Sensor

The SPR-based biosensor is constructed using a BK7 prism, a 40 nm silver layer, a graphene layer (0.35 nm thick), a 10 nm layer of silicon dioxide, and a thin 1 nm layer of silicon. Figure IV.29 illustrates the configuration under consideration.

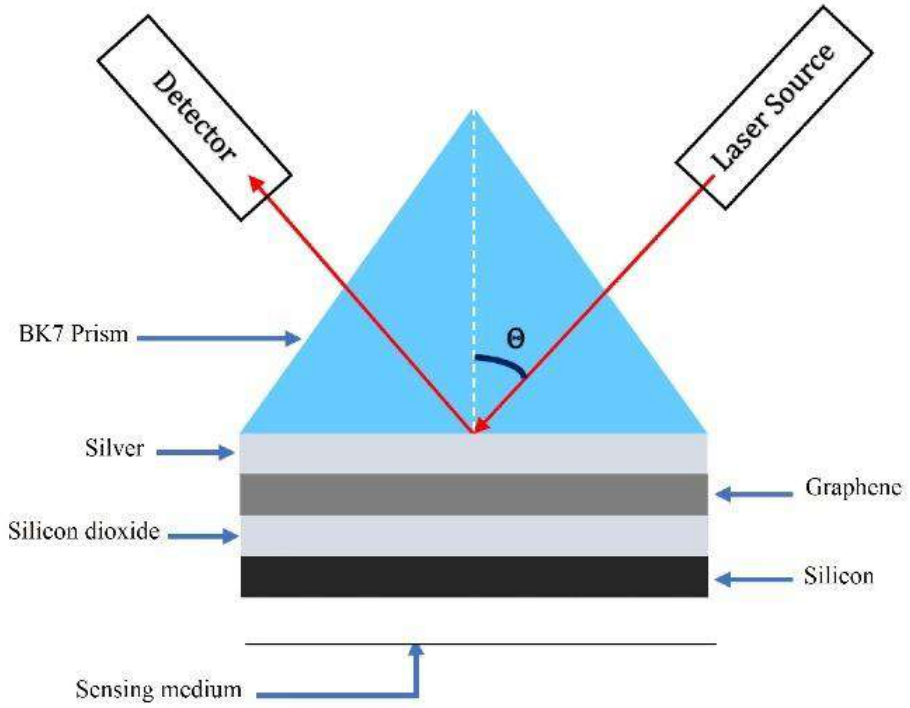

Figure IV.29 Representation of the proposed SPR sensor (Ouardi et Al. [144]).

The sensor's response was initially studied using water (n = 1.33) as the detection medium, with a refractive index variation of Δn = 0.005. Under these conditions, the sensor exhibited a sensitivity as high as 118 deg/RIU, as depicted by the SPR curve in Figure IV.30.

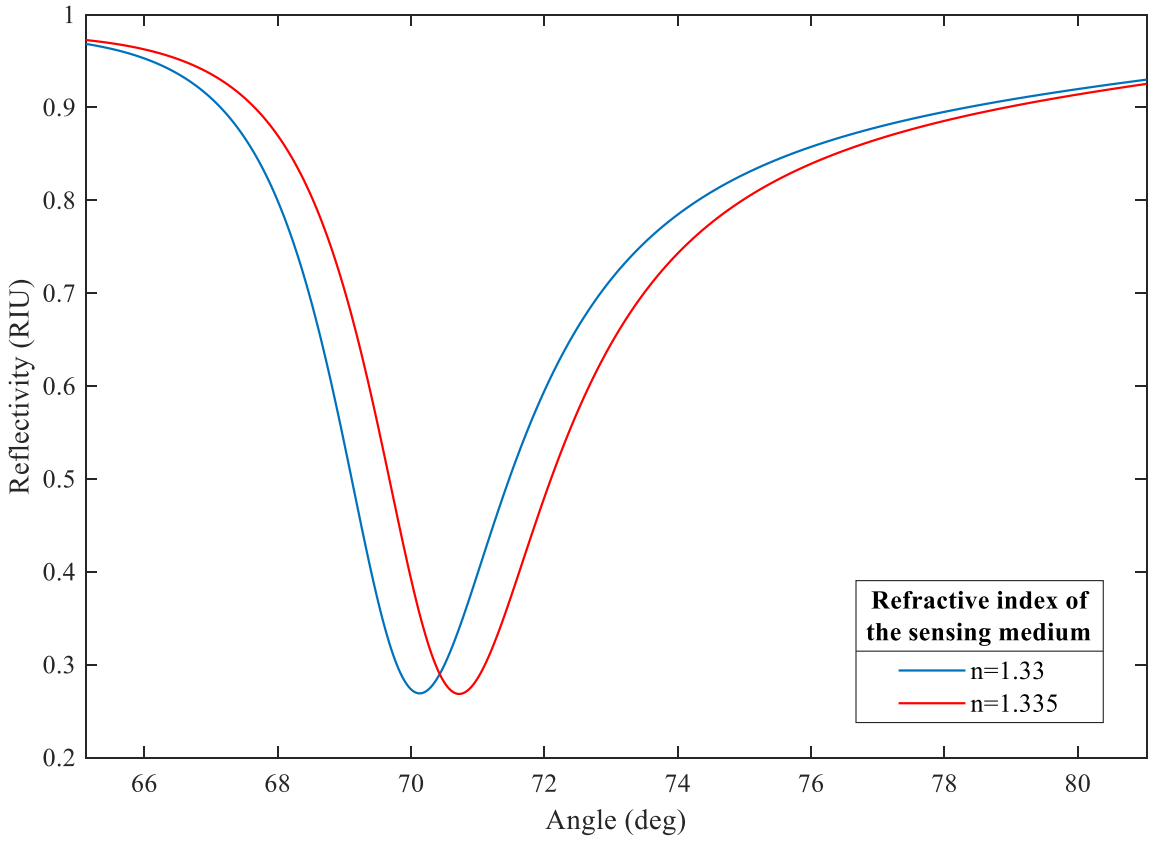

Figure IV.30 SPR curves of the HIV sensor using water as sensing medium (Ouardi et Al. [144]).

For the analyte in this study, the biosensor was tested with two distinct refractive index values corresponding to two types of blood samples: one from a healthy individual (n = 1.35) and another from an HIV-infected individual (n = 1.42) [142]. Figure IV.31 shows the two SPR curves obtained for these refractive index values. The maximum sensitivity achieved was 207 deg/RIU, with a figure of merit of 36.1 RIU^{-1}. These outstanding performance characteristics render the proposed sensor a promising candidate for HIV detection—a critical application in the medical field owing to its remarkable properties.

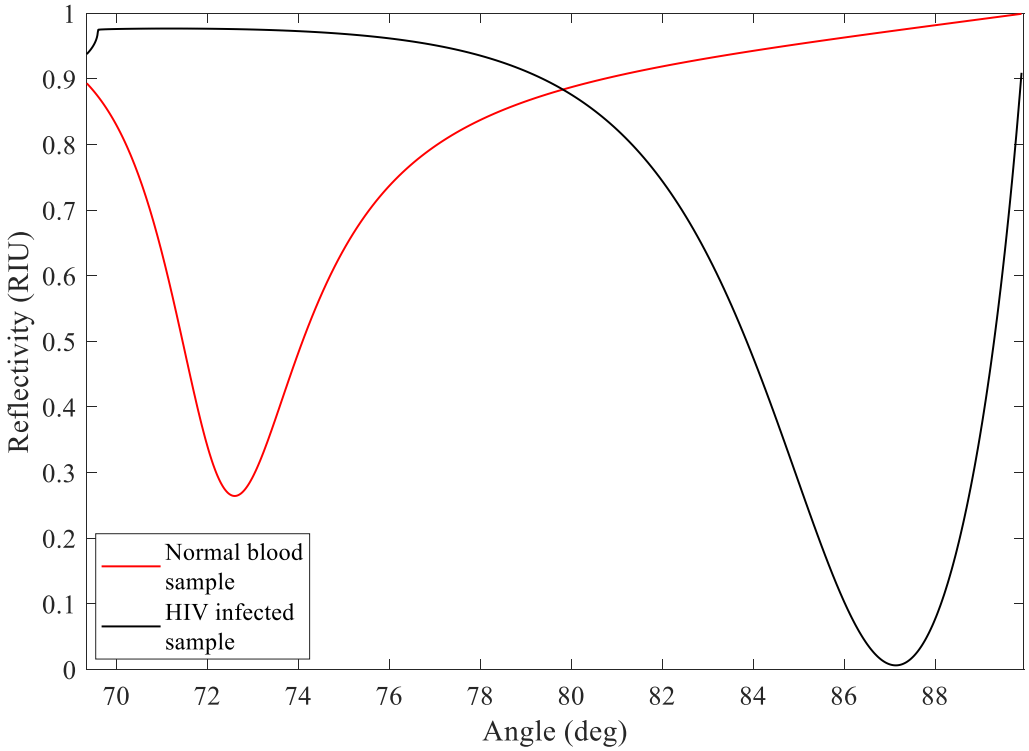

Figure IV.31 SPR curves of the proposed sensor for two samples, normal blood sample (in red) and HIV infected blood sample (in black) (Ouardi et Al. [144]).

In summary, the proposed SPR sensor is capable of rapidly and efficiently detecting the presence of HIV in a blood sample, demonstrating a sensitivity of 207 deg/RIU. The sensor's excellent performance was highlighted during an oral presentation at the International Conference on Multidisciplinary Sciences and Technological Developments (ICMUSTED 2024) held in Erzurum, Turkey [144]. Furthermore, the integration of graphene and ultrathin silicon layers not only enhances the sensor's electronic and plasmonic properties but also contributes to improved signal stability and reproducibility, making it a highly effective tool for early HIV diagnosis.

IV.9. Ninth Sensor: Leukemia Detection

The study presents a highly sensitive surface plasmon resonance (SPR) biosensor optimized for detecting blood cancer, specifically leukemia, by monitoring subtle changes in the refractive index of blood samples. The sensor structure comprises multiple layers: a BK7 glass prism for light coupling, a 45 nm silver (Ag) layer to generate strong surface plasmons, a 5 nm barium titanate ($BaTiO_3$) layer for its high dielectric constant and optical properties, a 5 nm silicon dioxide (SiO_2) layer to enhance sensor sensitivity, and two monolayers of black

phosphorus (BP) applied as an intermediate sensing layer. The configuration leverages these materials' optical properties to achieve excellent sensitivity and performance.

IV.9.1. Schematic of SPR Sensor

The sensor operates under the Kretschmann-Raether configuration, employing TM-polarized monochromatic light of 633 nm wavelength from a He–Ne laser directed through the BK7 prism. The interaction of light with the metal-dielectric interface excites surface plasmons whose resonance angle shifts in response to minute refractive index changes in blood samples, serving as the detection signal.

Testing revealed the sensor can distinguish between blood samples from healthy individuals and leukemia patients through the shift in SPR resonance angle, with the Leiden patient's sample showing a detectable increase indicative of disease presence.

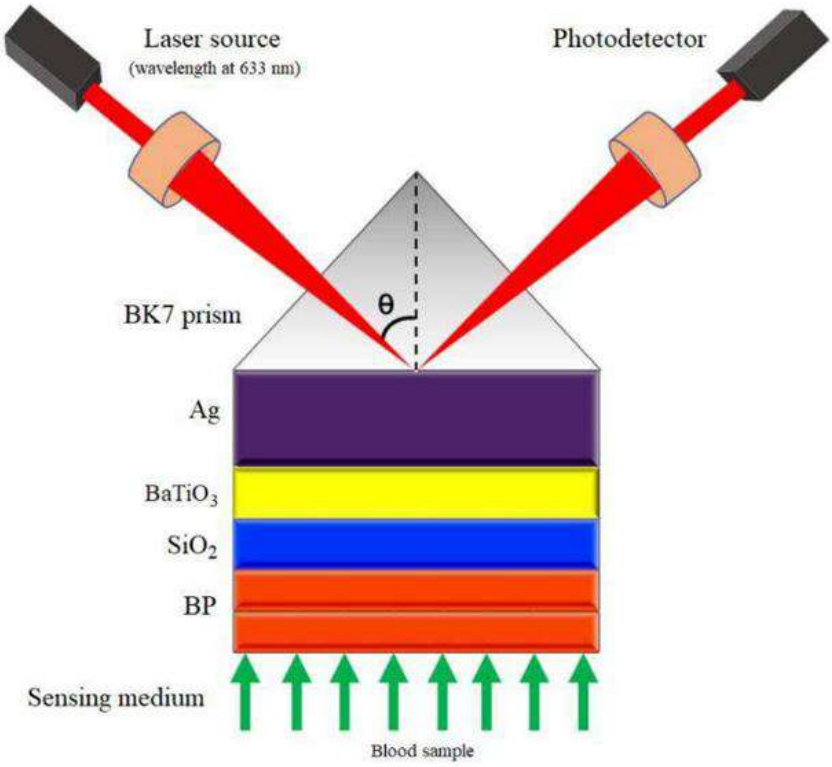

Figure IV.32 Schematic description of the proposed SPR sensor (Ouardi et Al. [145]).

Performance metrics demonstrate a remarkable angular sensitivity of 395 deg/RIU and a figure of merit (FoM) of 76.55 RIU^{-1}, surpassing many previous designs. The enhanced sensitivity especially benefits from the integration of $BaTiO_3$ and BP layers, which improve light-matter interaction and the resonance response to small refractive index variations. Optimal layer thicknesses were carefully determined through simulation using the transfer matrix

method (TMM), identifying 45 nm for Ag, 5 nm for $BaTiO_3$, 5 nm for SiO_2, and two BP monolayers as optimal for performance.

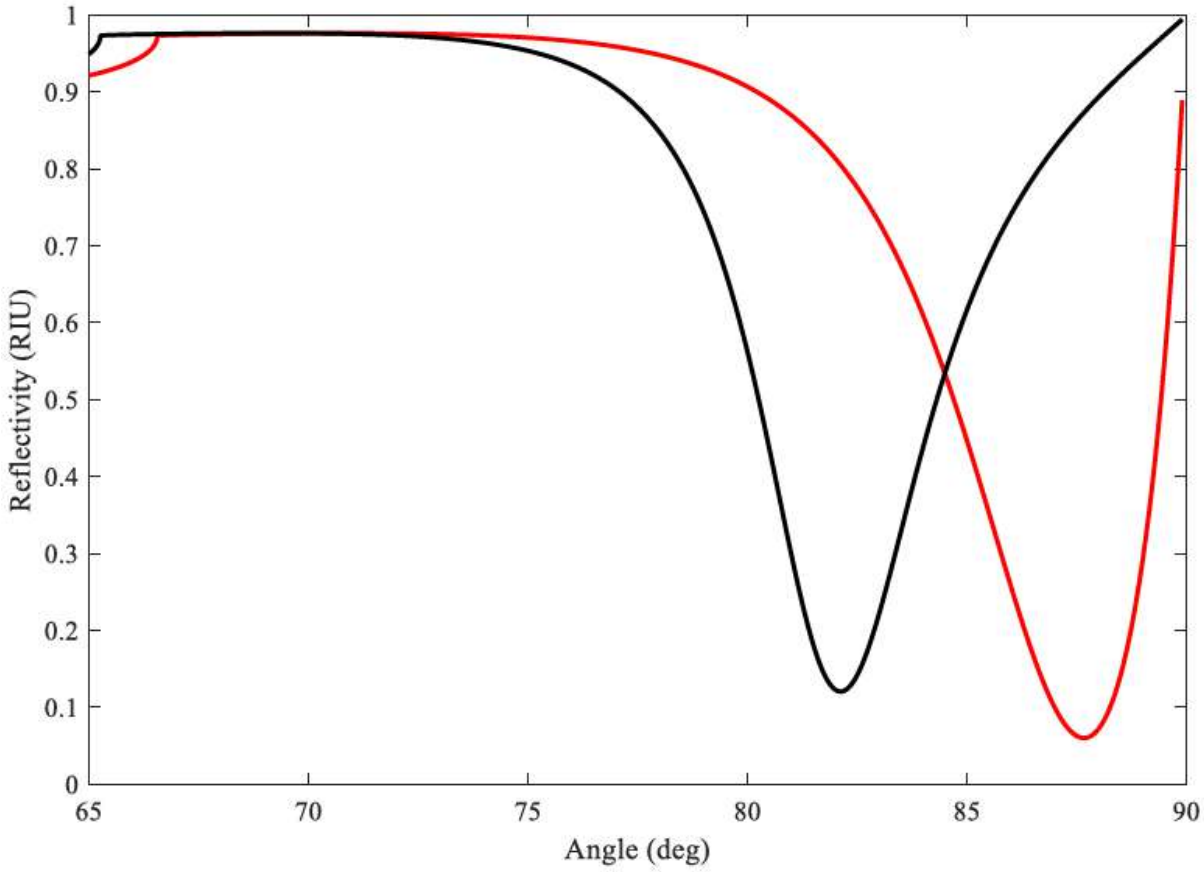

Figure IV.33 SPR curves of the proposed sensor loaded with blood samples from a healthy individual and a leukemia patient (Ouardi et Al. [145]).

In summary, this SPR biosensor offers a promising platform for early and accurate detection of blood cancer via label-free, real-time monitoring of refractive index changes, underscoring the potential of multilayer SPR designs with advanced 2D and dielectric materials in medical diagnostics, the results of the study of the sensor earned a publication in the Journal of Optics [145].

Conclusion

We have designed, simulated, and optimized a total of nine biosensors based on surface plasmon resonance (SPR): a sensor for water quality monitoring, a sensor for detecting alcohol content in water, a cancer cell detector, a sensor for monitoring blood glucose levels and another for both blood glucose and hemoglobin levels, a pregnancy test based on SPR, a sensor that measures the pesticide content in a solution, a biosensor for detecting HIV infections, and finally, a leukemia biodetector. In our work, we employed advanced numerical methods such

as the transfer matrix method (TMM) within the MATLAB environment to achieve precise modeling and optimization of these devices. Through the careful selection and integration of innovative materials—such as gold, silver, black phosphorus, graphene, zinc oxide, and others—we have been able to enhance the performance metrics of these sensors, including sensitivity, resolution, and the overall figure of merit.

Our sensors have demonstrated excellent performance factors, making them exceptional candidates for biosensing applications. Moreover, the proposed configurations are not only cost-effective and robust but also versatile enough to address a wide range of real-world challenges, from environmental monitoring and agricultural safety to early disease diagnosis and medical diagnostics. The promising results of our studies have been presented at various international conferences and have led to publications in reputable scientific journals, further underlining the potential impact of our research in the field of biosensors.

General Conclusion

General Conclusion

In this doctoral thesis, we have thoroughly investigated the fascinating domain of surface plasmons and their practical applications in biosensor design. We began by establishing the fundamental principles of electromagnetism—covering Maxwell's equations, constitutive relations, and the transfer matrix method (TMM)—which laid the groundwork for understanding the excitation and propagation of surface plasmons at metal–dielectric interfaces. This theoretical framework, enriched by a historical overview and detailed numerical demonstrations, enabled us to identify and quantify key performance parameters of SPR sensors, including sensitivity, figure of merit, detection limit, quality factor, and detection accuracy.

Building on this foundation, the diverse applications of SPR-based biosensors across several interdisciplinary fields have been explored. In our work, we harnessed advanced numerical methods—implemented in MATLAB—to model the reflectance of multilayer systems with precision. This allowed us to optimize sensor configurations rapidly and reliably, ensuring that our designs achieve the desired performance without excessive experimental trial and error.

A total of nine distinct biosensors, each tailored for a specific application, have been designed, simulated and optimized. The first sensor, targeting water quality monitoring, employs a BK7 glass prism coated with 50 nm of gold, a 0.7 nm layer of silicon dioxide, 2 nm of $PtSe_2$, and three layers of black phosphorus. This configuration effectively monitors subtle refractive index changes in water, proving its potential for assessing water purity. The second sensor was developed to measure alcohol content in water, utilizing a similar BK7 prism but with a silver layer (50 nm), eight layers of black phosphorus, and a 25 nm silicon dioxide layer, which together yield a notable enhancement in sensitivity. Additionally, for the medical diagnostics, the third sensor was dedicated to cancer cell detection, incorporating 45 nm of silver and a 3 nm layer of gallium arsenide on a BK7 prism. The fourth sensor focused on blood glucose monitoring, featuring a layered structure of 0.5 nm and 45 nm silver separated by a 0.5 nm rhodium layer and reinforced by six layers of black phosphorus. In the fifth sensor, designed as a pregnancy test, we integrated a 50 nm silver layer with a 1 nm MgF_2 layer and 14 layers of black phosphorus, achieving ultrahigh sensitivity for hormone detection. The sixth sensor presents a dual-analyte platform capable of simultaneously detecting blood hemoglobin and

urinary glucose levels by employing a configuration with 55 nm of silver, 6 nm of silicon dioxide, a 1 nm ZnO layer, and a single layer of black phosphorus on a BK7 prism. The seventh sensor was specifically engineered for agro-food applications, targeting the detection of the pesticide deltamethrin; it features a simple structure with a BK7 prism, 50 nm of silver, and 15 layers of black phosphorus, demonstrating the sensor's aptitude to detect even minute changes in refractive index associated with pesticide concentrations. The eighth sensor was optimized for the early detection of HIV. This design comprises a BK7 prism, 40 nm of silver, a graphene layer, 10 nm of silicon dioxide, and a 1 nm silicon layer, yielding promising results for rapid pathogen detection in blood samples. Finally, the ninth sensor was optimized for the detection of blood cancer (leukemia) comprising a BK7 prism, a 45 nm silver layer, a 5 nm barium titanate ($BaTiO_3$) layer, a 5 nm silicon dioxide layer, and two monolayers of black phosphorus (BP), delivering high sensitivity and promising results for rapid and label-free detection in blood samples.

All these biosensors have demonstrated outstanding performance in terms of both sensitivity and figure of merit, consistently outperforming many previously reported devices in the literature. Our integrated approach—combining rigorous theoretical analysis, state-of-the-art numerical simulation, and careful material selection—has not only yielded high-performance sensor configurations but has also underscored the versatility and potential of SPR-based biosensors for addressing critical challenges in healthcare, environmental safety, and industrial quality control.

Moreover, this work has highlighted the significant impact of advanced materials, such as black phosphorus, graphene, and various semiconductor oxides, on enhancing SPR sensor performance. By optimizing the thicknesses and combinations of these materials, we achieved improved resonance conditions, reduced reflectance minima, and increased sensitivity, thereby paving the way for the development of next-generation biosensors.

In conclusion, the research presented in this thesis contributes significantly to the field of plasmonics by offering a comprehensive study of SPR phenomena—from fundamental electromagnetic theory to practical sensor design and optimization. The successful demonstration of nine distinct biosensor models showcases the broad applicability and exceptional performance of SPR-based devices. Our findings not only validate the theoretical models and numerical methods employed but also establish a solid foundation for future research aimed at further refining these sensors and exploring new applications in precision diagnostics and environmental monitoring.

Bibliography and Webography

Bibliography and Webography

[1] LI, L. Manipulation of near field propagation and far field radiation of surface plasmon polariton. Springer, 2017.

[2] BARNES, W. L.; DEREUX, A.; EBESEN, T. W. Surface plasmon subwavelength optics. Nature, 424:824–830, 2003.

[3] HIRSCH, L. R.; STAFFORD, R. J.; BANKSON, J. A.; SERSHEN, S. R.; RIVERA, B.; PRICE, R. E.; HAZLE, J. D.; HALAS, N. J.; WEST, J. L. Nanoshell-mediated near-infrared thermal therapy of tumors under magnetic resonance guidance. Proc. Natl. Acad. Sci. USA, 100:13549–13554, 2003.

[4] ATWATER, H. A.; POLMAN, A. Plasmonics for improved photovoltaic devices. Nat. Mater., 9:205–213, 2010.

[5] FLEISCHM, M.; HENDRA, P. J.; MCQUILLA, A. Raman-spectra of pyridine adsorbed at a silver electrode. Chem. Phys. Lett., 26:163–166, 1974.

[6] SCHASFOORT, R. B. M. Handbook of Surface Plasmon Resonance. 2nd ed. London: The Royal Society of Chemistry, 2017.

[7] PINES, D. Collective energy losses in solids. Rev. Mod. Phys., 28(3):184–199, 1956.

[8] MOCHÁN, W. L. Plasmons. Reference Module in Materials Science and Materials Engineering, 2016. doi:10.1016/b978-0-12-803581-8.01192-9.

[9] KRETSCHMANN, E. The determination of the optical constants of metals by excitation of surface plasmons. Z. Physik, 241:313–324, 1971.

[10] SOUTO, D. E. P.; VOLPE, J.; GONÇALVES, C. C.; RAMOS, C. H. I.; KUBOTA, L. A brief review on the strategy of developing SPR-based biosensors for application to the diagnosis of neglected tropical diseases. Talanta, 205:120122, 2019.

[11] ANKER, J. N.; HALL, W. P.; LYANDRES, O.; SHAH, N. C.; ZHAO, J.; VAN DUYNE, R. P. Biosensing with plasmonic nanosensors. Nat. Mater., 7:442–453, 2008.

[12] MARADUDIN, A. A.; SAMBLES, J. R.; BARNES, W. L. (Eds.) Modern Plasmonics. Amsterdam: Elsevier, 2014, pp. 1–23. ISBN 9780444595263.

[13] PITELET, A. Théorie et simulation en nanophotonique : non-localité dans les nanostructures métalliques. Optique [physics.optics]. Université Clermont Auvergne, 2018.

[14] CAUCHETEUR, C. Plasmons de surface : principes physiques et applications. Physique Chimie, 2014.

[15] AKIMOTO, T.; SASAKI, S.; IKEBUKURO, K.; et al. Effect of incident angle of light on sensitivity and detection limit for layers of antibody with surface plasmon resonance spectroscopy. Biosens. Bioelectron., 15:355–362, 2000.

[16] QUINN, J. G.; O'NEILL, S.; DOYLE, A.; et al. Development and application of surface plasmon resonance-based biosensors for the detection of cell-ligand interactions. Anal. Biochem., 281:135–143, 2000.

[17] NGUYEN, H. H.; PARK, J.; KANG, S.; KIM, M. Surface plasmon resonance: a versatile technique for biosensor applications. Sensors (Basel), 15(5):10481–10510, 2015. doi:10.3390/s150510481.

[18] BIACORE AB. BIACORE Technology Handbook, 1994.

[19] AFTAB, M.; MANSHA, M.; IQBAL, T.; FAROOQ, M. Surface plasmon excitation: theory, configurations, and applications. Plasmonics, 19:1–19, 2023. doi:10.1007/s11468-023-02095-2.

[20] WELFORD, K. Surface plasmon-polaritons and their uses. Opt. Quant. Electron., 23:1–27, 1991.

[21] ROPER, D. K. Determining surface plasmon resonance response factors for deposition onto three-dimensional surfaces. Chem. Eng. Sci., 62(7):1988–1996, 2007. doi:10.1016/j.ces.2006.12.014.

[22] HOMOLA, J. Surface plasmon resonance sensors for detection of chemical and biological species. Chem. Rev., 108:462–493, 2008.

[23] GIÉ, H.; SARMANT, J. P. Électromagnétisme, vols. 1–2. Collection des sciences physiques, Technique et documentation, Lavoisier, 1985.

[24] COURJON, D.; BAINIER, C. Le champ proche optique : théorie et applications. Springer Science & Business Media, 2001, 344 p. ISBN 2-287-59720-4.

[25] LEROY, O.; BREAZEALE, M. A. Physical Acoustics: Fundamental and Applications. Springer Science & Business Media, 2012, 724 p. ISBN 978-1-4615-9575-5.

[26] PASCHOTTA, R. Evanescent Waves. RP Photonics Encyclopedia, retrieved 2024-02-25, https://doi.org/10.61835/c1l.

[27] RITCHIE, R. H. Plasma losses by fast electrons in thin films. Phys. Rev., 106:874–881, 1957.

[28] STERN, E. A.; FERRELL, R. A. Surface plasma oscillations of a degenerate electron gas. Phys. Rev., 120:130–136, 1960.

[29] TURBADAR, T. Complete absorption of light by thin metal films. Proc. Phys. Soc., 73:40–44, 1959.

[30] KRETSCHMANN, E. The determination of the optical constants of metals by excitation of surface plasmons. Z. Physik, 241:313–324, 1971.

[31] HO, A. H. P.; WU, S. Y.; KONG, S. K.; ZENG, Z.; YONG, K. T. SPR biosensors. In: HO, A. P.; KIM, D.; SOMEKH, M. (Eds.) Handbook of Photonics for Biomedical Engineering. Dordrecht: Springer, 2014. doi:10.1007/978-94-007-6174-2_38-1.

[32] CIALLA, D.; MARZ, A.; BÖHME, R.; et al. Surface-enhanced Raman spectroscopy (SERS): progress and trends. Anal. Bioanal. Chem., 403:27–54, 2012.

[33] ALEINER, I. L.; ALTSHULER, B. L.; RUBO, Y. G. Radiative coupling and weak lasing of exciton-polariton condensates. Phys. Rev. B, 85(12), 2012.

[34] SZUNERITS, S.; BOUKHERROUB, R. Introduction to plasmonics advances and applications. Taylor & Francis Group, 2015.

[35] MAIER, S. A. Plasmonics: Fundamentals and Applications. Springer Science & Business Media, 2007.

[36] KAYA, S. Photo-thermal control of surface plasmon mode propagation at telecom wavelengths. Physics [physics]. Université de Bourgogne, 2016.

[37] RAETHER, H. Surface plasmons on smooth and rough surfaces and on gratings. Berlin: Springer-Verlag, 1988.

[38] ZENG, S.; YU, X.; LAW, W. C.; ZHANG, Y.; HU, R.; DINH, X. Q.; HO, H. P.; YONG, K. T. Size dependence of Au NP-enhanced surface plasmon resonance based on differential phase measurement. Sensors and Actuators B: Chemical, 176:1128–1133, 2013. doi:10.1016/j.snb.2012.09.073.

[39] SARID, D.; CHALLENER, W. A. Modern introduction to surface plasmons: Theory, Mathematica modeling, and applications. New York: Cambridge University Press, 2010.

[40] KAVOKIN, V.; SHELYKH, I. A.; MALPUECH, G. Phys. Rev. B, 72:233102, 2005.

[41] KAVOKIN, A. V.; SHELYKH, I. A.; MALPUECH, G. Appl. Phys. Lett., 87:261105, 2005.

[42] TAMM, I. Über eine mögliche Art der Elektronenbindung an Kristalloberflächen. Z. Phys., 76(11-12):849–850, 1932.

[43] SASIN, M. E.; SEISYAN, R. P.; KALITTEEVSKI, M. A.; BRAND, S.; ABRAM, R. A.; CHAMBERLAIN, J. M.; EGOROV, A. Y.; VASIL'EV, A. P.; MIKHRIN, V. S.; KAVOKIN, A. V. Tamm plasmon polaritons: Slow and spatially compact light. Appl. Phys. Lett., 92:251112, 2008.

[44] DU, G.-Q.; JIANG, H.-T.; WANG, Z.-S.; YANG, Y.-P.; WANG, Z.-L.; LIN, H.-Q.; CHEN, H. Heterostructure-based optical absorbers. J. Opt. Soc. Am. B, 27:1757–1762, 2010.

[45] ZHANG, D.; CHEN, Y.; ZHU, L.; FU, Q.; WANG, R.; WANG, P.; MING, H.; LAKOWICZ, J. R.; BADUGU, R. Effect of metal, film thickness on Tamm plasmon-coupled emission. Phys. Chem. Chem. Phys., 2014.

[46] VETROV, S. Y.; BIKBAEV, R. G.; TIMO FEEV, I. V. Optical Tamm states at the interface between a photonic crystal and a nanocomposite with resonance dispersion. J. Exp. Theor. Phys., 117:988–998, 2013.

[47] BRAND, S.; KALITTEEVSKI, M.; ABRAM, R. Optical Tamm states above the bulk plasma frequency at a Bragg stack/metal interface. Phys. Rev. B, 79:2009, 2009.

[48] ZHANG, Y.; et al. Principles of optical interference sensors. J. Opt. Technol., 81(6), 2014.

[49] LEE, K.; et al. Optical fiber sensors: Principles and applications. Sensors, 18(12), 2018.

[50] JOANNOPOULOS, J. D.; et al. Photonic Crystals: Molding the Flow of Light. Princeton: Princeton University Press, 2008.

[51] TAVERNE, S.; CARON, B.; GÉTIN, S.; LARTIGUE, O.; LOPEZ, C.; MEUNIER-DELLA-GATTA, S.; GORGE, V.; REYMERMIER, M.; RACINE, B.; MAINDRON, T.; QUESNEL, E. Multispectral surface plasmon resonance approach for ultra-thin silver layer characterization: Application to top-emitting OLED cathode. J. Appl. Phys., 2018. doi:10.1063/1.5003869.

[52] KRETSCHMANN, E.; RAETHER, H. Radiative decay of non-radiative surface plasmons excited by light. Z. Naturforsch. A, 23(12), 1968.

[53] LIZ-MARZAN, L. M. Nanometre-sized metal colloids: From synthesis to applications. Adv. Colloid Interface Sci., 80, 1999.

[54] JAKSIC, Z. Optical metamaterials as the platform for a novel generation of ultrasensitive chemical or biological sensors, 2010.

[55] WANG, Y. Surface Plasmon Resonance Based Sensors Using Hydrogel Waveguide. LAP Lambert Academic Publishing, 2012.

[56] TURBADAR, T. Complete absorption of light by thin metal films. Proc. Phys. Soc., 73, 2002. doi:10.1088/0370-1328/73/1/307.

[57] YU, H.; PENG, Y.; YANG, Y.; et al. Plasmon-enhanced light–matter interactions and applications. npj Comput Mater., 5:45, 2019. doi:10.1038/s41524-019-0184-1.

[58] RAMAN, C. V. The molecular scattering of light. Nobel Lectures: Physics, 1922–1941, 267–275, 1930.

[59] OUYANG, Q.; ZENG, S.; JIANG, L.; et al. Sensitivity enhancement of transition metal dichalcogenides/silicon nanostructure-based surface plasmon resonance biosensor. Sci. Rep., 6:28190, 2016.

[60] SAID, F. A.; MENON, P. S.; RAJENDRAN, V.; SHAARI, S.; MAJLIS, B. Y. IET Nanobiotechnol., 11(8):981–986, 2017.

[61] WU, L.; GUO, J.; WANG, Q.; LU, S.; DAI, X.; et al. Sensitivity enhancement by using few-layer black phosphorus-graphene/TMDCs heterostructure in surface

plasmon resonance biochemical sensor. Sensors Actuators B: Chem., 249:542–548, 2017.

[62] BHAVSAR, K.; PRABHU, R. Investigations on sensitivity enhancement of SPR biosensor using tunable wavelength and graphene layers. IOP Conf. Ser. Mater. Sci. Eng., 499(1):012008, 2019.

[63] KUMAR, R.; KUSHWAHA, A. S.; SRIVASTAVA, M.; MISHRA, H.; SRIVASTAVA, S. K. Enhancement in sensitivity of graphene-based zinc oxide assisted bimetallic surface plasmon resonance (SPR) biosensor. Appl. Phys. A, 124(3):235, 2018.

[64] DOS SANTOS, J. P. S. S.; JORGE, P. A. S.; DE ALMEIDA, J. M. M. M.; CŒLHO, L. A simple spectral interrogation system for optical fiber sensors. MDPI Proc., 15(1):6, 2019.

[65] JIANG, H.; ZHENG, G.; RAO, W. F. Ultra-sensitive biosensor with hybrid coupling between molybdenum disulfide thin film and photonic waveguide mode. Results Phys., 13:102173, 2019.

[66] HAN, L.; WU, C. A phase sensitivity-enhancement surface plasmon resonance biosensor based on ITO-graphene hybrid structure. Plasmonics, 14(4):91–96, 2019.

[67] CHEN, S.; LIN, C. Sensitivity analysis of graphene multilayer based surface plasmon resonance biosensor in the ultraviolet, visible and infrared regions. Appl. Phys. A, 2019, pp.125–230.

[68] MARIANI, S.; MINUNNI, M. Surface plasmon resonance applications in clinical analysis. Anal. Bioanal. Chem., 406(9-10):2303–2323, 2014. doi:10.1007/s00216-014-7647-5.

[69] MERADI, K. A.; TAYEBOUN, F.; GUERINIK, A.; ZAKY, Z.; ARAFA, A. Optical biosensor based on enhanced surface plasmon resonance: theoretical optimization. Opt. Quantum Electron., 54:124, 2022. doi:10.1007/s11082-021-03504-8.

[70] KARKI, B.; JHA, A.; PAL, A.; et al. Sensitivity enhancement of refractive index-based surface plasmon resonance sensor for glucose detection. Opt. Quant. Electron., 54:595, 2022. doi:10.1007/s11082-022-04004-z.

[71] GUO, Z. SPR biosensor sensor principle and application progress. Highlights Sci. Eng. Technol., 73:238–242, 2023. doi:10.54097/hset.v73i.12978.

[72] MOHAMMED, I.; MULLETT, W. M.; LAI, E. P. C.; YEUNG, J. M. Anal. Chim. Acta, 444:97–102, 2001.

[73] SUN, M.; WU, H.; SONG, Y.; WANG, Q. Surface plasmon resonance alcohol sensor with $Ni(OH)_2$ nanoflowers/Au structure. Measurement, 210:112564, 2023. doi:10.1016/j.measurement.2023.112564.

[74] ZEDER-LUTZ, G.; ZUBER, E.; WITZ, J.; VAN REGENMORTEL, M. H. Thermodynamic analysis of antigen-antibody binding using biosensor measurements at different temperatures. Anal. Biochem., 246:123–132, 1997. doi:10.1006/abio.1996.9999101.

[75] COOPER, M. A.; WILLIAMS, D. H. Kinetic analysis of antibody-antigen interactions at a supported lipid monolayer. Anal. Biochem., 276:36–47, 1999. doi:10.1006/abio.1999.4333.

[76] KAUSAITE, A.; RAMANAVICIENE, A.; MOSTOVOJUS, V.; RAMANAVICIUS, A. Surface plasmon resonance and its application to biomedical research [Pavirsiaus plazmonu rezonansas ir jo pritaikymas biomedicininiams tyrinejimams]. Medicina (Kaunas), 43(5):355–365, 2007.

[77] BRULÉ, T.; GRANGER, G.; BUKAR, N.; DESCHÊNES-RANCOURT, C.; HAVARD, T.; SCHMITZER, A. R.; … MASSON, J.-F. A field-deployed surface plasmon resonance (SPR) sensor for RDX quantification in environmental waters. Analyst, 142(12):2161–2168, 2017. doi:10.1039/c7an00216e.

[78] MOHD DANIYAL, W.; YAP WING, F.; FAUZI, N.; HASHIM, H. S.; RAMDZAN, N. Recent advances in surface plasmon resonance optical sensors for potential application in environmental monitoring. Sensors and Materials, 32:4191, 2020. doi:10.18494/SAM.2020.3204.

[79] BALAA, K. Capteur à fibre optique basé sur le principe de résonance de plasmons de surface: optimisation pour la détection d'espèces chimiques. Matière Condensée [cond-mat]. Université de Nantes, 2007.

[80] KANSO, M. Modélisation, réalisation et caractérisation d'un capteur plasmonique à fibre optique: effets de la rugosité, des réactions de surface et de la

cinétique dans un système microfluidique. Matière Condensée [cond-mat]. Université de Nantes, 2008.

[81] LE RU, E. C.; ETCHEGOIN, P. G. Principles of Surface-Enhanced Raman Spectroscopy and Related Plasmonic Effects. Amsterdam: Elsevier, 2009.

[82] RAHMAN, M. S.; ANOWER, M. S.; HASAN, M. R.; HOSSAIN, M. B.; HAQUE, M. I. Design and numerical analysis of highly sensitive AuMoS$_2$-graphene based hybrid surface plasmon resonance biosensor. Opt. Commun., 396:36–43, 2017.

[83] ALMAWGANI, A. H. M.; AWASTHI, S. K.; MEHANEY, A.; ALI, G. A.; ELSAYED, H. A.; SAYED, H.; AHMED, A. M. A theoretical approach for a new design of an ultrasensitive angular plasmonic chemical sensor using black phosphorus and aluminum oxide architecture. RSC Adv., 13:16154–16164, 2023.

[84] COMSOL. COMSOL Multiphysics – RF Module, 2019. Available at: https://www.comsol.com/rf-module (Accessed: 22 June 2024).

[85] MATHWORKS. Simulink. Available at: https://ch.mathworks.com/products/simulink.html (Accessed: 22 June 2024).

[86] HRUNISYS. OptiFDTD Finite Difference Time Domain Simulation Design. Available at: https://www.hrunisys.com/product/7/OptiFDTD-Finite-Difference-Time-Domain-Simulation-Design (Accessed: 22 June 2024).

[87] MATHWORKS. MATLAB Product Description. Available at: https://ch.mathworks.com/help/matlab/learn_matlab/product-description.html (Accessed: 13 July 2024).

[88] AHN, H.; SONG, H.; CHOI, J.-R.; KIM, K. A localized surface plasmon resonance sensor using double-metal-complex nanostructures and a review of recent approaches. Sensors, 18:98, 2018. doi:10.3390/s18010098.

[89] WANG, M.; HUO, Y.; JIANG, S.; ZHANG, C.; YANG, C.; NING, T.; … MAN, B. Theoretical design of a surface plasmon resonance sensor with high sensitivity and high resolution based on graphene–WS$_2$ hybrid nanostructures and Au–Ag bimetallic film. RSC Adv., 7(75):47177–47182, 2017. doi:10.1039/c7ra08380g.

[90] SHARMA, A. K.; JHA, R.; PATTANAIK, H. S.; MOHR, G. J. Design considerations for surface plasmon resonance-based fiber-optic detection of human blood group. J. Biomed. Opt., 14(6):064041, 2009. doi:10.1117/1.3275476.

[91] KANSO, M. Modélisation, réalisation et caractérisation d'un capteur plasmonique à fibre optique: effets de la rugosité, des réactions de surface et de la cinétique dans un système microfluidique. Matière Condensée [cond-mat]. Université de Nantes, 2008. (in French).

[92] ZHANG, L.; HE, J.-A.; LI, T.; WU, X.; GU, D.; ZHANG, S.; YE, Y. Performance analysis of a Kretschmann-based Ag-ITO-Au surface plasmon resonance sensor through numerical simulations. Int. J. Opt., 2021:9975877, 10 pages, 2021. doi:10.1155/2021/9975877.

[93] SUKMA, F.; HANIF, M.; MASRUROH; SANTJOJO, D.; APSARI, R.; SUSANTO, H.; TAZI, I. Effects of thickness and roughness on plasmonic characteristics of gold thin films deposited on polished optical fiber. Mater. Res. Express, 11, 2024. doi:10.1088/2053-1591/ad17eb.

[94] GRANQVIST, N.; YLIPERTTULA, M.; VÄLIMÄKI, S.; PULKKINEN, P.; TENHU, H.; VIITALA, T. Control of the morphology of lipid layers by substrate surface chemistry. Langmuir, 30(10):2799–2809, 2014. doi:10.1021/la4046622.

[95] KORDI, S.; RAHMATI-YAMCHI, M.; ASGHARI VOSTAKOLAEI, M.; BARZEGARI, A.; ABDOLALIZADEH, J. Purification of a novel anti-VEGFR2 single chain antibody fragment and evaluation of binding affinity by surface plasmon resonance. Adv. Pharm. Bull., 9(1):64–69, 2019. doi:10.15171/apb.2019.008.

[96] SCHOTT. Zemax catalog 2017-01-20b. Available at: http://www.schott.com.

[97] TAN, C. Z. Determination of refractive index of silica glass for infrared wavelengths by IR spectroscopy. J. Non-Cryst. Solids, 223:158–163, 1998.

[98] AHN, H.; SONG, H.; CHOI, J.-R.; KIM, K. A localized surface plasmon resonance sensor using double-metal-complex nanostructures and a review of recent approaches. Sensors, 18:98, 2018. doi:10.3390/s18010098.

[99] ANDERSSON, J.; SVIRELIS, J.; FERRAND-DRAKE DEL CASTILLO, G.; SANNOMIYA, T.; DAHLIN, A. Surface plasmon resonance sensing with thin films of

palladium and platinum – quantitative and real-time analysis. Phys. Chem. Chem. Phys., 24:4588–4594, 2022. doi:10.1039/D1CP05381G.

[100] COHEN-TANNOUDJI, C.; DUPONT-ROC, J.; GRYNBERG, G. Photons et atomes: introduction à l'électrodynamique quantique. 2nd ed. Les Ulis et Paris: EDP Sci. et CNRS, 2001.

[101] SUN, M.; WU, H.; SONG, Y.; WANG, Q. Surface plasmon resonance alcohol sensor with $Ni(OH)_2$ nanoflowers/Au structure. Measurement, 210:112564, 2023. doi:10.1016/j.measurement.2023.112564.

[102] MALITSON, I. A. Interspecimen comparison of the refractive index of fused silica. J. Opt. Soc. Am., 55:1205–1208, 1965.

[103] KUC, A.; HEINE, T. Electronic properties of transition-metal dichalcogenides. Chem. Soc. Rev., 2014.

[104] KUC, A.; HEINE, T.; KIS, A. Electronic properties of transition-metal dichalcogenides. MRS Bull., 40:577–584, 2015.

[105] ERMOLAEV, G. A.; VORONIN, K. V.; TATMYSHEVSKIY, M. K.; MAZITOV, A. B.; SLAVICH, A. S.; YAKUBOVSKY, D. I.; TSELIN, A. P.; MIRONOV, M. S.; ROMANOV, R. I.; MARKEEV, A. M.; KRUGLOV, I. A.; NOVIKOV, S. M.; VYSHNEVYY, A. A.; ARSENIN, A. V.; VOLKOV, V. Broadband optical properties of atomically thin PtS_2 and $PtSe_2$. Nanomaterials, 11:3269, 2021.

[106] CIARROCCHI, A.; AVSAR, A.; OVCHINNIKOV, D.; KIS, A. Thickness-modulated metal-to-semiconductor transformation in a transition metal dichalcogenide. Nat. Commun., 9, 2018. doi:10.1038/s41467-018-03436-0.

[107] CASTELLANOS-GOMEZ, A.; VICARELLI, L.; PRADA, E.; ISLAND, J.; NARASIMHA-ACHARYA, K.; BLANTER, S.; GROENENDIJK, D.; BUSCEMA, M.; STEELE, G.; ALVAREZ, J.; ZANDBERGEN, H.; PALACIOS, J.; ZANT, H. Isolation and characterization of few-layer black phosphorus. 2D Mater., 1:025001, 2014. doi:10.1088/2053-1583/1/2/025001.

[108] SRIVASTAVA, A.; VERMA, R.; DAS, R.; PRAJAPATI, Y. K. A theoretical approach to improve the performance of SPR biosensor using MXene and black phosphorus. Optik, 203:163430, 2020.

[109] ASPNES, D. E.; KELSO, S. M.; LOGAN, R. A.; BHAT, R. Optical properties of Al_xGa_1−xAs. J. Appl. Phys., 60:754–767, 1986.

[110] DOUGLAS, B. E.; HO, S.-M. Structure and Chemistry of Crystalline Solids. Pittsburgh, PA: Springer Science + Business Media, Inc., 2006, 346 p. ISBN 0-387-26147-8, p. 64.

[111] CRADDOCK, P. T. The origins and inspirations of zinc smelting. J. Mater. Sci., 44(9):2181–2191, 2009. doi:10.1007/s10853-008-2942-1.

[112] TAYA, S. A.; DAHER, M. G.; ALMAWGANI, A. H. M.; HINDI, A. T.; ZYUOD, S. H.; COLAK, I. Detection of virus SARS-CoV-2 using a surface plasmon resonance device based on $BiFeO_3$-graphene layers. Plasmonics, 18:1441–1448, 2023. doi:10.1007/s11468-023-01867-0.

[113] WANG, X.; LU, D.; LIU, Y.; WANG, W.; REN, R.; LI, M.; LIU, D.; LIU, Y.; LIU, Y.; PANG, G. Electrochemical signal amplification strategies and their use in olfactory and taste evaluation. Biosens. (Basel), 12(8):566, 2022. doi:10.3390/bios12080566.

[114] OUARDI, M. E.; MERADI, K. A.; TAYEBOUN, F. Performance optimization of surface plasmon resonance sensor using 2D nanomaterials. Séminaire National sur le Laser et ses Applications SENALAP'10, 12–14 juin 2023, Alger, Algérie.

[115] ASHRAFI, T. M. S.; MOHANTY, G. Sensitivity calculation for different prism material based surface plasmon resonance sensor: A comparative study. J. Phys. Conf. Ser., 2267(1):012089, 2022.

[116] LIN, Z.; CHEN, S.; LIN, C. Sensitivity improvement of a surface plasmon resonance sensor based on two-dimensional materials hybrid structure in visible region: A theoretical study. Sensors (Basel), 20(9):2445, 2020.

[117] WIELOSYŃSKA, A.; PYRCHLA, K.; JAKÓBCZYK, P.; LENTKA, D.; SAWCZAK, M.; SKOWROŃSKI, Ł.; BOGDANOWICZ, R. Tailoring optical constants of few-layer black phosphorus coatings: Spectroscopic ellipsometry approach supported by ab-initio simulation. J. Ind. Eng. Chem., 127:579–589, 2023. doi:10.1016/j.jiec.2023.07.043.

[118] SIMMONDS, C. Alcohol: Its Production, Properties, Chemistry, and Industrial Applications. Macmillan and Co, 1919.

[119] MERADI, K. A.; TAYEBOUN, F.; GUERINIK, A.; et al. Optical biosensor based on enhanced surface plasmon resonance: Theoretical optimization. Opt. Quant. Electron., 54:124, 2022. doi:10.1007/s11082-021-03504-8.

[120] KUSHWAHA, A. S.; KUMAR, A.; KUMAR, R.; SRIVASTAVA, S. K. A study of surface plasmon resonance (SPR) based biosensor with improved sensitivity. Photonics Nanostructures – Fundam. Appl., 31:99–106, 2018. doi:10.1016/j.photonics.2018.06.003.

[121] OUYANG, Q.; ZENG, S.; DINH, X.-Q.; COQUET, P.; YONG, K.-T. Sensitivity enhancement of MoS_2 nanosheet based surface plasmon resonance biosensor. Proc. Eng., 140:134–139, 2016.

[122] DAHER, M. G.; AHMED, N. M.; PATEL, S. K.; et al. Novel surface plasmon resonance detector for the detection of various alcohols with ultra-high sensitivity. Opt. Quant. Electron., 55:1102, 2023. doi:10.1007/s11082-023-05418-z.

[123] OUARDI, M. E.; MERADI, K. A.; TAYEBOUN, F.; et al. Detection of water-alcohol content using surface plasmon resonance. Plasmonics, 2024. doi:10.1007/s11468-024-02285-6.

[124] PATIL, H.; SANE, V. G.; TS, I.; SHARAN, P. Gallium arsenide based surface plasmon resonance for glucose monitoring. International Conference on Optical and Photonic Engineering (icOPEN 2015), 2015.

[125] MAURYA, J.; PRAJAPATI, Y. A comparative study of different metal and prism in the surface plasmon resonance biosensor having MoS_2-graphene. Opt. Quant. Electron., 48:280, 2016.

[126] BIJALWAN, A.; SINGH, B. K.; RASTOGI, V. Analysis of one-dimensional photonic crystal based sensor for detection of blood plasma and cancer cells. Optik, 165994, 2021.

[127] OUARDI, M. E.; MERADI, K. A.; TAYEBOUN, F. Conception of SPR-based sensor for cancer cell detection. The 3rd International Conference on Materials Science and Engineering and Their Impact on the Environment (ICMSE'2024), 29–30 May 2024, Sidi-Bel-Abbes, Algeria.

[128] BELAY, A.; ASSEFA, G. Concentration, wavelength and temperature dependent refractive index of sugar solutions and methods of determination contents of sugar in soft drink beverages using laser lights. J. Lasers Opt. Photonics, 5(2):1–5, 2018.

[129] OUARDI, M. E.; MERADI, K. A.; TAYEBOUN, F. Conceptual study of surface plasmon resonance sensor for glucose level monitoring. INTERNATIONAL CONFERENCE ON ENGINEERING, NATURAL SCIENCES, AND TECHNOLOGICAL DEVELOPMENTS (ICENSTED 2024), Erdek, Türkiye, July 19–21, 2024.

[130] KUMAR, S.; YADAV, A.; MALOMED, B. A. High performance surface plasmon resonance based sensor using black phosphorus and magnesium oxide adhesion layer. Front. Mater., 10:1131412, 2023. doi:10.3389/fmats.2023.1131412.

[131] Ouardi, M.E., Meradi, K.A., Tayeboun, F. *et al.* Development of a Novel SPR Biosensor for Early Pregnancy Detection. *Sens Imaging* **26**, 56 (2025). https://doi.org/10.1007/s11220-025-00582-w

[132] MOSTUFA, S.; PAUL, A. K.; CHAKRABARTI, K. Detection of hemoglobin in blood and urine glucose level samples using graphene-coated SPR based bio-sensor. OSA Continuum, 10. doi:10.1364/OSAC.433633.

[133] RILEY, R. S.; MCPHERSON, R. A. Basic examination of urine. MCPHERSON, R. A.; PINCUS, M. R. (Eds.) Henry's Clinical Diagnosis and Management by Laboratory Methods. 24th ed. Philadelphia, PA: Elsevier, 2022, chap. 29.

[134] ZHERNOVAYA, O.; SYDORUK, O.; TUCHIN, V.; DOUPLIK, A. The refractive index of human hemoglobin in the visible range. Phys. Med. Biol., 56(13):4013–4021, 2011. doi:10.1088/0031-9155/56/13/017.

[135] OUARDI, M.E., MERADI, K.A., TAYEBOUN, F. *et al.* Multi-purpose Surface Plasmon Resonance Sensor with Enhanced Sensitivity for Detecting Anemia and Monitoring Glucose Levels. *Plasmonics* (2025). https://doi.org/10.1007/s11468-025-02813-y

[136] TUDI, M.; RUAN, H. D.; WANG, L.; LYU, J.; SADLER, R.; CONNELL, D.; CHU, C.; PHUNG, D. T. Agriculture development, pesticide application and its impact on the environment. Int. J. Environ. Res. Public Health, 18(3):1112, 2021. doi:10.3390/ijerph18031112.

[137] HÉNAULT-ETHIER, L. Health and environmental impacts of pyrethroid insecticides: What we know, what we don't know and what we should do about it - Executive summary and scientific literature review. 2016. doi:10.13140/RG.2.1.2304.8721.

[138] ADAMS, A. J. A review of the efficacy and uses of deltamethrin for wood preservation. International Research Group on Wood Preservation, Sweden, 1996.

[139] SAYEED, I.; et al. Oxidative stress biomarkers of exposure to deltamethrin in freshwater fish, Channa punctatus Bloch. Ecotoxicol. Environ. Saf., 56(2):295–301, 2003.

[140] YOUSEF, M. I.; AWAD, T. I.; MOHAMED, E. H. Deltamethrin-induced oxidative damage and biochemical alterations in rat and its attenuation by Vitamin E. Toxicol., 227(3):240–247, 2006.

[141] TEERTSTRA, D. Photon refraction in dielectric crystals using a modified Gladstone-Dale relation. J. Phys. Chem. C, 112, 2008. doi:10.1021/jp800634c.

[142] KUMAR, B. M. H.; VAIBHAV, A. M.; SRIKANTH, P. C. Si/SiO_2 based nano-cavity biosensor for detection of anemia, HIV and cholesterol using refractive index of blood sample. Indian J. Sci. Technol., 15(18):899–907, 2022. doi:10.17485/IJST/v15i18.186.

[143] OUARDI, M. E.; MERADI, K. A.; TAYEBOUN, F.; et al. High-precision chemical sensor using surface plasmon resonance for deltamethrin analysis. Sensing and Imaging, 2025. doi:10.1007/s11220-025-00550-4.

[144] OUARDI, M. E.; MERADI, K. A.; TAYEBOUN, F. High-sensitivity surface plasmon resonance-based sensor for HIV detection. International Conference on Multidisciplinary Sciences and Technological Developments (ICMUSTED 2024), Erzurum, Türkiye, December 13–15, 2024.

[145] OUARDI, M. E.; MERADI, K. A.; TAYEBOUN, F. Sensitivity enhanced surface plasmon resonance biosensor for blood cancer detection. J Opt (2025) https://doi.org/10.1007/s12596-025-02843-z.

Our Articles

1- Detection of Water-alcohol Content Using Surface Plasmon Resonance, Plasmonics, published online : 08 April 2024. https://doi.org/10.1007/s11468-024-02285-6
2- **High-Precision Chemical Sensor Using Surface Plasmon Resonance for Deltamethrin Analysis**, Sensing and Imaging, published online : 11 February 2025. https://doi.org/10.1007/s11220-025-00550-4 **[Article of thesis]**
3- Multi-purpose Surface Plasmon Resonance Sensor with Enhanced Sensitivity for Detecting Anemia and Monitoring Glucose Levels, Plasmonics, published online : 11 March 2025. https://doi.org/10.1007/s11468-025-02813-y
4- Development of a Novel SPR Biosensor for Early Pregnancy Detection, Sensing and Imaging, published online : 13 May 2025. https://doi.org/10.1007/s11220-025-00582-w
5- Sensitivity enhanced surface plasmon resonance biosensor for blood cancer detection, Journal of Optics, published online : 19 July 2025. https://doi.org/10.1007/s12596-025-02843-z

Our Conferences

International Conferences

1. Conception of SPR-Based Sensor for Cancer Cell Detection, ICMSE 2024, 29-30 May 2024.
2. Conceptual Study of Surface Plasmon Resonance Sensor for Glucose Level Monitoring, ICENSTED 2024, 19-21 July 2024.
3. High-sensitivity Surface Plasmon Resonance Based Sensor For HIV Detection, ICMUSTED 2024, 13-15 December 2024.
4. High-Sensitivity Atrazine Sensor Using Aluminum Plasmonics and Molecular Imprinting, ICMUSTED 2025, 12-15 December 2025 (to be presented)
5. Mercury Sensing in Fish via Gold-Based SPR and Chitosan Composite Functionalization, ICMUSTED 2025, 12-15 December 2025 (to be presented)

National Conferences

1. Performance Optimization of Surface Plasmon Resonance Sensor Using 2D Nanomaterials, SENALAP' 10, 12-14 June 2023.
2. A Multilayer Surface Plasmon Resonance Platform for Rapid SARS-CoV-2 Detection, NCCAE 2025, 18-19 November 2025.
3. Ultrasensitive Bimetallic SPR Biosensor for Label-Free Malaria Stage Differentiation, NCCAE 2025, 18-19 November 2025.

Abstract

Over the last decades, a big number of scientific publications (articles, books, presentations, etc.) has been produced in photonic physics, most especially in the field of sensors, for the optimization of their accuracy and their miniaturization and make them cost-efficient. The aim of this work is to design SPR biosensors under the Kretschmann-Raether configuration. With simple and achievable structures. We have studied the effect of many materials such as black phosphorus, silicon dioxide, zinc monoxide, transition metal dichalcogenides (TMDC), rhodium, gallium arsenide and magnesium fluoride on the SPR-based sensor's response. In comparison with other works in the same field, simulations show that the proposed biosensors deliver excellent performances. With sensitivities going from 238 to 499 deg/RIU for various applications in the medical, environment and agri-food fields. Results were provided using the transfer matrix method (TMM).

Keywords NanoPhotonics, Plasmonics, TMM.

Résumé

Durant les dernières décennies, un grand nombre de travaux scientifiques (articles, livres, présentations, etc.) ont été réalisés en physique photonique, plus précisément dans le domaine des capteurs, dans le but d'améliorer leurs précisions tout en les miniaturisant et en réduisant leur coût de production. Ce travail a pour but la conception théorique de plusieurs capteurs basés sur la résonance des plasmons de surface (SPR) sous la configuration de Kretschmann-Raether. Avec des structures réalisables pour leur simplicité. Nous avons étudié l'effet de plusieurs matériaux tel que le phosphore noir, le dioxyde de silicium, l'oxyde de zinc, les dichalcogénures de métaux de transition (TMDC), le rhodium, l'arséniure de gallium et le fluorure de magnésium sur la réponse des capteurs SPR tout en comparant chaque capteur avec d'autres travaux sur le même sujet. Les simulations réalisées montrent que les biocapteurs proposés dans ce travail de thèse présentent d'excellentes performances. Avec des sensibilités variant de 238 à 499 deg/RIU pour différentes applications dans le domaine médical, environnemental et agroalimentaire. Les résultats des simulations ont étés réalisés en suivant la méthode de matrice de transfert (TMM).

Mots clés NanoPhotonique, Plasmonique, TMM.

ملخص

خلال العشريات الأخيرة، تم إنتاج عدد كبير من الأعمال العلمية (مقالات، كتب، عروض، إلخ.) في مجال الفيزياء الفوتونية، خصوصا في مجال المستشعرات، بهدف تحسين دقتها مع تصغيرها وتقليل تكاليف إنشائها. يهدف هذا العمل إلى تصميم نظري للعديد من المستشعرات البلازمية وفق رنين البلازمونات السطحية (SPR) استنادا على تكوين كريتشمان Kretschmann-Raether. باستعمال هياكل بسيطة سهلة التحقيق على أرض الواقع. لقد درسنا تأثير العديد من المواد، نذكر على سبيل المثال الفوسفور الأسود، ثنائي أوكسيد السيليكون، أوكسيد الزنك، ثنائي كالكوجينيدات معادن الانتقال (TMDC)، الروديوم بالإضافة إلى زرنخيد الغاليوم وفلوريد المغنيزيوم على إستجابة المستشعرات. مع مقارنة كل مستشعر بالأعمال الأخرى السابقة في نفس المجال. تظهر المحاكاة التي قمنا بها أن المستشعرات المقترحة في هذا العمل تعطي أداء ممتازا. مع حساسية تتراوح بين 238 و499 deg/RIU من أجل تطبيقات مختلفة في الطب، البيئة، وحتى الزراعة. تم الحصول على نتائج المحاكاة باتباع طريقة مصفوفة الانتقال (TMM).

الكلمات المفتاحية النانوفوتونيات، البلازمونيات، TMM.